Thunderstorms: Life cycle analyses and nowcasting based on multi-source data

Isabella Zöbisch

München 2019

Thunderstorms: Life cycle analyses and nowcasting based on multi-source data

Isabella Zöbisch

Dissertation
an der Fakultät für Physik
der Ludwig–Maximilians–Universität
München

vorgelegt von
Isabella Zöbisch
aus Eisenstadt

München, den 28.11.2019

Erstgutachter: Prof. George Craig
Zweitgutachter: Prof. Markus Rapp
Tag der mündlichen Prüfung: 28.01.2020

Zusammenfassung

Ziel dieser Dissertation ist es den Lebenszyklus von Gewittern zu analysieren und dadurch deren Kürzestfristvorhersage (Nowcasting) zu verbessern. Zu diesem Zweck wurden basierend auf Satelliten-, Radar-, Blitz- und Modelldaten Lebenszykulsanalysen sowie ein Nowcasting erstellt. Die Lebenszylusanalysen umfassen Gewitter von unterschiedlichen Organisationsarten (Einzelzellen, Multizellen, Superzellen), die in den Sommermonaten Juni 2016, Mai, Juni, Juli 2017 und Juni 2018 über Deutschland detektiert wurden. Ein Gewitter wird anhand eines auf Satellitendaten basierenden Algorithmus (Cb-TRAM) definiert, der Gewitter detektiert, verfolgt und ihre zukünftige Position bis zu 60 min vorhersagt. Diese über 1900 Gewitter wurden nach ihrer Lebensdauer sortiert und in die Lebenszyklusstadien *frühes Wachstum, fortgeschrittenes Wachstum, Reife* und *Zerfall* unterteilt. Dadurch konnten unterschiedliche Charakteristika des Lebenszyklus im Bezug auf Lebensdauer und Lebenszyklusstadium identifiziert werden. Parameter die für die Lebenszyklusanalysen verwendet wurden sind zum Beispiel: optische Dicke (τ), Helligkeitstemperatur (BT), Zellgröße des Gewitters (A_{cb}), vertikal integriertes Flüssigwasser (VIL), sowie die Modellparameter Convective Available Potential Energy ($CAPE$) und die relative Feuchte (RH). Im Allgemeinen zeigten die Beobachtungsdaten spezifische Merkmale für jedes Lebenszyklusstadium. Im Gegensatz dazu weisen die Modellparameter keine signifikanten Eigenschaften in den einzelnen Lebenszyklusstadien auf. Dennoch konnten Unterschiede zwischen den Lebenszyklen kurz- und langlebiger Gewitter sowohl in den Beobachtungs- wie auch in den Modelldaten ausgemacht werden. Zusätzlich wurden Lebenszyklusanalysen für *intensive* ($\geq$ 46 dBZ) und *nicht-intensive* ($<$ 46 dBZ) Gewitter sowie für Gewitter in einer *front* Umgebung und *nicht-front* Umgebung erstellt.

Die Erkenntnisse aus den Lebenszyklusanalysen werden unter anderem für die Erstellung eines Nowcastingalgorithmus verwendet, der die verbleibende Lebensdauer eines bereits existierenden Gewitters vorhersagt, sowie sein aktuelles Lebenszyklusstadium bestimmt (*LOC-lifetime*). Zusätzlich wird ein erster Ansatz vorgestellt, wie die zukünftige Intensität eines Gewitters - mit derselben mathematischen Methode wie die der Lebensdauervorhersage - vorhergesagt werden kann (*LOC-intensity*). Die Vorhersage des Nowcastingalgorithmus *LOC-lifetime* zeigt eine Verbesserung im Vergleich zu der eines auf reinen Extrapolationsmethoden basierenden Algorithmus. Des Weiteren wird gezeigt, dass die Modellparameter den geringsten positiven Effekt und die Radarparameter den größten positiven Effekt auf die Qualität der Vorhersage von *LOC-lifetime* haben. Je größer das Toleranzinterval ist, welches mittels der Standardabweichung berechnet wird, desto größer die Verbesserung von *LOC-lifetime* gegenüber der Vorhersage der Extrapolationsmethode. Nichtsdestotrotz sind große Toleranzintervalle notwendig um verlässliche Vorhersagen zu erhalten, da diese durch die hohe Variabilität der einzelnen Gewitter stark geprägt ist. Des Weiteren wird gezeigt, dass eine Vorhersage ausschließlich basierend auf den Informationen die zum Zeitpunkt der ersten Detektion verfügbar sind, nur für die Vorhersage der verbleibenden Lebensdauer und nicht für die Intensität verlässlich ist.

Abstract

This study analyses the life cycle of thunderstorms over Germany with the aim to select relevant parameters with predictive skill to improve the description and nowcasting of the thunderstorm life cycle. In contrast to previous analyses, multiple high resolution (in space and time) data sources are used and the life cycle from *early development* over *advanced development* and *mature* to *decay* of several organization types is investigated in detail. Basis are Cb-TRAM (Thunderstorm Tracking and Monitoring) cells in the period June 2016, May, June, and July 2017, and June 2018. Cb-TRAM is an algorithm to detect, track, and nowcast thunderstorms up to one hour using satellite data. For each of these thunderstorms the time series of selected parameters from satellite, ground-based radar, lightning, and model data were inspected. These include e.g. cloud optical thickness (τ), Brightness Temperature (BT), Area of the Cb-TRAM cell (A_{cb}), Vertically Integrated Liquid water (VIL), and the model parameters Convective Available Potential Energy ($CAPE$) and Relative Humidity at 700 hPa (RH). In order to learn more about differences between long- and short-lived thunderstorms, all thunderstorms were sorted by their lifetime and separated into the life cycle stages. Generally, satellite, radar and lightning data are the most suitable data to determine the actual life cycle stage of a thunderstorm. It is shown that the observational data parameters from satellite, ground-based radar and lightning show characteristic behavior in at least one of the four life cycle stages. Model parameters do not show these life cycle stage dependent characteristics. Nevertheless, there are parameters with predictive skill concerning lifetime in observational data as well as in model data. Additionally, the life cycle was analyzed for *non-severe* ($<$ 46 dBZ) and *severe* ($\geq$ 46 dBZ) thunderstorms, and for thunderstorms in a *frontal* and *non-frontal* environment.

These results were used to select meaningful parameters with respect to the nowcasting of the remaining lifetime, the calculation of the current stage of the thunderstorm (*LOC-lifetime*) and the prediction of the future intensity (*LOC-intensity*). One result is that *LOC-lifetime* is more reliable than a lifetime prediction of an extrapolation method based algorithm. Another result is that the parameters of the model data has the lowest positive impact on the fuzzy logic-based nowcasting model. Whereas radar parameters are crucial for the remaining lifetime prediction. The larger the tolerance interval around the predicted lifetime gets, the bigger is the improvement of *LOC-lifetime* compared to extrapolation method based predictions. The tolerance interval is calculated from the standard deviation. Nevertheless, high tolerance intervals are needed to get a reliable output as the prediction is limited by the high variability of single thunderstorms. Further results show that predictions using only the first detection step are only reliable for the remaining lifetime and not for the future intensity.

Contents

1 Introduction

1.1 Motivation

A modest thunderstorm cloud contains about $8x10^6$ kg of condensed water (Doswell III, 2001). For condensation of this water, almost 10^{14} J of latent heat is released over a period of roughly 25 min. This, during condensation released energy, can be compared to the latent heat of a "25 kiloton" bomb. A part of this energy creates severe weather events like hail, lightning, strong wind gusts and heavy precipitation sometimes followed by flooding or localized flash floods. Due to these weather phenomenons that occur together with thunderstorms, it is not surprising that thunderstorms have fascinated humans since the year dot and gave birth to myths and superstition. In ancient times, for instance, people believed that thunderstorms were a message from outer space, and in medieval times, lightning was seen to be a punishment of god. The Greek god "Zeus", as well as the Nordic god "Thor" might be one of the most known explanations for lightning and thunder during this time. Thus, it is not surprising that these mystical weather events inspired poetry. Many poets describe the threatening and at the same time beautiful appearance of thunderstorms. Heinrich Heine ("Gewitter"), Otto Ernst ("Nach dem Gewitter"), or Emily Dickinson ("A Thunderstorm") are just a few examples.

One of the first who studied the phenomenon of lightning scientifically was Benjamin Franklin in the 18th century. But the occurrence of thunderstorms and lightnings, and their underlying mechanisms, are not fully understood until today. The complexity of the underlying physics is only one reason for the difficulty of thunderstorm prediction in addition to the limited operationally available observation methods. As well as the research of thunderstorms, weather prediction has a long history. Synoptic weather prediction began in the period of 1850-1870 (Murphy, 1998). First computational weather models were developed in the early 20th century. Due to a better resolution of available data and increased power of processors, weather forecasting improved greatly in the last decades.

Today, thunderstorms are well known to still have high impact on society and safety (Brooks and Dotzek, 2008). This high impact results from the thunderstorms' related weather events. These severe weather events cover a wide horizontal and especially vertical area, from the surface up to the tropopause in 11 km. On the ground, hail,

lightning and heavy rain affect society and safety. In May 2013, for instance, the effects of tornadoes injured nine people and destroyed 230 buildings with assumed losses of about 50 million euro in Germany, as the insurance agency "Munich Re" reported [1]. In 2016, the music festival "Rock am Ring" was spontaneously interrupted by a severe thunderstorm event. As the warning and, consequently, the security measures came to late, more than 50 people got hurt by a lightning stroke. 15 of them were injured severely, some of them even critically [2]. An earlier warning could have contributed to an earlier start of security measures, and might have avoided these injuries. Although, losses that result from destroyed buildings can not be avoided by an improved thunderstorm nowcasting, personal injuries might be reduced.

In addition to these severe weather events on the ground, thunderstorms also contain severe regions at high altitude (for example, near the tropopause). For example, thunderstorms in higher heights cause icing of airplane turbines in the upper troposphere, leading to malfunctions (Tafferner et al., 2008). Other well known dangerous weather events connected to thunderstorms are convective turbulence and lightning. These severe weather events affect flight times negatively and pose a risk for crew and passengers. Therefore, thunderstorms are one of the most significant threats for aviation.

Since thunderstorms occur all over the world, an improved forecasting of thunderstorms would benefit many people. With regard to the fact that the frequency of severe thunderstorms over Europe will increase in future (Rädler et al., 2019), an improved nowcasting becomes more meaningful. However, forecasting of thunderstorms is still a challenge to date. Based on dynamical and thermodynamic equations numerical weather forecast models are able to calculate the atmospheric state hours and days in advance. However, the model forecasts are not accurate enough to predict the exact location and time of the occurrence of thunderstorms, since observations to exactly describe the initial state for such calculations do not exist in the necessary resolution. Model forecasts can only give a rough estimate of the future atmospheric state and are not suitable to plan appropriate measures related to the mitigation of the impact of a thunderstorm.

In contrast, observations from satellite and weather radar enable the exact detection of existing thunderstorms and allow a short-term forecast up to a few hours (called nowcasting) based on the extrapolation of historic observations. Examples for such nowcasting algorithms are Cb-TRAM (Zinner et al., 2008), KONRAD (Lang, 2001), and CellMOS (Hoffmann, 2008). They provide an overview of the current thunderstorm situation and its predicted development in the near future. The inaccuracy grows

[1] `https://www.munichre.com/topics-online/en/climate-change-and-natural-disasters/natural-disasters/storms/thunderstorms-germany-2016.html`, 15.05.2019

[2] `https://www.faz.net/aktuell/gesellschaft/unwetter-bei-festival-bei-rock-am-ring/-schlaegt-der-blitz-ein-14269078.html`, 15.05.2019

rapidly for nowcastings beyond one hour, since the extrapolation is just based on the development seen in the historic data and no physical equations are used to calculate the forecasts. In addition, the remaining lifetime of a thunderstorm and the trend of its intensity still remain unknown.

In a nutshell, thunderstorms have a huge vertical extended area, from the surface up to the tropopause, that is full of severe weather events. Additionally to the already severe weather events, accompanied with thunderstorms, climate change will lead to more intense thunderstorms (Sander, 2011). In order to be able to take appropriate actions to mitigate a thunderstorm's impact, warning and rescue services, the public, aviation stakeholders, and further affected parties need accurate and reliable information on the occurrence, lifetime, and intensity of thunderstorms. Already today, thunderstorm nowcasting can be used to optimize flight routes spontaneously (Forster et al., 2016), resulting in reduced delays, fuel savings, and improved safety.

In the following, the basic knowledge of thunderstorm life cycle and organization is presented as preparation for the subsequent state of the art of thunderstorm life cycle analyses and nowcasting.

1.2 Background: Life cycle of convective clouds

In this chapter, the basic knowledge about the underlying mechanisms and physics of thunderstorms, the typical life cycle of a single thunderstorm, and different types of organization are presented.

The following introduction in convection is based on Doswell III (2001) if no other references are mentioned. The underlying mechanism behind thunderstorms is convection. Convection is – beside radiation and conduction – one of the three main processes of transportation of heat.

There are many forms of convection as described in Emanuel (1994). One form of convection is Deep Moist Convection (DMC) which is associated with thunderstorms. A detailed description of the underlying mechanisms of DMC is given in the next paragraphs.

The vertical component of heat transportation by convection is called buoyancy. A simplified way to describe buoyancy is:

$$B \equiv g\frac{T - T'}{T'}$$

where g is the acceleration of gravity, T is the temperature of an air parcel and T' is the temperature of the surrounding environment. A positive buoyancy describes an

updraft and a negative buoyancy a downdraft. Buoyancy is a product of heat release and therefore a crucial aspect of thunderstorms.

The following explanations of the process of convective initiation are based on Schumann (2012). Beside an environmental temperature gradient rapidly decreasing with height, moisture must be abound in the lower troposphere for thunderstorm development. In many cases a trigger mechanism (a source of lift) is also necessary. An air parcel that is warmer at the surface than its environment rises due to the density differences between the parcel and the environment (warm air is less dense than cold air). The parcel rises dry adiabatically with a temperature decrease of ~ -10 K km^{-1} due to adiabatic expansion, as long as it is warmer than its environment and not saturated. If it rises further until it reaches the dewpoint and hits a saturation of 100%, water vapor condensates. At this height the Lifted Condensation Level is reached (LCL, see Figure 1.1). As long as the water vapor in the air parcel condensates, it rises moist adiabatically (usually between -5 to -9 K km^{-1}), and the temperature decreases less with height than in case of a dry adiabatic ascent, as latent heat is released during the phase change in the process of condensation. If the air parcel is no longer warmer than its environment, the air parcel has to be lifted to the Level of Free Convection (LFC), for further rising. Some of these trigger mechanisms that may lift the parcel are convergence, orographic forcing or solar heating. At the height of LFC the parcel is able to further rise moist adiabatically due to its higher temperature compared to the environment until the temperature of the parcel is equal or less than that of its surrounding environment. This is for example the case at the tropopause because of the reversed environmental temperature gradient in the stratosphere. The height where further vertical growth stops is called Equilibrium Level (EL).

The area between the temperature of the parcel and its surrounding environment from the LFC to the EL is called Convective Available Potential Energy (CAPE) and is a measure of instability. The definition of CAPE is given by

$$CAPE = \int_{z_{LFC}}^{z_{EL}} g\frac{T - T'}{T'}dz \equiv \int_{z_{LFC}}^{z_{EL}} B(z)dz$$

Where the buoyancy is integrated from the height of LFC (z_{LFC}) to the height of EL (z_{EL}).

High CAPE values indicate a high potential for thunderstorms (Markowski and Richardson, 2010). For instance, marginal convection is associated with CAPE values of 0-1000 J kg^{-1}, CAPE values of 1000-2500 J kg^{-1} indicate moderate convection, and CAPE values of 2500-4000 J kg^{-1} contribute to strong convection. If CAPE reaches higher values than 4000 J kg^{-1}, potential extreme convection is indicated. However while high CAPE values are necessary for DMC, they are not sufficient. For instance, if an inversion layer at the planetary boundary layer inhibits the air parcel to lift to LFC, no DMC occurs. This inhibition can be measured in energy, that is necessary to

lift a reference air parcel to its LFC and is called Convective INhibition (CIN). The calculation of CIN is very similar to CAPE, only the integration limits differ. For CIN calculation it is integrated from the surface to the LFC. If the storage of CAPE occurs over several days it is possible, that the accrued instability finally releases in form of severe convection. Large CAPE values and small CIN values are required for DMC, although CIN is necessary for large CAPE values to build up. Many further indices exists, which describe the physical state of the low- and mid-troposphere to estimate the probability of thunderstorm development. Most of them describe the instability of the atmosphere, such as the indices Showalter Index (SI, Showalter, 1953) and Lifted Index (LI, Galway, 1956). LI and SI are simpler calculations for the probability of thunderstorm development than CAPE and describe only single-level bouyancy. In contrast CAPE is calculated by vertical integration and includes the bouyant energy up to the level of free convection (LFC).

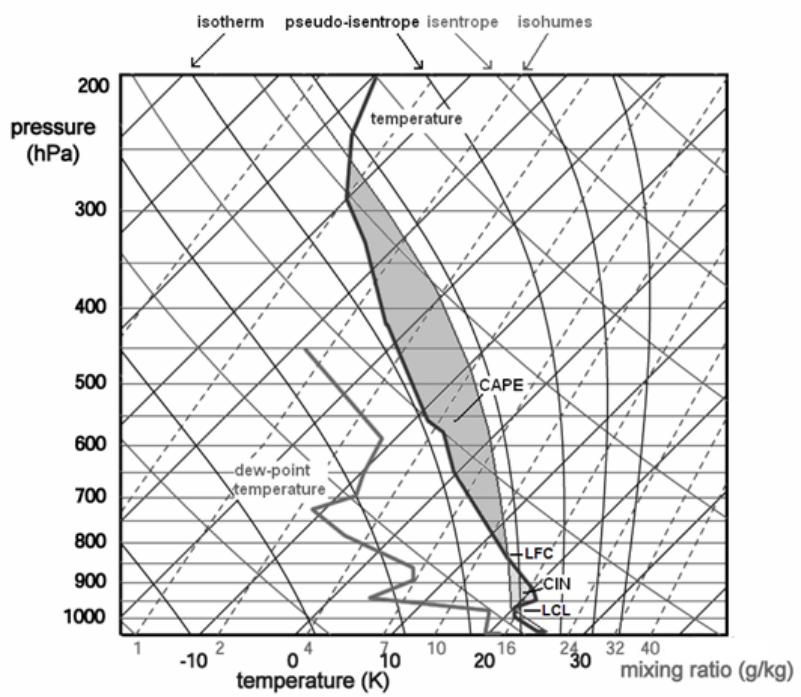

Figure 1.1: The temperature and dew point temperature (measured via radiosonde ascent) are plotted in this Skew-T log p diagram. Isotherms and isobars are shown together with isohumes (lines of equal mixing ration), isentropes (also called dry adiabats, lines of equal potential temperature), and pseudo-isentropes (also called moist adiabats, lines of equal pseudo equivalent potential temperature). In this example, the ascent curve of T(p) of a parcel having an initial temperature of 26°C at the surface and a dewpoint temperature of 21°C has been constructed. (Diagram taken from `http://www.estofex.org/guide/`,15.11.2019).

1.2.1 The thunderstorm life cycle

The life cycle of thunderstorms was defined by Byers and Braham Jr. (1948) for the first time. They separated the life cycle into three stages: towering cumulus stage, mature stage, and dissipation stage. The life cycle as described in detail in Doswell III (1985) is presented in the following paragraphs. This definition describes a textbook life cycle of single thunderstorm cells. The persistence of each life cycle stage depends on the type of organization as described in the next section (Section 1.2.2).

1. Towering cumulus stage

The first stage of the thunderstorm life cycle is named "growing stage" or "towering cumulus stage". Characteristics of the growing stage are depicted in Figure 1.2. The towering cumulus stage is characterized by beginning of visible cloud formation and the initiation of an updraft. This updraft is accompanied by small scale downdrafts. The updrafts increase rapidly with height, since the temperature difference between the air parcel and the environment increases due to their different lapse rates (see Figure 1.1); thunderstorms typically show updrafts of about 10 m s^{-1} in 5 km height.

The warm moist air is transported upward and expands adiabatically, to higher levels. If relative humidity supersedes 100% (LCL in Figure 1.1), the water vapor in the air parcel condensates and further rises moist adiabatically. Consequently, cloud formation starts (convective initiation). The strong condensation leads to an intensifying updraft and cloud droplets reach high altitudes. If cloud droplets reach radii of 20 μm or larger, coalescence starts to contribute to cloud droplet growth. The larger cloud droplets fall faster than small cloud droplets, collide with the smaller cloud droplets and merge together. Finally, precipitation and downdraft are initiated. The underlying physics for downdraft development is presented in the next paragraph. Ordinary thunderstorm cells reach diameters of about 5-8 km during their "growing stage". Most clouds dissipate after this stage and do not evolve to the mature stage, because the downdraft impedes further buoyancy supply.

2. Mature stage

Once precipitation reaches the ground, the "mature stage" begins. In this stage the thunderstorm cell reaches its maximum intensity. This intense period is dominated by strong up- and downdrafts of which the updrafts lead to an ongoing vertical growth. Air masses rise, until the EL is reached (see Figure 1.1). During the growth, water droplets grow and become supercooled at high altitudes. These supercooled water droplets might freeze to ice particles. The ice particle growth can be described by the Wegener-Bergeron-Findeisen Process (Wegener, 1911; Bergeron, 1935; Findeisen, 1938): Since supercooled water droplets and ice particles coexist above freezing level, the ice particles grow at the expense of supercooled water droplets. This is the case because

the saturation vapor pressure is lower for ice than for water. Hail, for example, mostly occurs if a strong updraft is present. For a more detailed description of precipitation forms see, for example, Tessendorf et al. (2005). In general, the upcoming air masses reaching the tropopause can not rise higher, therefore, an anvil is built via divergence at the tropopause. In case of a very strong updraft the upcoming air even overshoots into the dry warm stable conditions of the stratosphere. Due to mixing with relatively warm and dry stratospheric air cloud droplets evaporate rapidly and further vertical growth is impeded mostly by the stable stratification in the stratosphere.

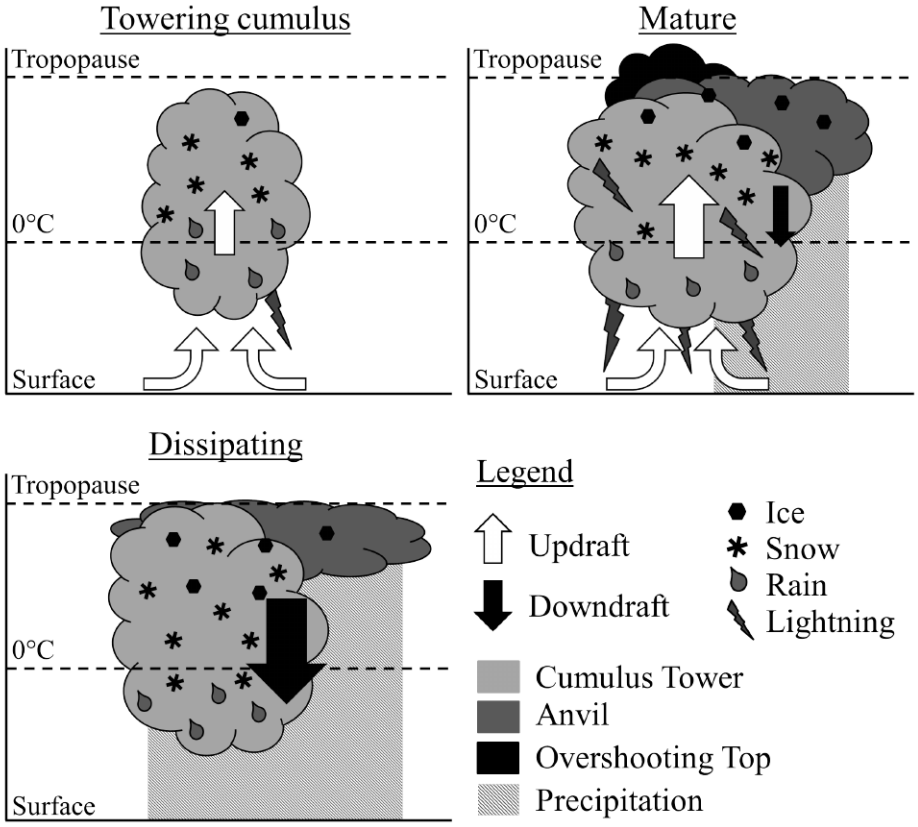

Figure 1.2: Sketch of the three life cycle stages of a single thunderstorm cell after Byers and Braham Jr. (1948)

For the development of a downdraft, two different origins are possible. One possibility is the evaporation of cloud droplets by entrainment of dry air. Evaporation of condensed air leads to a cooling of the surrounding air by up to 3.7°C. Consequently, the colder air starts to sink building a cold pool at the surface. The second possibility for onset of downdraft is that falling precipitation droplets transport some of the surrounding air downwards.

During "mature stage" lightning occurs. The responsible factors for electrification of

the storms are not well understood until today. It is assumed that the collision of ice particles with supercooled water is crucial for cloud electrification (Reynolds et al., 1957; Saunders, 1993; Wallace and Hobbs, 2006). Lightning occurs if the electrical field caused by charge separation into positive (at cloud top and surface) and negative (at cloud bottom) ions due to friction becomes too strong. The discharge happens by inner cloud lightning (Cloud-to-Cloud, CC) or by lightning between cloud and surface (Cloud-to-Ground, CG). The process of lightning is described in detail in Feynman et al. (1964).

3. Dissipating stage

The "dissipating stage" supersedes the "mature stage" once the source of the updraft is stopped by the previously developed cold pool that spreads out horizontally at the surface. Finally, the updraft diminishes rapidly due to the missing buoyancy supply. The dissipating stage is characterized by precipitation and downdrafts. Generally no lightning activity exists during the dissipating stage. The persistence of the dissipating stage depends on the type of organization as described in the next section (Section 1.2.2)

1.2.2 Organization of thunderstorms

Thunderstorms can be classified into three different types of organization: single cells, multicells and supercells (Höller, 1994). This classification is based on a method developed by Foote (1985), and implies a differentiation of storms depending on their lifetime, evolutionary features, and forming processes.

The organization types and their main characteristics by (Höller, 1994) are summed up in the following and described afterwards:

- Single cells: The complete life cycle (growth, mature, and decay) of the thunderstorm takes place in one isolated cell. Typical lifetimes of single cells are 20-30min.
- Multicells: A group of single cells in which each cell is in different life cycle stages. Multicells can last a few hours.
- Supercells: One enormous cell, in which all life cycle stages coexist. Supercells have a deep rotating updraft named mesocyclone. They can last up to 12 hours.

Single cells do not show any organized subsequently initiated convection. Thus, only one updraft is present. Typically single cells develop in an environment with weak wind shear. Single cells often develop due to the diurnal circle of the boundary layer and therefore occur during the time of maximum daytime heating and decay after sunset. To predict whether or not single cells produce hail is often difficult, because of their

short time range and the possible large range of CAPE values (a few hundred J kg^{-1} to > 2000 J kg^{-1}). Usually severe weather occurs in an environment with CAPE values of > 2000 J kg^{-1} (Markowski and Richardson, 2010).

The most common form of convection are multicells. In multicells several cells are grouped in an organized cluster, thus different life cycle stages exist. If for example one cell is already decaying, while another cell is in its mature stage and another in its growing stage, more than one updraft region exists simultaneously. This co-existence of several life cycle stages is possible, because the vertical wind shear is moderate (0-6 km wind field difference usually has a magnitude of 10-20 m s^{-1}) for multicells and separates the updraft and downdraft region. Additionally, the cold pool acts as source of lift for neighboring air parcels. Multicells can occur in environments with high or low CAPE (Markowski and Richardson, 2010).

Hail with a diameter of 5 cm or larger, or tornadoes are often the results of supercells. More than 200 flashes per minute can occur in those supercells. Lifetimes of 1 to 4 hours are usual, although some supercells last up to 8 hours. Supercells have only one dominant updraft region that shows a quasi-steady appearance. Additionally, a persistent mesocyclone within the updraft is essential for the occurrence of supercells. The mesocyclone is defined by a region of vertical vorticity. For the development of such a mesocyclone, a large vertical wind shear extended over most parts of the troposphere is necessary. Since the dynamic effects due to the vertical wind shear and the presence of the mesocyclone can enhance the updraft, large CAPE values are no necessary condition. Supercells exists already for CAPE values of about > 1000 J kg^{-1} (Markowski and Richardson, 2010).

Since the aim of this thesis is to predict the lifetime of convective systems in general, no differentiation is done for these three types of organization. Therefore, the characteristics of thunderstorms of any type of convective system are considered in the life cycle analyses and nowcasting.

1.3 State of the art

1.3.1 Thunderstorm life cycle

In order to improve the nowcasting of thunderstorms, profound knowledge of the typical life cycle of thunderstorms is essential. Nowadays a large variety of observational methods is available to investigate small scale atmospheric processes. First, the major methods for an operational thunderstorm observation that are available high-resolution in time and space over Germany are introduced including satellite, ground-based radar

and lightning detection. Afterwards, studies about the thunderstorm life cycle are presented.

The satellites, which measurements are used in this thesis, is geostationary and at a height of about 36.000 km. It is able to detect outgoing electromagnetic radiation via a radiometer and measure twelve different spectral ranges, from visible (VIS) / near infrared (NIR) to water vapor (WV) and infrared (IR) to high-resolution visible (HRV). Generally, clouds have high reflectivities in the visible range, resulting in bright clouds in the VIS. The NIR channels are able to measure ice, therefore, they can be used for identification of ice clouds. While the VIS channels can be used for observing the thickness of clouds, the IR channels are able to provide information about the state of aggregation and the particle size. As the radiation emitted increases with temperature and spectral emission coefficient, the cloud top height can be measured indirectly by the IR channels. Since the temperature decreases with increasing altitude, high clouds (low temperatures) show smaller values of IR. Additionally, the WV channels provide information about the water vapor content in the atmosphere and its layers.[3]

Ground-based radar systems can also be used to analyze some thunderstorm characteristics. RADAR is the acronym for "RAdio Detection And Ranging" which implies that radio waves are measured. This is done via the "Doppler Effect" to get information about particle movement. The radar sends a high frequent electromagnetic wave in a desired direction into the atmosphere, where a part of the signal will be reflected, for example, off a precipiation particle. The reflected part of the electromagnetic wave is measured at the radar and transformed into a digitalized signal. This way the location of the particle and the intensity (intensity of the reflected signal) of, for example, precipitation can be measured. These continuous high-resolution radar measurements in varying azimut and elevation angle are used for operational weather observations.[4]

Another thunderstorm observational method used operationally is the lightning detection. As previously described, thunderstorms are defined by thunder which a lightning must precede, consequently, lightning detections act as indicator for thunderstorm occurrence. Since lightning produces electromagnetic radiation a net of measurement systems can detect the location of a lightning due to arrival differences of the signal. In general, it is possible to measure the intensity, the height, the location and the type (cloud-to-ground or cloud-to-cloud) of the lightning.[5]

The first model describing the life cycle of a thunderstorm was presented by Byers and Braham Jr. (1948). They separated the life cycle on the basis of observations and measurements (especially airplane data) from the "Thunderstorm Project" into

[3] https://www.dwd.de/DE/forschung/atmosphaerenbeob/wettersatelliten/satelliten_meteosat_node.html,15.11.2019

[4] https://www.dwd.de/DE/forschung/atmosphaerenbeob/wetterradar/wetterradar_node.html,15.11.2019

[5] https://www.nowcast.de/technologie/funktionsweise-von-linet.html,15.11.2019

three stages: Growth, mature, and dissipation (as explained in the previous section). The stages were characterized and defined by wind-field and microphysics. During the early cumulus stage surface convergence happens 20-30 min before a radar echo can be measured. Machado et al. (1997) analyzed the life cycle of Mesoscale Convective Systems (MCS) in satellite data with a temporal resolution of 3 hours. There, a MCS is defined as a "mesoscale cluster of deep convection". They especially focused on the trend of the cloud top temperature and the coverage area of the cloud system of deep convective systems over the Americas (tropical and middle latitude). The study showed that size and lifetime of thunderstorm cells correlate nearly linearly. This was also seen by Feng et al. (2012). Furthermore, long-lived cells reach larger sizes than short-lived cells, while no differences between long- and short-lived cells were found for the cloud top temperature gradient. A correlation between updraft and cloud droplet size can be seen for increased reflectivity, caused by strong updrafts that tends to produce great amounts of small ice particles (Setvák and Doswell, 1991). The life cycle of Sahelian MCS was analyzed by Mathon and Laurent (2001) with a temporal resolution of 30 min. They confirmed that the mean radius of MCSs correlates roughly linearly with their lifetime. Roberts and Rutledge (2003) analyzed the convective initiation of thunderstorms on basis of satellite and radar data with a temporal resolution of 15 min. They confirmed high cooling rates at cloud tops 30 min before 35 dBZ are measured. In thermal radiation, growing clouds show a rapid cooling of cloud tops, indicating a release of Convective Available Potential Energy (CAPE) (Senf et al., 2015). CAPE can also be related to the maximum updraft velocity according to Emanuel (1994). Freud et al. (2008) analyzed the size of convective cloud droplets by in-situ measurements. They showed that cloud droplet size increases with cloud depth. MacKeen et al. (1998) analyzed the correlation of lifetime and radar reflectivity. Almost 1000 thunderstorms were observed over the analyzed area in Memphis, Tennessee. It was shown that radar reflectivity parameters do not show any predictive skill concerning lifetimes. Pope et al. (2008) found cloud top temperature decreases slowly once the size of a thunderstorm reached its maximum. The anvil formation is suggested to lead to a horizontal growth right before mature stage. A detailed study about the life cycle of thunderstorms and lightning occurrence was given from Mattos and Machado (2010). They depict that a relationship between the area, cloud top temperature and the lightning occurrence exists. The cloud-to-ground lightning occurrence correlates positively with the size of the observed thunderstorm area. Additionally, high cloud tops are strongly correlated with areas of increased electrical activity. However, high cloud tops are no essential criterion for lightning activity (Goodman et al., 1988). Further Goodman and MacGorman (1986) remarked that lightning activity appears to be independent of thunderstorm size and life cycle duration.

Jurković et al. (2015) observed a correlation between spatial distribution of lightning and of detected overshooting tops. Whereas, this correlation is less pronounced in southeastern Germany where lightning occur in the vicinity of overshooting tops. Higher

values of lightning activity were detected slightly before an overshooting top occurred. Additionally, Mikus and Mahovic (2013) showed that overshooting tops are associated to precipitation and wind gusts rather than to temperature and humidity changes. Mecikalski et al. (2011) used satellite data to describe and understand the physical attributes of growing single cell thunderstorms. They found that during the growing phase, cloud optical thickness and cloud droplet size increase until cloud tops glaciate, and initiate a decrease in cloud droplet size. The study by Mecikalski et al. (2012) presented a more detailed life cycle definition than Byers and Braham Jr. (1948) and proposed five stages: Pre-convection, convective initiation, deep convective growth, mature, and dissipation. Description of the pre-convection and convective initiation stages were possible due to a higher temporal and spatial resolution of satellite data. The pre-convection stage is represented by a 4D wind field, before convective initiation occurs. Multi-spectral satellite radiance can be used in combination with temperature and moisture profiles to describe this stage. Additionally, the characteristics of the pre-convective environment can be observed by rawinsonde profiles. The key forcing mechanisms upper level divergence and low level convergence can be measured this way. The beginning of convective initiation is defined by the onset of vertical growth. This is indicated by the first detection of a 35 dBZ radar echo, for instance. During the convective initiation, cloud tops cool and glaciate. Existing precipitation in clouds can be detected by radar. After Mecikalski et al. (2012), the mature stage is characterized by a region of strong vertical motion that advects ice hydro-meteors into the upper troposphere and lower stratosphere.

Davini et al. (2012) analyzed the life cycle of storms in northwestern Italy on the basis of radar data with a temporal resolution of 10 min. They showed that the maximum reflectivity is detected predominantly in the first half of the life cycle and is higher for long-lived thunderstorms than for short-lived thunderstorms. The maximum of areal extent was observed in the last half of the life cycle. Further they found that reflectivity values at the beginning of a thunderstorm allow to draw conclusions about the thunderstorm's lifetime. Liu and Li (2016) analyzed the life cycle of severe thunderstorms via radar and lightning data and examined the spatial and temporal distribution of the lifetime of thunderstorms. They differentiated between the categories initiation, development, termination, merge, and split. The highest number of thunderstorms was detected in May. Most of the analyzed thunderstorms had a lifetime between 5 and 20 min and were initiated during 2100 to 0000 UTC and terminated during 2100 to 0300 UTC. In a study of the life cycle of hailstorms over Germany on basis of lightning and radar data, Wapler (2017) revealed that the lightning intensity of hailstorms is much higher than that of ordinary thunderstorms. Furthermore, hailstorms exhibit a lightning jump just before hail onset. A positive correlation of the maximum cloud top height, anvil expansion rate, maximum precipitation intensity and core size was found by Senf and Deneke (2017) for thunderstorms over Central Europe. They also proved that precipitation already occurs 30 min prior to maximum

cloud top cooling. On thundery days, an especially strong conditionally unstable layer is present between 850 and 500 hPa (Huntrieser et al., 1997). They also showed that the vertical wind shear and the relative humidity correlate well with the occurrence of thunderstorms.

All these studies either focus on specific aspects of the thunderstorm life cycle or mainly make use of observations from only one or two data sources. In this thesis, the life cycle of thunderstorms is analyzed for the first time on the basis of a variety of data sources from observations high-resolution in space and time and a NWP model. The previous studies analyze mostly one special type of thunderstorm organization, for example, single cells or MCSs. In this thesis, no differentiation is done between the different types of organization with respect to a future nowcasting. In order to find typical characteristics in every life cycle stage, thunderstorms are analyzed in a data set of five months. The aim of this thesis is to identify relevant parameters with predictive skill and to use them to improve the nowcasting of thunderstorms concerning their lifetime and intensity. Several studies about the nowcasting of thunderstorms were conducted and an overview is given in the following.

1.3.2 Thunderstorm nowcasting

Now, important studies on the predictive skill of certain analyzed parameters are presented, followed by a summary of existing nowcasting methods.

Parameters for nowcasting

The parameter CAPE is a well known predictor for severe storms (Rasmussen and Blanchard, 1998). Rosenfeld et al. (2008) analyzed the predictive skill and relation of the cloud top temperature and cloud droplet size. According to them, strong updrafts connected with hail occurrence are responsible for a delayed growth of cloud droplet size and lower cloud top temperatures. Therefore, hail as well as tornadoes can be predicted with lead times of up to 2 hours by taking the relationship criteria into account. The areal growth rate, detected in satellite data is greater for severe storms than for non-severe thunderstorms during their vertical expansion (Adler and Fenn, 1979). The parameter Vertically Integrated Liquid water (VIL) is commonly used as an estimate of the total mass of precipitation and further can be used to differentiate between severe and non-severe thunderstorms (Kitzmiller et al., 1995). An algorithm was developed to detect severe storms, on basis of the radar parameter VIL and the areal expansion. The correlation between high VIL values and severe storms was first published in 1970s (Greene and Clark, 1972). Additionally, a positive correlation between VIL and lightning occurrence was observed by Watson et al. (1995). As they found, one criterion for lightning occurrence is that VIL values are greater than

1 kgm^{-1}. Hartung et al. (2013) showed that there is a correlation between cloud top cooling rates during convective initiation, rainfall intensity and hail occurrence in the later stages of the life cycle. Correspondingly to this, Cintineo and Stensrud (2013) analyzed the predictive skill of temporal change of satellite derived cloud properties for future severity. They found that the trend of the optical thickness, the cloud particle size, emissivity and cloud top phase are parameters with predictive skill.

Several groups already worked on the prediction of thunderstorm intensity. Dvorak (1975) estimates the intensity of a cyclone by summarizing parameters, derived from satellite pictures. To detect severe thunderstorms early in their development, Nisi et al. (2014) developed the "context and scale oriented thunderstorm satellite predictors development" (COALITION) algorithm. This object-oriented algorithm uses satellite, radar, and model data, as well as climatology. The aim is to predict whether or not a thunderstorm cell will develop to a severe thunderstorm within the next 30 min. Lead times of 5 to 60 min were analyzed, resulting in reliable predictions for lead times up to 20 min. For lead times greater than 20 min the prediction became less reliable. Already Mecikalski et al. (2015) combined data from satellite observations with the model data parameters CAPE and convective inhibition energy to improve the prediction of convective initiation. They successfully reduced the ratio of the false alarms by combining these two data sources, compared to predictions based on only one of these two data sources. A more recent study was made by Mecikalski et al. (2016) in which they analyzed satellite fields and their prediction ability in the early life cycle stages of severe thunderstorms and their future intensity. Especially the cloud top temperature and cloud droplet size ratio played a significant role in their analysis. Farnell et al. (2017) developed an algorithm that predicts severe storms based on the occurrence of lightning jumps (Williams et al., 1999). The algorithm is based on the assumption that a lightning jump occurs right before a storm intensifies. This indicator is presented in other studies as well (Darden et al., 2010; Wapler, 2017). Several detection algorithms (Roberts and Rutledge, 2003; Zinner et al., 2008) use the cloud top cooling rate for detection and nowcasting of strong vertical growth (which is an indicator for convection initiation, as previously mentioned).

Methods for nowcasting

In the following paragraphs, an overview of the current research on nowcasting models is presented. Basically, three categories of nowcasting methods exist: extrapolation techniques, numerical weather prediction models (NWP), and expert knowledge-based systems that combine extrapolation techniques and NWP (Wilson et al., 1998, 2010; Sun et al., 2014).

An example for a nowcasting model based on extrapolation techniques is the algorithm "Thunderstorm Identification, Tracking and Nowcasting" (TITAN, Dixon and Wiener,

1993). TITAN is a radar based nowcasting algorithm that uses the centroid tracking method. Thus, the algorithm was not developed to nowcast the lifetime of single thunderstorm cells, but to calculate motion vectors of radar echoes. Neither storm initiation nor thunderstorm life cycle can be predicted by this algorithm. Another example for an extrapolation based algorithm to nowcast thunderstorms is the satellite based algorithm "CumulonimBus TRacking And Monitoring" (Cb-TRAM, Zinner et al., 2008). Since this algorithm plays a crucial role for this thesis, it will be explained in great detail in Chapter 2.1.

Today, several methods are used for nowcasting thunderstorms. There are on the one hand the commonly used extrapolation methods and on the other hand newly developed methods such as fuzzy logic or machine learning. The fuzzy logic-based algorithm Auto-Nowcast System (ANC) nowcasts the future location of storms for 0-1 hour (Mueller et al., 2003). They added a combination of predictor fields based on radar, satellite, sounding, mesonet and profiler data and a numerical boundary layer model to a forecaster input and detection algorithms. In this algorithm, the life cycle is separated into the stages initiation, growth, and decay. This life cycle information is used to decide, if the contour of a predicted thunderstorm is newly developed, increasing, or decreasing comparison to a currently existing contour. In contrast to extrapolation techniques, the nowcasting of storm location is improved by the fuzzy logic-based ANC method in regards to the probability of detection. However, the false alarm ratio also showed increased values for ANC. One example for the application of machine learning for nowcasting thunderstorms is presented in Han et al. (2017). Within the machine learning framework, they developed a support vector machine box-based nowcasting method using variational Doppler radar analysis system data. They improved the nowcasting of thunderstorm movement and growth within the next 30 min compared to TITAN.

Most of the presented nowcasting tools were developed to predict the convective initiation of thunderstorms or their severity, in addition to the movement and local displacement. Hence, nowcasting of remaining lifetime is neglected often. It is a challenge to predict the remaining lifetime of thunderstorms, primarily because thunderstorm cells can split into several thunderstorm cells or they merge during their life cycle. Westcott (1994) showed that radar echoes of merging thunderstorm cells are initially taller and slightly larger than those without merging. After merging, more than half of the thunderstorms were growing again. Consequently, this uncertain behavior impedes the prediction of future development and remaining lifetime of thunderstorms.

The aim of this thesis is to describe the life cycle of thunderstorms detailed by using a multi-sourced data set and to improve the nowcasting of the remaining lifetime and intensity of thunderstorms. An overview of the basic concept is given in the following.

1.4 Basic concept, aims & outline

Nowadays, the resolution in time and space of observational and model data increases rapidly. Also the variety of operationally available parameters is getting more diverse. Hence, the aim of this thesis is, to select parameters with predictive skill from satellite, radar, lightning and model data, to combine them and to improve the nowcasting of thunderstorms. Especially the lifetime prediction is focused in this thesis, due to its high impact on society as described in Brooks and Dotzek (2008).

This thesis is separated into two main parts: The first part is about the analyses of the thunderstorm life cycle and the second about the development and verification of two nowcasting models. A thunderstorm includes a broad variety of possible thunderstorm organization types and is often a thunderstorm complex (for example, a multicell) than a single thunderstorm cell, consequently the following named thunderstorm is described by thunderstorms of various organization types. The basic concept is outlined in Figure 1.3, including the main work packages and aims. At the start, the data sources satellite, radar, lightning, and model were chosen as data sources, due to their operational availability, and spatial and temporal resolution. The satellite based algorithm "CumulonimBus TRAcking and Monitoring" (Zinner et al., 2008) was used to define the thunderstorms. As it is crucial to understand and learn more about the behavior during the life cycle of a thunderstorm life cycle to predict future developments, the thunderstorm life cycles were analyzed for parameters from these data sources. Additionally, differences between the life cycle of short- and long-lived thunderstorms, as well as, differences between the life cycle of severe and non-severe thunderstorms were analyzed.

The second part of this thesis contains the development and verification of the nowcasting models. These models calculate the current stage and predict the remaining lifetime (*LOC-lifetime*), and nowcast the future intensity (*LOC-intensity*). Parameters with predictive skill were selected for the two nowcasting models *LOC-intensity* and *LOC-lifetime*. After the parameter selection, the parameters were combined and integrated into the nowcasting models. This has done via the mathematical method "fuzzy logic".

The life cycle analyses and the development of the nowcasting models *LOC-lifetime* and *LOC-intensity* are based on the following hypotheses:

1. Model and observational data are able to represent the thunderstorm life cycle or to indicate the thunderstorm lifetime

2. The nowcasting of thunderstorms can be improved using such a life cycle description compared to extrapolation methods, as shown by a reduced false alarm ratio

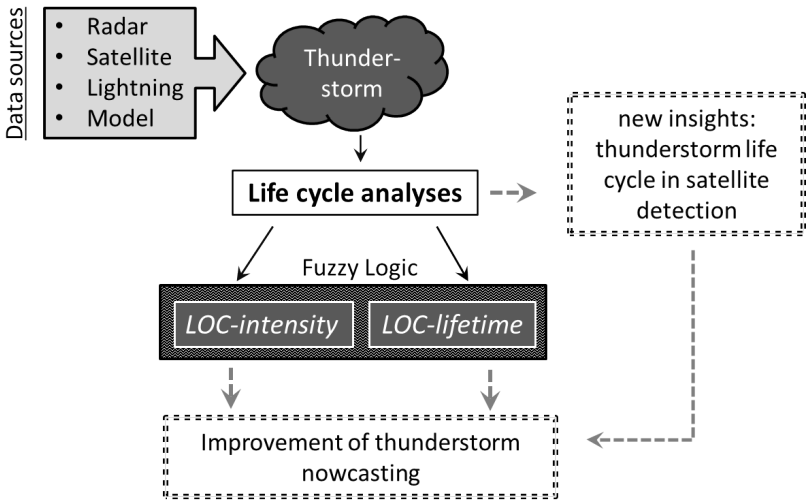

Figure 1.3: Concept of the thesis and primary aims (dashed lines), where a thunderstorm is defined by a satellite detection method.

The data sources satellite, radar, lightning, and model, are described in detail in Chapter 2.1, together with their corresponding parameters. Additionally parameter allocation of thunderstorms and the method fuzzy logic that is used for nowcasting is explained. At the end of this chapter, the methods used for validation of the nowcasting model, are presented, as well as the thunderstorm definition used for the life cycle analyses.

The approaches for the life cycle analyses and for the development of the nowcasting models *LOC-lifetime* and *LOC-intensity* are outlined in the following. The results of the life cycle analyses and the nowcasting model are presented in Chapter 3 and 4. The first part of this thesis, the analyses of the thunderstorm life cycle in multi-sourced data for June of 2016; May, June, and July of 2017; and June of 2018, is contained in Chapter 3. For these analyses the thunderstorms were sorted by their lifetime and nominated to one lifetime class. Therefore, the differences between life cycles of long- and short-lived thunderstorms, as well as, differences between the single life cycle stages can be characterized. The variability between thunderstorms is presented, additionally to a brief study about life cycle differences with regard to the synoptic situation and the thunderstorm intensity.

The nowcasting models *LOC-lifetime* and *LOC-intensity* and their results are the second part of this thesis and presented in Chapter 4. The nowcasting model *LOC-intensity* is a first approach for intensity prediction with fuzzy logic and is presented in a separate section at the end of the chapter. The *LOC-lifetime* model calculates the remaining lifetime and current life cycle stage. The *LOC-intensity* model predicts the future intensity and categorizes the thunderstorms into non-severe ($<$ 46 dBZ) and severe

($\geq$ 46 dBZ). In the previous life cycle analyses parameters with predictive skill were determined. After the parameter selection, the fuzzy logic-based nowcasting model *LOC-lifetime* is described and the results are presented. Afterwards, the *LOC-lifetime* model is verified. Additionally, the sensitivity of the nowcasting model *LOC-lifetime* is analyzed with respect to the input data sources, as well as to the shape of the membership function and its thresholds. At the end of this chapter, a first approach for intensity prediction, called *LOC-intensity*, is presented.

Afterwards, the results are discussed in Chapter 5. In Chapter 6 the results are compared to the hypotheses. The future work is outlined in Chapter 7.

Concluding, the following questions will be answered in this thesis:

(a) Can the thunderstorm life cycle be described by observational and model data, and what are the characteristics for each life cycle stage and lifetime?

(b) Does the information of the thunderstorm life cycle data improve the thunderstorm nowcasting?

A wide variety of related work, and a profound knowledge about thunderstorms already exists as shown in the literature review. Although, thunderstorms are studied well, this thesis contains some unique features. The most unique features of this thesis are summed up in the following:

- multi-sourced data set, observational (satellite, radar, lightning) and model data, available for almost 2000 thunderstorms
- wide variety of thunderstorm organizations included in life cycle analyses
- systematic parameter selection for nowcasting models
- methodical determination of membership thresholds
- remaining lifetime prediction on basis of a multi-sourced data set for every thunderstorm individually for every detection time step

The most noteworthy point of these is the multi-sourced data set. On basis of this, it is possible to compare parameters from satellite, radar, lightning, and model data by the same method of analyses. This systematical analyses enable the comparison of the results between a variety of data sources.

2 Data sources and methods

2.1 Data sources

In the last decades, the temporal and spatial resolution of observational and model data got more detailed. Therefore physical processes can be build up that could not be identified with observations before. Due to the development of high performance computers, weather models are able to resolve smaller physical processes as well. Core of this study is to analyze parameters from satellite data from METEOSAT-8, ground-based radar data from the German RX-radar network, lightning data provided by "nowcast GmbH" and Numerical Weather Prediction (NWP) model data from the Deutschen Wetterdienst (DWD, German Weather Service) with the aim to extract those parameters that show any predictive skill concerning the lifetime or intensity of thunderstorms. Due to the variety of the data sources it is possible to investigate the thunderstorm life cycle from micro-scale to macro-scale. Satellite, radar, and lightning data are available in 5 min frequency. The model data with lower temporal resolution is interpolated to 5 min resolution in order to enable a comparison with the observations. The high temporal and spatial resolution over Germany, and the operational availability of these data sources is the reason for choosing this data set. In the following, the analyzed parameters from the different data sources are described in detail. A summary of all available parameters is given in Table 2.1. The way the single parameters are calculated and assigned to a thunderstorm is described in Section 2.2.

2.1.1 Observational data

Satellite data

The visible (VIS) and infrared (IR) channels from the rapid scanning mode of METEOSAT "Spinning Enhanced Visible and Infra-Red Imager" (SEVIRI) are used to determine the parameters cloud optical thickness (τ) , effective radius (r_e), ice fraction at the cloud top ($phase$), and Brightness Temperature (BT) with the "Algorithm for the Physical Investigation of Clouds with SEVIRI" (APICS) developed at "Deutsches Zentrum für Luft- und Raumfahrt e.V." (DLR, German Aerospace Center) and described in Bugliaro et al. (2011). Values of 1 for $phase$ indicate cloud top in water phase

and values of 2 an ice phased cloud top. Values between 1 and 2 indicate a mixed phase. The data has a temporal resolution of 5 min and a spatial resolution of 3 km x 3 km at the sub-satellite point. The here mainly used satellite METEOSAT-8 is located 41.5 °E and 36,000 km above the Equator. The parameter BT follows from measurements in the IR 10.8 μm window channel and the black-body assumption. The parameters τ and r_e are calculated on basis of two channels, VIS 0.6 μm and NIR 1.6 μm, where NIR 1.6 μm accounts for water or ice absorption and is thus sensitive to particle size while both provide information on optical thickness. While the actual optical thickness of deep convection can easily reach values of several 100s or even 1000, the change of solar reflectivity with increasing optical thickness diminishes. Limited by measurement accuracy the retrieved values of τ are limited to a maximum of 100. Due to the fact, that thunderstorm cloud tops are not at ground level and the satellite observes from higher heights, it has to take care of the parallax correction before assigned to the thunderstorm. The parallax correction is further explained in the next Section (2.2).

Cb-TRAM

In this study, a thunderstorm is defined as an object identified by "CumulonimBus TRacking And Monitoring" (Cb-TRAM), an algorithm that detects, tracks, and nowcasts deep convective cells based on Meteosat Second Generation (MSG) rapid scanning data (Zinner et al., 2008, 2013). Three different development stages are distinguished by Cb-TRAM using two IR, one water vapor (WV), and the high-resolution visible (HRV) channels. Convective cells that belong to the Cb-TRAM warning level "early development" show strong vertical and/or horizontal growth indicated by rapid cooling in the IR 10.8 μm channel and a significant increase in the HRV reflectivity. The Cb-TRAM warning level "rapid development" is detected through a strong cooling in the WV 6.2 μm channel, and the level "mature-thunderstorm" is determined using a difference of WV 6.2 μm and IR 10.8 μm and a strong local texture in the HRV channel. Based on an image matching algorithm a displacement vector field is derived and used to track each thunderstorm in time. In addition, the displacement vector field is used here to perform a backward-extrapolation of all cell positions for 30 min before the first detection by Cb-TRAM and a forward-extrapolation of positions for 60 min after the last detection. Although detection in satellite data is expected to cover the earliest and last parts of developments better than any other observation data set (under clear air conditions), the coverage in time by the basic object definition is extended this way. This will allow a more complete analysis of observational signals of otherwise excluded parts of convective initiation and dissipation. This way an analysis of cloud and environmental parameters becomes possible shortly before the point in time that Cb-TRAM considers as a convection detection as well as the last decaying when no active convection cell is detected anymore. The Area inside A_{cb} where $\tau > 0.1$ ($A_{\tau>0.1}$) is considered for further analysis. The life cycle of a Cb-TRAM

detected thunderstorm starts as soon as $A_{\tau>0.1}$ is greater than 0 and ends when $A_{\tau>0.1}$ is equal to 0 again. Since the HRV channel is used to calculate τ only thunderstorms occurring in the daytime are considered in the life cycle analysis. Cb-TRAM uses for the analyzed period a constant cloud top height of 10 km for parallax correction. No distinction between different organization types is done, as indicated in Figure 2.1, most Cb-TRAM cells contain several updraft regions (indicating multicells). Therefore, the life cycle analyses of this study comprises single cells, multicells and supercells.

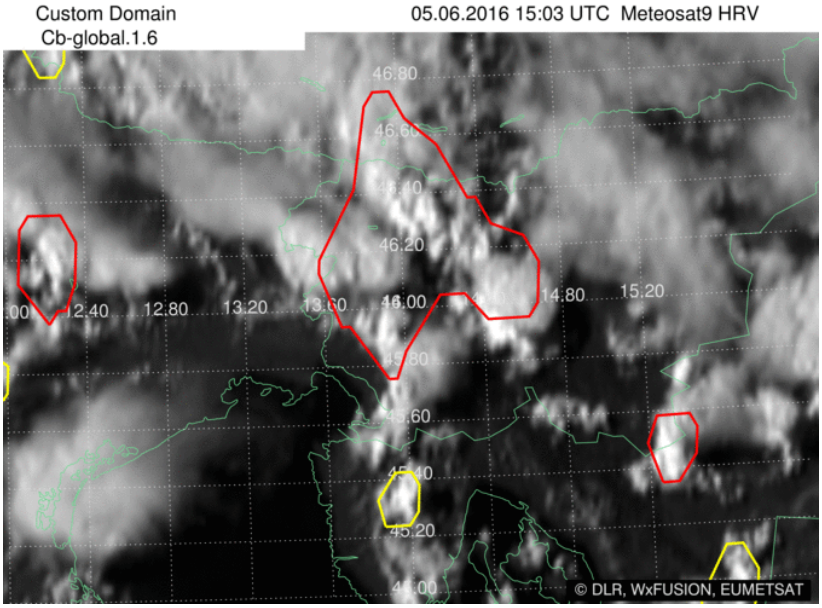

Figure 2.1: Example for Cb-TRAM detection based on satellite data in the East of the Alps on June 5, 2016 at 3 pm GMT. Red contours show cells assigned to warning level "mature-thunderstorm" and yellow cells indicate thunderstorms with warning level "early development".

Radar data

The DWD operates a network of weather radars (Helmert et al., 2014). Radar measurements allow area-wide precipitation detection, local and regional. 17 polarimetric Doppler C-Band radar systems are distributed over Germany (see Figure 2.3, dark grey shaded area over Germany). Each of it provides a new volume scan every 5 min with a horizontal radius of up to 180 km and a vertical extent from surface near layers to the upper troposphere (about 10 km height). These polarimetric measurements provide information of microphysical precipitation processes. The reflectivity represents the magnitude of the reflected radar pulse (Schumann, 2012), where the reflectivity factor z is the sum of the diameter to the power of six D^6 of all particles within the unit

volume V with the assumption, that water particles much smaller than the wavelength are measured

$$z = \frac{1}{V} \sum_{i=1}^{n} D_i^6$$

The reflectivity factor is expressed as a logarithmic ratio ralated to the reflectivity factor of a raindrop with a diameter of 1 mm (Schumann, 2012). This logarithmic reflectivity is given in dBZ (dezibel Z).

$$Z = 10\log\left(\frac{z}{1\mathrm{mm}^6\mathrm{m}^{-3}}\right)$$

The intensity of precipitation is categorized into 255 classes and provide information about microphysical precipitation processes.

The DWD 3D radar reflectivity products Vertically Integrated Ice (VII) and Vertically Integrated Liquid water (VIL) in kg m^{-2} are analyzed over the life cycle of thunderstorms. VIL is the sum of all radar reflectivities measured in vertical direction from the surface to the highest radar measurement. VII is calculated from the -10°C line up to the highest radar measurement. Therefore VII is part of the VIL column. The integration that is used for the calculation of VII and VIL is described in detail in Greene and Clark (1972).

Rad-TRAM

Beside the volume scan, the precipitation scan is used for the life cycle analyses as a measure of precipitation where the radar elevation angle is "terrain following" (elevation angle dependent on orography) and varies its azimuth angle as usual. An algorithm that uses the precipitation scan to detect, track, and nowcast precipitation cells is "Radar TRacking And Monitoring" (Rad-TRAM, Kober and Tafferner, 2009). In addition, the maximum reflectivity for each precipitation cell is determined by a mean over 30% of the highest reflectivities within the Rad-TRAM contour. Rad-TRAM output of the maximum reflectivity (R_{max}) and Area of the 46 dBZ contour (RA_{46}) are used in the life cycle analyses, if the Rad-TRAM cell overlaps with a Cb-TRAM cell. The RA_{46} is chosen to analyze the behavior of the area of very heavy precipitation.

Lightning data

Data of the European ground-based Lightning NETwork (LINET) from "nowcast GmbH" (Betz et al., 2009) with a statistical average accuracy of approximately 150 meters are used in this study. LINET operates over Europe and other parts of the world (see Figure 2.2). With the very low frequency and low frequency (VLF/LF) lightning detection technique it is possible to measure cloud-to-ground (CG) and intra cloud (IC)

lightning. In the life cycle analyses cloud-to-ground (CG) and intra cloud (IC) lightning will be considered. All lightning observations (CG and IC) inside a Cb-TRAM cell are summed up that occur 2.5 min before and 2.5 min after the Cb-TRAM detection. The resulting parameter is called Lightning detection (Li).

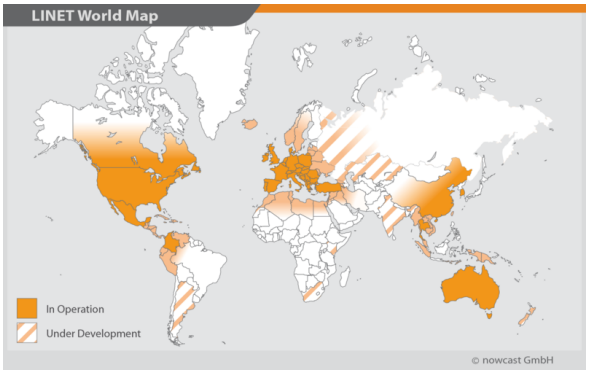

Figure 2.2: World wide distribution of LINET measurements (source: `https://www.nowcast.de/aktuell/network-expansion.html`).

2.1.2 Model data

The COnsortium for Small-scale MOdeling (COSMO) was formed in 1998. The model COSMO-DE has been operated since January 2007 at the DWD (Baldauf et al., 2006) and complements the global model "ICON". The COSMO-DE model has a spatial resolution of 2.8 km x 2.8 km (0.025° x 0.025°). It is separated in 50 model layers where the lowest is at 0 m and the highest at 22 km altitude above surface. The levels are constant over time. The coverage area comprises Germany, Austria and Switzerland with 421x461 data points (see Figure 2.3, squared area). In May 2018, COSMO-DE was replaced by COSMO-D2 with a higher spatial resolution (2.2 km x 2.2 km) and 65 layers which is used for a part of the period (June of 2018) analyzed in this study (see Chapter 2.2). The update cycle of both COSMO-DE and COSMO-D2 is 3 hours (00, 03, 06, 09, 12, 15, 18, and 21 UTC). Forecasts are output with an interval of 1 hour until 21 hours and then interpolated to a temporal resolution of 5 min. Always the latest available forecast relative to the observation of the thunderstorm is taken for the life cycle analyses. For example, the 2 h forecast of the 06 UTC run is used for a thunderstorm detected at 8 UTC. The model parameters Convective Available Potential Energy ($CAPE$), Relative Humidity at 700 hPa (RH), and vertical velocity at 700 hPa (ω) are analyzed over the life cycle of thunderstorms due to their predictive skill as shown in, for example, Huntrieser et al. (1997).

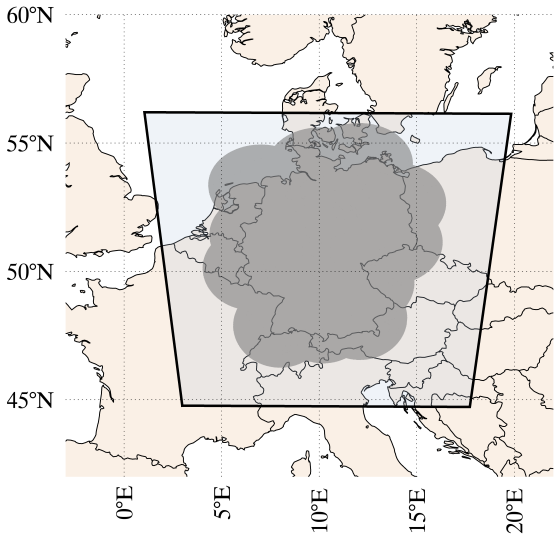

Figure 2.3: Map of Central Europe with coverage of COSMO-DE data (squared light grey shaded area) and the coverage of the German radar network (dark grey shaded area).

2.2 Data treatment

Table 2.1 summarizes all parameters relevant for this study. The availability of every parameter for every analyzed cell is crucial for the significance of the life cycle analyses. Consequently, the analyzed area is limited to the data source covering the smallest area and additionally overlapping with the other data sources, in this case the radar data. Therefore, every cell is considered in the life cycle analyses, that occurs inside the radar net covering Germany (see Figure 2.3, dark grey shaded area) and fulfills the criterion of a "mature-thunderstorm" detection with Cb-TRAM minimum for one time step during its life cycle. Overall, almost 2000 thunderstorms are considered in the life cycle analyses.

Since thunderstorms over Germany are analyzed and METEOSAT-8 is located 41,5 °E and 36,000 m over the equator, a parallax correction has to be done. The satellite's large viewing angle from nadir leads to a local shift of clouds relative to the surface. This displacement is called parallax. For this thesis, parameters from different data sources are used to describe and nowcast thunderstorms. All data sources are available with latitude-longitude grid or location information, each with or without parallax correction. Consequently, the parameter allocation has to be done with regard to a possible parallax displacement.

Table 2.1: All available parameters that are used to describe the life cycle of thunderstorms.

Data source	Parameter	Abbrev.	unit
Satellite	Brightness Temperature	BT	K
	cloud optical thickness	τ	-
	effective radius	r_e	μm
	ice fraction at the cloud top	$phase$	-
	Area inside A_{cb} where $\tau > 0.1$	$A_{\tau>0.1}$	km^2
Cb-TRAM	Area of the Cb-TRAM cell	A_{cb}	km^2
	propagation velocity	c	m s^{-1}
Radar	Vertically Integrated Ice	VII	kg m^{-3}
	Vertically Integrated Liquid water	VIL	kg m^{-3}
Rad-TRAM	Area of the 46 dBZ contour	RA_{46}	km^2
	maximum Reflectivity	R_{max}	dBZ
LINET	Lightning detection	Li	# 5min^{-1}
COSMO-DE	Convective Available Potential Energy	$CAPE$	J kg^{-1}
	Relative Humidity at 700 hPa	RH	%
	vertical velocity at 700 hPa	ω	Pa s^{-1}

For each thunderstorm, one single value of every of the previously described parameters is calculated for every single lifetime step: The parameter BT as well as τ, r_e, and $phase$ are determined by their average over 10% of the pixels with the lowest BT values inside Area of the Cb-TRAM cell (A_{cb}), respectively. The radar parameters VII and VIL are the mean over 10% of their respective highest values within A_{cb}. The parameter R_{max} represents 30% of the highest reflectivity values inside a Rad-TRAM contour with a threshold of 19 dBZ and an overlap with A_{cb}. All lightning detection inside A_{cb} that occur 2.5 min before and 2.5 min after the detection with Cb-TRAM are summed up to calculate the parameter Li. Finally, in order to account for uncertainties of the model regarding the location of thunderstorms the Cb-TRAM cells are enlarged with a radius of 50 km. For these enlarged Cb-TRAM cells $CAPE$ and ω are determined by their average over 10% of the pixels with the highest $CAPE$ and the lowest ω values, respectively. The parameter RH is an average of the RH values over all pixels within A_{cb}.

Thunderstorms that occur in June 2016, May, June, and July 2017, and June 2018 within the dark grey shaded area (see Figure 2.3) are studied. This period is taken due to reasons of availability. Almost 2000 cells with lifetimes between 5 (one time step) and 300 (60 time steps) min have been detected in these five months and are sorted in lifetime classes with 5 min bins (Figure 2.4). Short-lived cells (< 90 min) occur relatively seldom (20 thunderstorms per lifetime class). More than the half of all detected thunderstorms have a lifetime class between 90 min and 175 min.

Thunderstorms that exist longer than 300 min occurred very rarely and will not be considered in the life cycle analyzes.

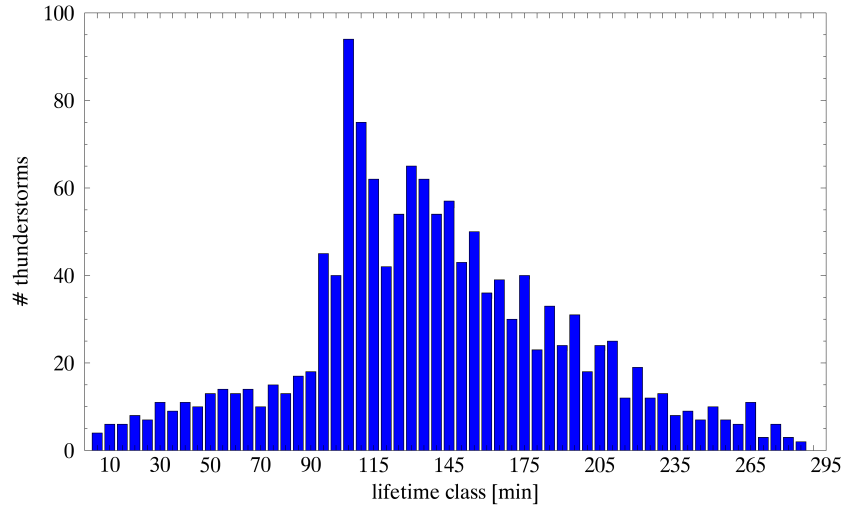

Figure 2.4: Thunderstorms that occurred over Germany in June 2016, May, June, July 2017 and June 2018 sorted by their lifetimes into lifetime classes in [min]. The sum of all thunderstorms with the same lifetime class is depicted for each lifetime class.

This frequency distribution differs from the usual picture of thunderstorm occurrence (maximum for lifetimes less than 60 min) as presented, for example, in Wilson et al. (1998). The strong increase of the number of thunderstorms with lifetime classes greater than 90 min occurred, due to the lifetime class separation and the $A_{\tau>0.1}$ criterion. As described in Section 2.1 the lifetime of the Cb-TRAM cell is extended of up to 90 min as soon as $A_{\tau>0.1}$ is greater than 0 within A_{cb} and ends when $A_{\tau>0.1}$ is equal to 0 again. Thus, the satellite parameter τ can be determined in the daytime only, a sudden end of the thunderstorms life cycle due to sunset or another source of missing data is possible when using this criterion. Most of the cases a thunderstorm, detected by Cb-TRAM shows already 30 minutes before and 60 min after its detection cloudy pixels, as a result the number of thunderstorms with lifetimes greater than 90 min is large compared to the number of thunderstorms with lifetimes less than 90 minutes. In the following, the thunderstorm lifetimes are normalized to a lifetime progress 0-100%, in order to be able to compare the specific characteristics of each life cycle stage independent of the individual lifetime of the storms. Thus, short- and long-lived thunderstorms are rare, the thunderstorms with a lifetime of 5-45 min, 50-90 min, 210-255 min, and 260-300 min are combined and each treated as one lifetime class. For thunderstorms with a lifetime class between 90 and 210 min every thunderstorm class is treated as its own lifetime class in the life cycle analyses.

The previously described data sources are used for the life cycle analyses in Chapter 3. The life cycle analyses are the first part of this thesis. Based on the results of the life cycle analyses a nowcasting of the remaining lifetime (*LOC-lifetime*) and future intensity (*LOC-intensity*) is done in Chapter 4. The nowcasting models are based on the method *fuzzy logic*. This method is chosen for the nowcasting in this thesis since it has been commonly applied in meteorological settings and is a suitable way to combine parameters of several data sources. The basic concept of fuzzy logic is described in the following. Afterwards the verification method of the nowcasting models is explained in Chapter 2.4.

2.3 Fuzzy logic

The method *fuzzy logic* was introduced by Zadeh (1965). The basic principle of fuzzy logic are blurred boundaries, so not a sharp allocation to one category for example 0 or 1 takes place, but values between 0 and 1. Several categories can be defined, not only two but an arbitrary number so called subsets, for instance: hot, warm, moderate, cool, and cold. The transition between the subsets occurs subsequently via the likelihood (values between 0 and 1) of the subsets. In general, the mathematical method fuzzy logic is a classification that is more similar to the way of human thinking than for example the Boolean notation. The fuzzy logic scheme has no sharp boundaries and can therefore be used to describe processes in nature. It is explicitly used in weather forecasting. For example, Hansen (1997) created a fuzzy logic-based model to improve the marine forecasting. Additionally, Hansen (2007) developed a fuzzy logic-based model to forecast the cloud top temperature and the vertical temperature profile. Another fuzzy logic-based model was introduced by Hertl and Schaffar (1998) to forecast temperature and icing on streets. Stich (2013) used fuzzy logic to combine parameters from lightning, satellite, and model data to improve the detection and nowcasting of convective initiation.

One example for the allocation to the different classes is presented in Figure 2.5, there the fuzzy sets (classes) are *growth* (red line) and *decay* of a thunderstorm (blue line). If BT is about 220 K the thunderstorm is categorized as *decay* with a value of 0.7 and as *growth* with a value of 0.3. This allocation step is named fuzzification. The function of each subset that describes the fuzzy set (class) is called membership function. One benefit of the mathematical method fuzzy logic is the possibility to combine different parameters and categorize them individually. The lower part of Figure 2.5 depicts the trend of the thunderstorm area. A decrease is allocated to the subset *decay* and an increase to the subset *growth*. The area trend value is about -25 %/5min, a value of 0.75 is determined for the class *decay* by the membership function and a fuzzy logic value of 0.25 is allocated to the class *growth*.

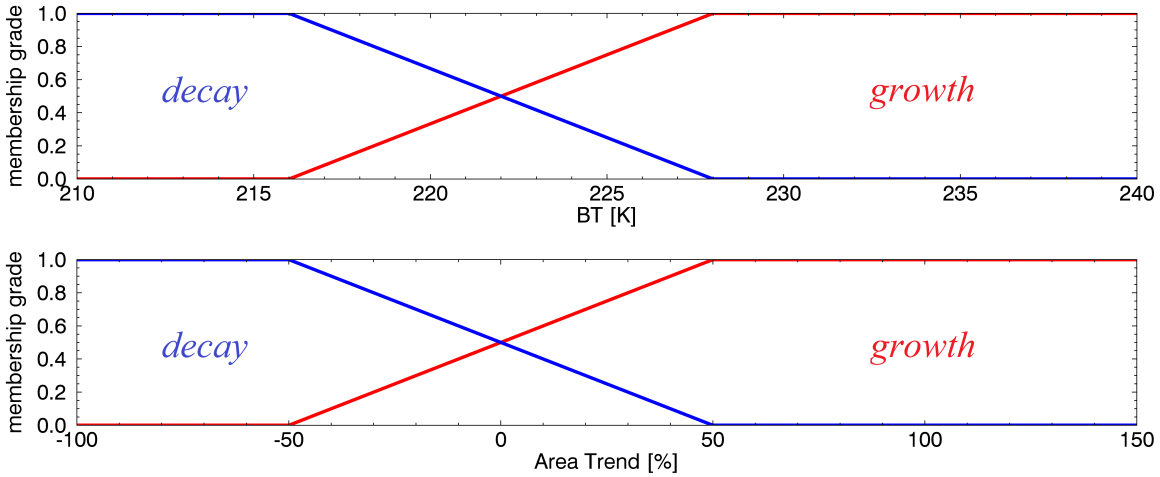

Figure 2.5: Membership function of the fuzzy sets *decay* (blue) and *growth* (red) for the parameters BT (upper figure) and the temporal change of 5 min in percent of A_{cb}.

In Figure 2.6, an outline of the principle procedure of the method fuzzy logic is shown. In the previously mentioned example the actual value of BT and the temporal change in percent of A_{cb} represent the input data as depicted in Figure 2.6. The membership functions shown in Figure 2.5 represent the fuzzifiers in order to calculate the fuzzified input from the input parameters. Expert knowledge is necessary to define the input parameters and to set the thresholds of the membership functions reasonably. In this thesis, the thresholds of the membership functions are derived by statistical analyses. The combination of the fuzzified input data is done via a set of rules, composed of "if ... then ..." conditions. This way the fuzzified input can be combined to one fuzzified output. Again, expert knowledge is required to set up reasonable rules. To make this fuzzified output "readable" a defuzzifier is necessary. There are several methods for defuzzification. One example of such defuzzification, commonly used for fuzzy sets considered as a probability distribution is the "center of gravity" (Leekwijck and Kerre, 1999). This method calculates the center of gravity for the area under the membership function. Another method is called "maximum-method". For this method, only the class with the maximum value is valid and therefore selected as output. After the defuzzification the "readable" output is determined.

In this thesis, fuzzy logic is used for combining all selected parameters from the different data sources with respect to their ability to describe the actual stage and to nowcast the remaining lifetime and intensity of a thunderstorm. For this purpose the thunderstorm life cycle stages are separated into the fuzzy sets *growth* and *decay*, and *non-severe* and *severe*. The parameters from satellite, radar, lightning, and model data are used as input (parameters selection is described in Chapter 4). Although, the actual stage is categorized into growth, mature and decay, the fuzzy sets exist only for *growth*

and *decay*. Consequently, the mature stage is represented by the overlapping area of *growth* and *decay*. For the purpose of defuzzifying, the maximum-method is used for the nowcasting of the intensity. A new defuzzification method is implemented for the calculation of the current stage and the remaining lifetime prediction, also explained in detail in Chapter 4.

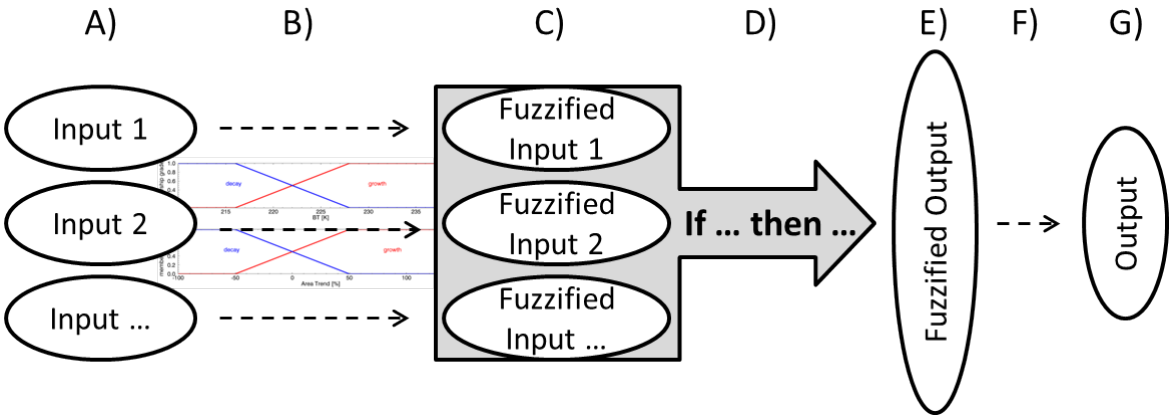

Figure 2.6: Scheme of the fuzzy logic setup. A) input, B) fuzzifier (membership functions), C) fuzzified input, D) set of rules, E) fuzzified output, F) defuzzifier, and G) output.

2.4 Verification

In order to evaluate whether or not the developed nowcasting models *LOC-lifetime* and *LOC-intensity* improve the forecast quality, they have to be verified and compared to an already existing extrapolation method. There is a broad variety of verification methods for forecasting models available. Verification scores based on the contingency table (see Figure 2.7) are calculated, since an "improvement" of the nowcasting is here defined on the one hand as a reduction of false alarms as well as an inrease of right detected events, and the prediction compared to a random prediction. On the other hand the differences between the predicted and the real lifetime is of interest and therefore the standard deviation and root-mean-square-error (RMSE) are calculated. This contingency table contains four combinations to combine the forecast "yes" and "no" with the observed "yes" or "no" to verify the type of forecast. These four combinations are called joint distribution and are in detail:

- *hit* - event forecast and occurred
- *miss* - event not forecast and occurred
- *false alarm* - event forecast and not occurred

- *correct negative* - event not forecast and not occurred

Two of the most common verification method is the calculation of the probability of detection (POD) and the false alarm ratio (FAR). POD and FAR contain relevant information for validation concerning hits, misses, and false alarms. Therefore, they are used beside others to verify the life cycle models and compare them to other models.

		Observed	
Forecast		YES	NO
	YES	*Hit*	*False alarm*
	NO	*Misses*	*Correct negative*

Figure 2.7: Contingency Table

The POD or *hit rate* is a measure of the ratio of the observed "yes" events that were correctly forecast and those events that actually occurred.

$$\text{POD} = \frac{hits}{hits + misses}$$

To calculate this statistical value the sum of *hits* (all correctly forecast events) is divided by the sum of *hits* and those events that occurred but were not forecast (*misses*). POD can obtain values between 0 (worst forecast) and 1 (perfect forecast). For instance, if every event (for e.g. tornadoes) that occurs was forecast than POD has its perfect score 1.

One disadvantage of this score is that the *false alarms* are not considered. Therefore, it is possible that a forecasting has a POD of 1 if it always predicts an event (tornado), but only in 1 of 100 cases a tornado is observed indeed. Consequently the statistical value FAR is considered in combination with POD.

$$\text{FAR} = \frac{false\ alarms}{hits + false\ alarms}$$

The FAR is a measure of the ratio of events that were forecast but not observed (*false alarms*) and all events that were forecast. The sum of *false alarms* is divided by the sum of *hits* and *false positive events (false alarms)*. Hence, the number of *false alarms* is divided by the number of all "yes" predicted events. Consequently, the perfect score of FAR is 0 and the worst 1.

As the POD contains only the information of *hit* and *miss*, and the FAR contains only the information of *false alarms* and *hits*, additional statistical values have to be calculated for the model verification.

The fraction of the forecast events that is correct is evaluated by the accuracy.

$$\text{Accuracy} = \frac{hits + correct\ negative}{total}$$

All events that are correct forecast and those that are correct not forecast are summed up and divided by the total forecast. Therefore, the *correct negatives* are considered as well. Consequently, the perfect score is 1 and no skill is indicated by 0.

Additionally, the frequency bias (BIAS) is calculated to identify whether the nowcasting system has a tendency to over or under forecast events. The BIAS is calculated as follows:

$$\text{BIAS} = \frac{hits + false\ alarms}{hits + misses}$$

The BIAS score has a range between 0 and infinity, whereas the perfect score is 1. It only measures the relative frequency of forecasts and does not consider right forecasts indeed. Consequently, it is possible to obtain a BIAS score of 1 if no *hit* occurred. Therefore, BIAS only is representative in combination with other statistical parameters.

The critical success index (CSI) is calculated to identify how well the forecast "yes" events correspond to the observed "yes" events. The CSI takes *hits*, *misses*, and *false alarms* into account:

$$\text{CSI} = \frac{hits}{hits + misses + false\ alarms}$$

The CSI has a range between 0 and 1 where 0 indicates no skill and 1 is the perfect score. Comparing to POD and FAR, the *false alarms* as well as the *misses* are considered here. It is a measure of the fraction of observed and forecast events that are correctly predicted. But it depends on the climatology of the event, rare events show poorer scores. The *hit* due to random chance is not considered here. Indeed no one of the recently presented statistical scores takes the statistical hit rate into account. Thus, it is crucial for evaluating the gain of a nowcasting model compared to forecast based on a random chance, two further statistical parameters are calculated.

First the Gilbert Skill Score (GSS) is calculated to indicate the fraction of observed events that are correctly predicted and adjusted for *hits* associated with random chance. The formula shows that the GSS is similar to the formula of CSI but deduced by a hit chance due to a random chance:

$$\text{GSS} = \frac{hits - hits_{random}}{hits + misses + false\ alarms + hits_{random}}$$

where the parameter $hits_{random}$ that takes the probability of hits due to a random chance into account is defined by:

$$hits_{random} = \frac{(hits + misses)(hits + false\ alarms)}{total}$$

where *total* is the number of all events. The GSS has a range between $-1/3$ and 1, where 0 indicates no skill and 1 is the perfect score. As seen in the calculation of GSS the *correct negative* values are not considered here.

The second score that takes the forecast of a random chance into account is called Heidke Skill Score (HSS). It calculates the Accuracy of the forecast relative to that of a random chance:

$$\mathrm{HSS} = \frac{(hits + correct\ negative) - (expected\ correct)_{random}}{N - (expected\ correct)_{random}}$$

where the parameter that describes the correct forecasts due to a random chance $(expected\ correct)_{random}$ is defined by:

$$(expected\ correct)_{random} = \frac{1}{N}\Big[(hits + misses)\,(hits + false\ alarms) + (correct\ negative + misses)\,(correct\ negative + false\ alarms)\Big]$$

where N is the number of thunderstorms. The formula shows that the HSS is the Accuracy deduced by the *hit rate* due to a random chance.

For validation of the remaining lifetime forecast, the *standard deviation* of the thunderstorms that are used as basis data set is calculated as well. It is calculated for the purpose of indicating how variable the fuzzy logic values of thunderstorms with the same total lifetime at one detection time step are. The standard deviation takes 68% of all thunderstorms into account. The standard deviation s is calculated as the following:

$$s = \sqrt{(\frac{1}{N}\sum_{i=1}^{N}(x_i - \bar{x})^2)}$$

Where $\bar{x}$ is the mean value of the fuzzy logic values and x_i the fuzzy logic value of the current thunderstorm. N is the number of thunderstorms with the same lifetime considered. The *standard deviation* is used to calculate a tolerance interval in minutes that indicates the time range that is needed to predict the remaining lifetime right, for example, 68% of all thunderstorms in case of a tolerance interval based on s. Especially of interest is the change of the probability of a correct forecasting inside a variable interval where a multiple of s is added. This is an indicator for accuracy of the forecast of remaining lifetime.

Additionally to the *standard deviation* the root-mean-squared-error (RMSE) is calculated for forecasting the remaining lifetime. The RMSE is similar to s a measure of the forecast quality where POD, FAR, BIAS, CSI, Accuracy, GSS, and HSS are a measure of the forecast quantity. The RMSE is calculated as the following:

$$\mathrm{RMSE} = \sqrt{\frac{\sum_{\mathrm{i=1}}^{\mathrm{n}}(P_i - O_i)^2}{N}}$$

Where P_i is the predicted remaining lifetime and O_i the observed remaining lifetime.

In Chapter 4, *LOC-lifetime* and *LOC-intensity* will be evaluated with the statistical values POD, FAR, BIAS, CSI, Accuracy, GSS, HSS, RMSE and the *standard deviation*. In detail, there will be the forecast of intensity categorized into two classes: *non-severe* and *severe*, additionally to the forecast of remaining lifetime, also categorized into two categories: *short-* and *long-lived*. In case of these predictions, every mentioned statistical value is calculated for validation. However, the remaining lifetime forecasting is also done with a separation into 27 categories (from 5 to 135 min in 5 min interval). Since some of the statistical values contain *correct negatives*, and *correct negatives* is in this case every prediction that is no *false alarm* or no *hit*, the number of *correct negatives* is enormous. Consequently, the significance of these statistical values is low. Therefore, only statistical values that do not contain *correct negatives* are considered for the validation of the remaining lifetime prediction in form of a 5 min interval, these are POD, FAR, CSI, RMSE and *s*.

The statistical values are calculated for five different model runs. With respect to evaluating the life cycle model, four month are used to form the basis of the fuzzy logic model and the fifth month presents the independent data set taken for nowcasting. The basis of the model is defined by determination of the thresholds for the membership functions and calculating the defuzzification basis table (see Chapter 4). This procedure will be repeated with every possible combination of month. Consequently, each of the five month is used as independent validation month. This validation method is also called *cross validation*.

2.5 Definition of the thunderstorm life cycle in the analyzed data

As explained in Chapter 2.1.1, a thunderstorm is defined by a Cb-TRAM cell including its backward-extrapolation up to 30 min before the first detection, and its forward-extrapolation up to 60 min after the last detection while $A_{\tau>0.1}$ is greater than 0. Since the aim of the thesis is to nowcast the lifetime and intensity of a thunderstorm defined by Cb-TRAM detection and Cb-TRAM is not able to identify the different types of thunderstorm organization or individual cells inside thunderstorm lines, it is necessary to consider the life cycle of all organization types together. Consequently, the definition of a single cell as done by Mecikalski et al. (2012), for example, can not be used in these analyses, especially multicells contain several life cycle stages simultaneously and differ from single cells among others. To define the life cycle for various organization types and lifetimes, the duration of the life cycle stages normalized to the thunderstorms total lifetime, is defined by the trend of BT and A_{cb} averaged over all lifetime classes (see Figure 2.8). These two parameters are selected due to their predominant signals

during the life cycle. A stage transition is defined by strong characteristics in this averaged life cycle.

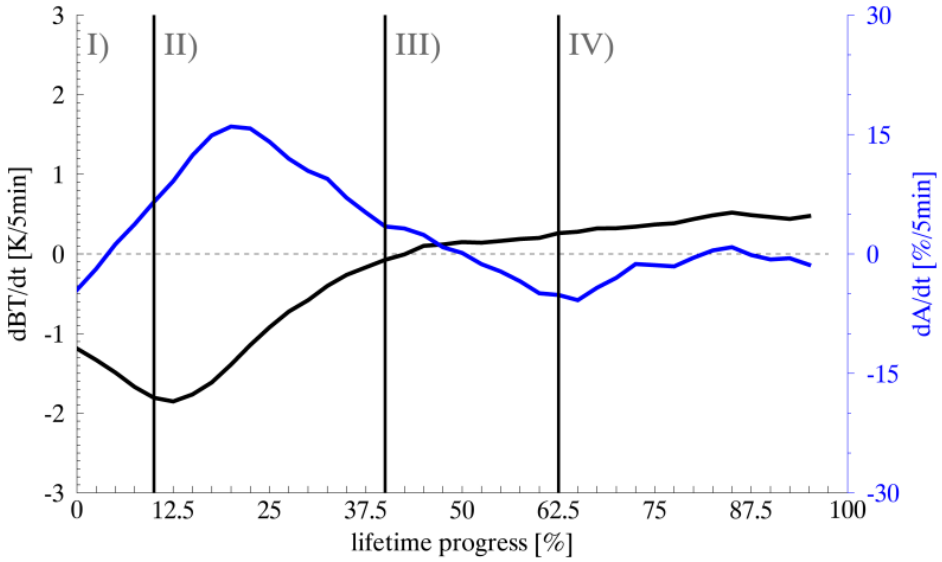

Figure 2.8: Method for life cycle stage separation
Mean temporal changes of Brightness Temperature (BT) (black line) in Kelvin per 5 min period and of Area inside A_{cb} where $\tau > 0.1$ ($A_{\tau>0.1}$) (blue line) in percent over 5 min of all thunderstorms normalized to their lifetime in June of 2016; May, June, July of 2017; and June of 2018 and separated into the life cycle stages *early growth* (I), *advanced growth* (II), *mature* (III), and *decay* (IV).

The *early growth* (stage I) is defined from 30 min before the first Cb-TRAM detection up one time step before the cooling trend of BT reaches its maximum indicating a rapid vertical cloud growth and beginning of cloud formation. The *advanced growth* (stage II) begins and lasts one time step until the cooling stops. This stage shows rapid vertical cloud growth until the maximum height is reached, for example, at the tropopause. The *mature* (stage III) is defined as the time when the maximum A_{cb} decrease is reached. This strong decrease marks the beginning of the last stage, the *decay* (stage IV).

The life cycle definition just presented is used for the life cycle analyses in the next chapter (Chapter 3) to compare the trends of several parameters in single life cycle phases. The fuzzy logic-based nowcasting model *LOC-lifetime* (Chapter 4) only differentiates between a growing or decaying thunderstorm. Whereas a growing thunderstorm is comparable to a thunderstorm in stage I (early growth) and a decaying thunderstorm is equal to stage IV (decay). Stage III (mature) is comparable in the nowcasting with the overlap between an early growing and a decaying thunderstorm and therefore more or less equal to the recently presented stages II (advanced growth) and III (mature)(see

Chapter 2.3 and 4.1.2). The phase separation ("warning levels") as done in Cb-TRAM (see Chapter 2.1) only is used for the thunderstorm object definition and, therefore, not further used in the life cycle analyses or nowcasting.

In these analyses, the life cycle of all thunderstorms that occurred over Germany in the analyzed period are considered. It is important to take all thunderstorm organizations into account for the life cycle analyses, since the analyses are the basis for the following nowcasting models. An analysis of single thunderstorm cells would be probably disadvantageous for the development of the nowcasting models as the models are supposed to predict the future intensity and lifetime of a wide variety of thunderstorm organizations.

3 Analyses of the thunderstorm life cycle

3.1 Thunderstorm life cycle characteristics in the analyzed data

The aim of this section is to gain detailed information about the characteristics of each life cycle stage and differences between the life cycles of long- and short-lived cells. Therefore, all cells are sorted by their lifetimes for every selected parameter. Each life cycle stage is described separately using the selected observational parameters Brightness Temperature (BT), Area inside A_{cb} where $\tau > 0.1$ ($A_{\tau>0.1}$), cloud optical thickness (τ), effective radius (r_e), ice fraction at the cloud top ($phase$), propagation velocity (c), maximum reflectivity (R_{max}), Vertically Integrated Liquid water (VIL), Lightning detection (Li) and the model parameters Convective Available Potential Energy ($CAPE$), Relative Humidity at 700 hPa (RH), and vertical velocity at 700 hPa (ω) (summarized in Table 2.1). Additionally, the variability of each parameter is visualized by the 25th and 75th percentiles (Chapter 3.2).

Since one aim is to predict the future intensity of thunderstorms in Chapter 4.3, life cycles of *severe* and *non-severe* thunderstorms (depending on their maximum reflectivity) are analyzed in Chapter 3.3. Additionally, an analysis of the differences between the thunderstorms life cycle in *frontal* and *non-frontal* environments is done.

3.1.1 Life cycle characteristics in observational data

The model parameters as well as the observational parameter c do not show any changes between the life cycle stages. They are categorized environmental parameters and analyzed in detail in the next section (Section 3.1.2). Every single life cycle stage is described in the following for the other parameters (observational parameters only).

The life cycle of thunderstorms in observational data sources is presented in the Figures 3.1 and 3.2. The average life cycle of the thunderstorms of one lifetime class is depicted (colored lines) there. Since there is only a small number of thunderstorms with very

short and long lifetimes, thunderstorm with those lifetimes are combined to the lifetime classes 5-45 min, 50-90 min, 200-255 min and 260-300 min. The life cycle is separated into the stages: *early growth* (I), *advanced growth* (II), *mature* (III), and *decay* (IV) as defined in Chapter 2.5.

Early growth

In the analyzed data, the early growth (stage I) is on average over all cells represented by a steady decrease of satellite observed BT (Figure 3.1, dashed black line). At the beginning, it has a mean value of 240 K and decreases with about -1 K/5min. The cloud area $A_{\tau>0.1}$ shows low values (< 500 km^2) without any temporal changes during this stage. Optical thickness τ and cloud particle size r_e are both increasing during this stage. The cloud top *phase* begins at mean values of 1.8 as a mixed value between liquid (=1) and ice (=2) and increases further towards almost complete glaciation (Figure 3.2). The radar parameters R_{max} and VIL show an increase as well. In stage I, hardly any lightning is observed. The general picture provided is a cloud cell which mainly grows vertically with increasing droplet sizes and starting glaciation. Horizontal growth is not detected yet.

Differences between lifetime classes are very systematic. It is most striking that short-lived thunderstorms start at colder temperatures BT, higher optical thickness τ, larger particle size r_e, and larger area $A_{\tau>0.1}$ than long-lived ones. In addition, cloud tops of the shortest-lived cells are already completely glaciated while longest-lived are observed as mixed phase. Probably the short-lived cloud cell classes are dominated by cells which develop from existing larger scale systems, "out-of-sight" under existing high cloud cover and already at their dissipation stage when detected for the first time. Consequently, most of the here presented short-lived thunderstorms actually have longer lifetimes but are briefly detected. The inspection of radar based parameter R_{max} shows that most lifetime classes show high maximum precipitation reflectivity values already early in the observed life cycle, as well.

Advanced growth

In the observation data, the advanced growth (stage II) is dominated by a quickly rising cloud top, with cloud tops cooling at almost -2 K/5min in BT, the start of horizontal growth of the cell ($A_{\tau>0.1}$) and an increase of τ (Figure 3.1 and 3.2). Most interestingly values of r_e display a clear decrease of particle size starting just from the beginning of this stage, while the *phase* shows progressing glaciation. The R_{max}, as a proxy of surface precipitation, slowly approaches a maximum mean value of about 44 dBZ. Additionally, the vertical cloud water integral VIL reaches its maximum (8 kg m^{-2}) and subsequently decreases afterwards. First lightning occurs and intensifies. The

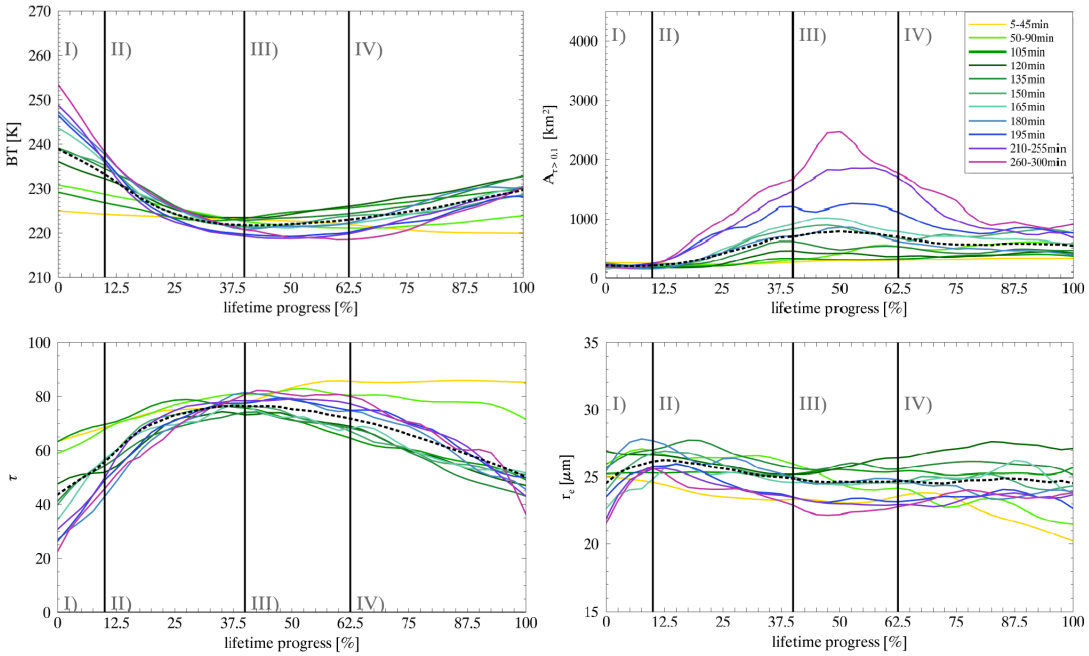

Figure 3.1: All lifetime classes are normalized to one lifetime progress [%]. The parameters Brightness Temperature (BT), Area inside A_{cb} where $\tau > 0.1$ ($A_{\tau>0.1}$), cloud optical thickness (τ) and effective radius (r_e) are depicted. The mean values over the life cycle are smoothed over the nearest time steps. Each lifetime class is depicted in another color (colored lines). The averaged life cycle of all lifetime classes is depicted in the dashed black line. Life cycle stages are stage I (*early growth*), stage II (*advanced growth*), stage III (*mature*), and stage IV (*decay*) and separated by vertical black lines

general picture provided is a cloud cell for the most part in ice phase, which reached its maximum VIL and r_e, and spreads out horizontally.

These observations are consistent with literature: Machado et al. (1997) and Feng et al. (2012) also show a decreasing BT in the growth for Mesoscale Convective Systems over America (tropical and mid latitude), and an increase in τ. Davini et al. (2012) mention a maximum of reflectivity in the first half (growth phase) of a thunderstorm life cycle. Wapler (2017) also described the increase in lightning activity during the growth of hailstorms.

The parameters BT, $A_{\tau>0.1}$ and Li of longer-lived cells start to show clear signs to have a stronger updraft, to reach higher cloud top altitudes, to cover a larger area and to show more lightning activity compared to shorter-lived ones. Differences for τ disappear during this stage as all values approach the maximum sensitivity of optical thickness observations. Over the full stage, longer-lived cells show smaller r_e than

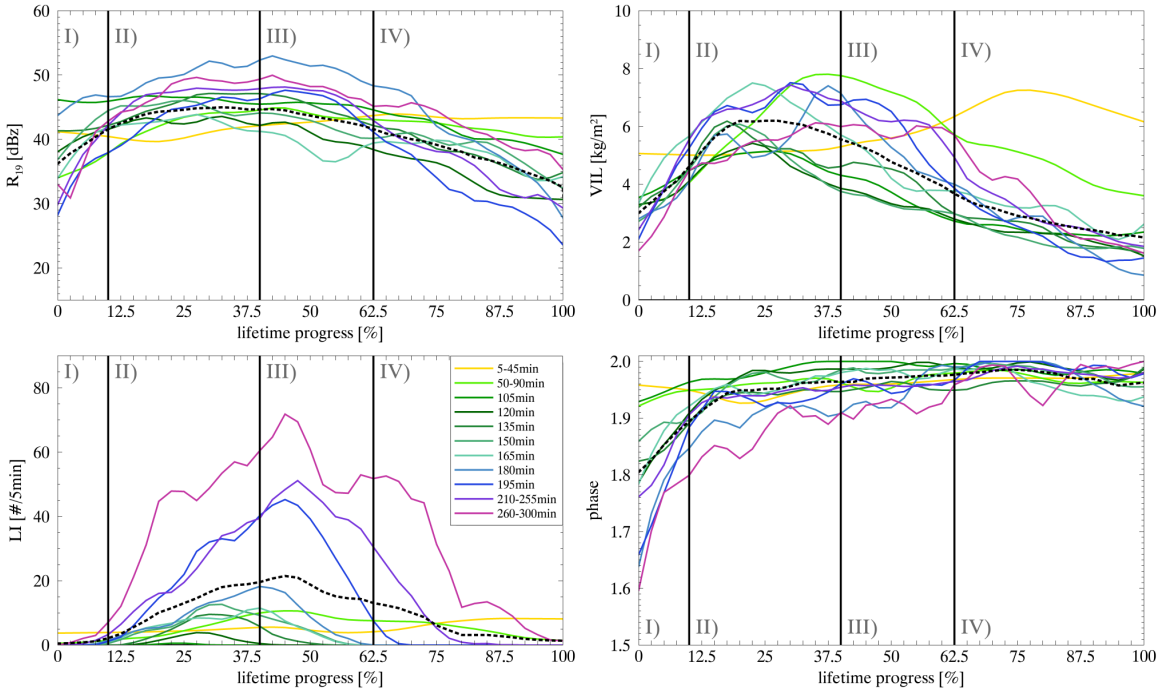

Figure 3.2: As in Figure 3.1. The parameters maximum reflectivity (R_{max}), Vertically Integrated Liquid water (VIL), Lightning detection (Li) and ice fraction at the cloud top ($phase$) are depicted.

shorter-lived. There are weak signs of precipitation strength (comparable to values of R_{max}) being larger for long-lived cells and VIL being higher.

Mature

In general, BT is a measure of the altitude of the cloud top, for instance, on average very high cloud tops are related to the lowest values of BT along the life cycle due to the atmospheric temperature gradient in the tropopause. Once the tropopause is reached, vertical development (further cooling) stops as the Level of Equilibrium is reached due to the stable stratification in the stratosphere (see Chapter 1.2). This stop of vertical growth can occur also at lower altitudes than the tropopause if the atmospheric conditions support this. For this reason, the minimum of BT during the mature (stage III) indicates that this stage is characterized by the highest cloud tops of the life cycle. The parameters $A_{\tau>0.1}$ and τ reach or stay at their maximum. The slight decrease of r_e continues, as the increase of $phase$ shows an ongoing glaciation. VIL values start to decrease as the largest part of the cloud water mass reached altitudes above freezing level in this stage. Precipitation starts to decrease (see R_{max} values). Li reaches its maximum at the beginning of stage III and starts to decrease afterwards.

The general picture provided is an intense cloud cell with its maximum altitude and lightning occurrence.

Long-lived thunderstorms reach lower minimum of BT, higher maximum of $A_{\tau>0.1}$, smaller r_e and higher Li values than short-lived thunderstorms. The longer-lived still tend to show more precipitation.

Decay

The decay of a thunderstorm (stage IV) is characterized by a slow increase of 0.5 K/5min in BT. The satellite parameters $A_{\tau>0.1}$, τ and r_e decrease. As $A_{\tau>0.1}$ is defined with a certain optical thickness threshold, thinnest still growing parts of anvil clouds might be missed in this parameter. The parameter *phase* almost reaches a value of 2: Almost all clouds within the considered cloud area are ice clouds. Precipitation as represented by the radar parameter R_{max} weakens and VIL decreases further. Last lightning activity comes to an end. The general picture provided is an almost completely in its ice phase existing cloud cell, that dissolves.

With respect to lifetime hardly any differences can be detected in this stage. Only remaining $A_{\tau>0.1}$ and Li show detectable systematic differences.

3.1.2 Life cycle characteristics in environmental data

The environmental parameters can not be treated as individual characteristics of observed thunderstorms but can possibly serve to characterize the large scale convective environment. Therefore, $CAPE$, RH at 700 hPa and ω at 700 hPa from the NWP model are interpreted for observed thunderstorms. Although these of course interact with convective cloud physics in the model, they are not related to reality in full detail in time and space. Instead, large scale convective processes in the NWP model atmosphere large enough to be resolved have detrimental local impact on the diagnostic potential these parameters. E.g. $CAPE$ would be reduced by resolved convection, leading to the misinterpretation of a low convection risk nearby. In a similar way the parameter c does not describe the physics of individual thunderstorms but is footprint of the environmental situation.

As a consequence of their consideration as non-local environmental information averaged over a radius of 50 km, they do not show significant changes during individual life cycle stages (see Figure 3.3). Nonetheless, they might help to distinguish between long- and short-lived thunderstorms.

To evaluate whether or not there exist indicators for the lifetime at the beginning of the thunderstorm detection, the median with 25th and 75th percentiles are calculated for

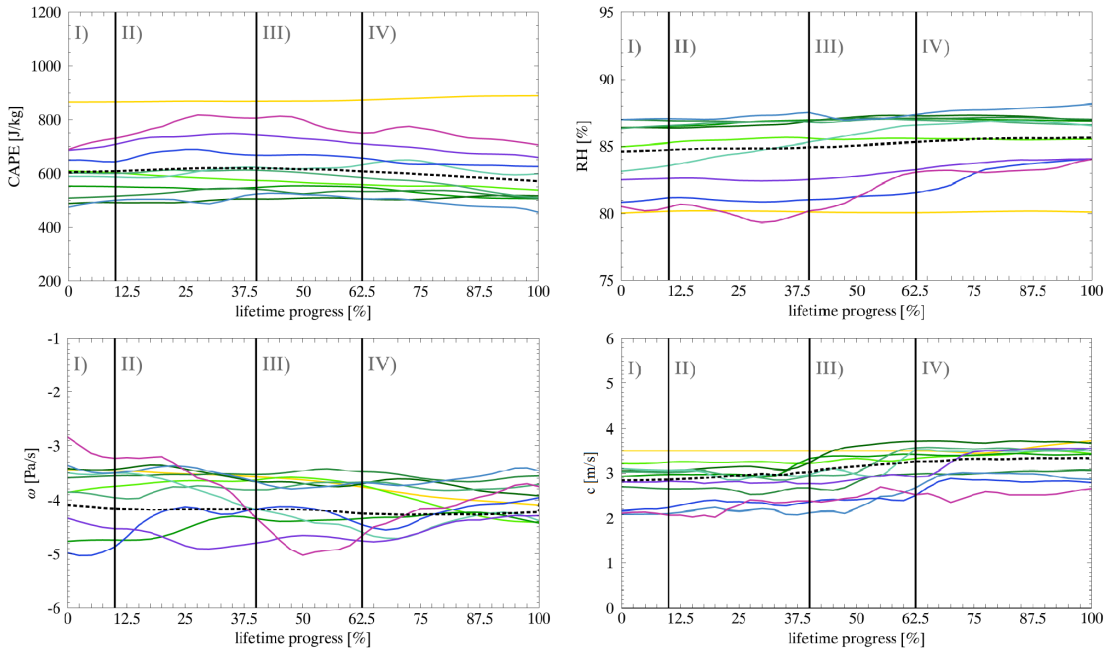

Figure 3.3: As in Figure 3.1. The parameters Convective Available Potential Energy ($CAPE$), Relative Humidity at 700 hPa (RH) and vertical velocity at 700 hPa (ω) from the COSMO-DE model data and propagation velocity (c) from the satellite data are depicted.

thunderstorms with a lifetime of $\leq$ 1 h, 1-2 h, 2-3 h, 3-4 h, and 4-5 h. As depicted in Figure 3.4, the median and percentiles of the model parameters are relatively constant for lifetimes less than 3 h. For lifetimes between 3-4 h, the parameter RH often shows lower values than for short lifetimes (see 25th percentile) and larger values of $CAPE$ (see 75th percentile), however, the median does not differ from the 25th-75th percentile range of shorter-lived thunderstorms. The tendency of longer-lived thunderstorms getting lower RH values and higher $CAPE$ values as indicated in thunderstorms with a lifetime between 3-4 h is more pronounced for very long-lived thunderstorms with lifetimes between 4-5 h. There, lower values of RH and higher values of $CAPE$ are more often, shown by the 25th and 75th percentiles. The median value of $RH/CAPE$ is smaller/larger compared to the 25th/75th percentile of shorter-lived thunderstorms. Nevertheless, large variations exist due to a small number of thunderstorms with lifetimes between 4-5 h. A positive correlation with lifetime of $CAPE$ already has been evaluated by several studies, for example, Rasmussen and Blanchard (1998). These lifetime dependent characteristics are not seen in the model parameter ω. Although, the median of thunderstorms with lifetimes between 4-5 h is higher (smaller updrafts) than covered by the 25-75th percentile range of thunderstorms with lifetimes less than 4 h, the smaller updrafts (higher values of ω) present in very long-lived thunderstorms (4-5 h) are also seen in shorter-lived thunderstorms (see median of the other lifetimes).

To conclude, the high variability of thunderstorms is present in the model data, as seen in weak differences of model parameters for thunderstorms with lifetimes of less than 4 h. Nevertheless, very long-lived thunderstorms contain smaller values of RH and larger values of $CAPE$ and ω. Since the 25-75th range of ω covers most of the median values of shorter-lived thunderstorms, the predictive skill of ω in relation to the lifetime is not graded as high as of RH and $CAPE$. More than half of the thunderstorms with a lifetime less than 4 h show higher values of RH and smaller values of $CAPE$ at the beginning of the detection than 75% of thunderstorms with a lifetime between 4-5 h.

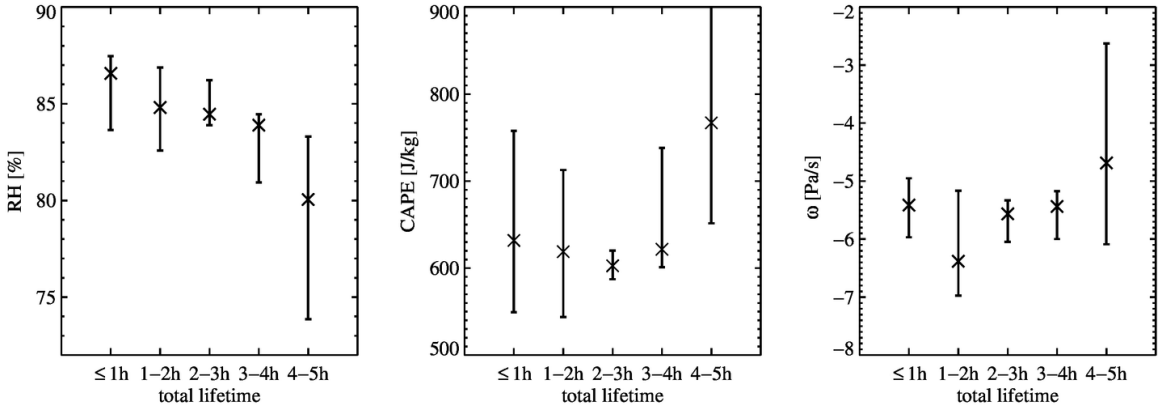

Figure 3.4: Median (x-symbol), 25th and 75th percentiles of the first life cycle time step of thunderstorms in June 2016, May, June, and July 2017, and June 2016 for the lifetimes $\leq$ 1h (5-60 min), 1-2 h (65-120 min), 2-3 h (125-180 min), 3-4 h (185-240 min), 4-5 h (245-300 min) for the analyzed model parameters Relative Humidity at 700 hPa (RH), Convective Available Potential Energy ($CAPE$), and vertical velocity at 700 hPa (ω).

3.2 Variability of thunderstorm life cycle

Thunderstorms are known as highly variable systems and therefore are difficult to nowcast. How variable are the previously identified characteristics of the life cycle in the analyzed parameters? This is a crucial question, respectively to a possible usage of the characteristics in the life cycle model *LOC-lifetime*. If the life cycle is too variable to form the typical characteristics of an averaged life cycle, they can not be considered in the life cycle based nowcasting model *LOC-lifetime*. To analyze the variability of the life cycle, the median life cycle of all thunderstorms normalized to one lifetime process, and the 25th and 75th percentile values are calculated (see Figure 3.5). Only the parameters that showed strong characteristics for each life cycle stage in the previous life cycle analysis are presented. Thus, the median and percentile values of BT, $A_{\tau>0.1}$,

τ, and Li are presented. Additionally, the parameter r_e is depicted, due to its high variability compared to the characteristics of the single life cycle stages.

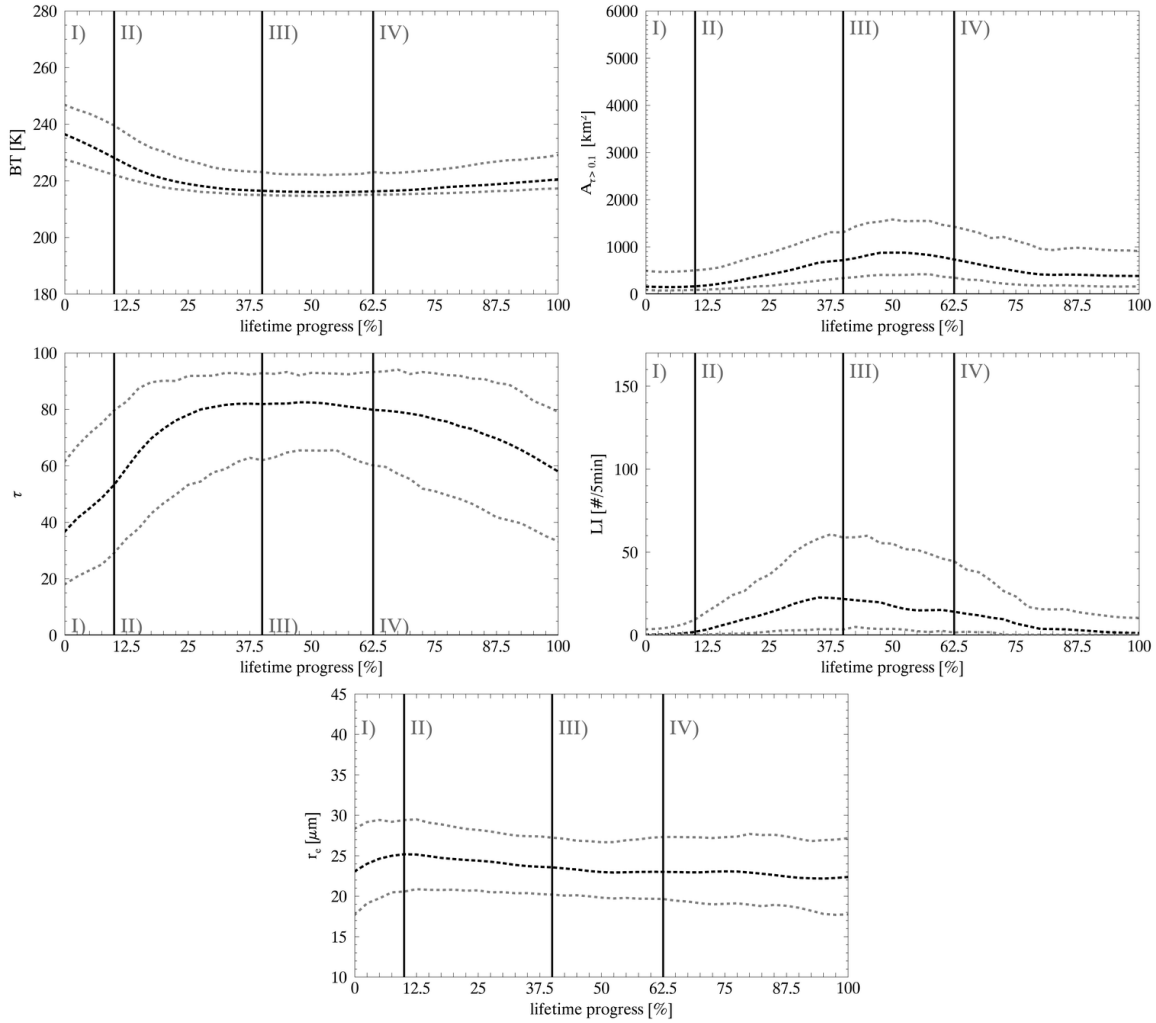

Figure 3.5: Median value (black dashed line) of the life cycle for all thunderstorms detected in the analyzed period, normalized to one lifetime progress and separated into stage I (*early development*), stage II (*advanced development*), stage III (*mature*) and stage IV (*decay*). Additionally, the 25th and 75th percentiles (grey dashed lines) are presented for the parameters Brightness Temperature (BT), Area inside A_{cb} where $\tau > 0.1$ ($A_{\tau>0.1}$), cloud optical thickness (τ), Lightning detection (Li), and effective radius (r_e).

The BT values are most variable during stage I, already indicated in Figure 3.1, which shows that short-lived thunderstorms start with lower BT values than long-lived thunderstorms. This variability is a result of the missing detection of the initial phase, for instance due to cloud masking. The 25th percentile line of BT is near

the median line, especially during stage III. Much lower BT values than the median are rare due to the vertical temperature profile of the atmosphere. The temperature decreases relative to the altitude from the surface to the tropopause and increases from the tropopause to higher levels, whereas the potential temperature increases continuously with height. During stage IV, the difference between the median and the 25th percentiles increases. The 25th percentile line shows a slight increase during stage IV, indicating merging events, in which a thunderstorm dissipate but fuse with a newly developing thunderstorm. During the whole life cycle the difference between the median and the 75th percentile line is almost constant. The high BT values represented by the 75th percentile line, might be an indicator of thunderstorms that never reach the tropopause. Additionally to relatively high BT values, relatively high Li and $A_{\tau>0.1}$ values indicate a possible merge during the dissipation stage. The consideration of already at the beginning well developed events is depicted in stage I of $A_{\tau>0.1}$ and Li with a greater difference between the median and 75th percentile line than the median and the 25th percentile line. Larger $A_{\tau>0.1}$ and Li values are an indicator for an already well developed thunderstorm. Throughout the entire life cycle, the parameter Li varies greatly. During stage III, very low Li values exist, shown by the 25th percentiles. One reason for these low Li values can be a miss of detected Li, due to a local shift by parallax correction. The parameter τ shows high variations to lower and higher values during the whole life cycle. The parameter r_e is highly variable between the thunderstorms, as seen in Figure 3.5. Making it difficult to differentiate between the single life cycle stages by the 25th and 75th percentile lines of r_e. Additionally, the characteristics of the life cycle of r_e are not represented by the 75th percentile line.

As these high variabilities show, some parameters have more robust characteristics and therefore more predictive skill. Parameters with more robust characteristics are, for example, BT, $A_{\tau>0.1}$, τ, and Li and an example for a parameter with weak predictive skill due to high variability compared to the characteristic temporal changes is the parameter r_e (maximum value of 25th percentile never reach minimum value of the mean temporal change). Consequently, a parameter selection is likely to improve for the quality of *LOC-lifetime*. The parameter selection based - beside others - on this variability analysis. The parameter selection is described in detail in Chapter 4.1.1.

3.3 Thunderstorm life cycles in special conditions

The previous analyses of the thunderstorm life cycle considered all thunderstorms, independently of their synoptic environment. Additionally, *severe* and *non-severe* thunderstorms were not analyzed independently. To identify the influence of the synoptic situation on the life cycle characteristics of thunderstorms, the thunderstorms are separated into *frontal* and *non-frontal* with regard to their synoptic situation. This separation was done, since it is possible that thunderstorms in *frontal* situations are

more often already well developed at the first detection than in *non-frontal* situations due to high cloud masking that inhibits an earlier detection. Since one aim of this thesis is to nowcast the future intensity of a thunderstorm it is crucial to analyze the life cycle characteristics depending on the thunderstorm intensity. For this purpose, thunderstorms are separated into the two intensity categories *non-severe* (< 46 dBZ) and *severe* (≥ 46 dBZ).

3.3.1 Synoptic situation: *Frontal* and *non-frontal*

Precise determination of the actual synoptic situation is difficult, since several synoptic situations often happen simultaneously. Accordingly, no algorithm is available that is able to differ between *frontal* and *non-frontal* situations reliable. Thus, the analyzed thunderstorms are categorized by "eye-ball tracking" into *frontal* or *non-frontal*. Due to this time intensive method, only thunderstorms which occurred in June 2016 are analyzed. Only days are considered that can be clearly assigned to solely one of the two synoptic categories. For this purpose the criterion for *frontal* situation is the presence of a cluster of thunderstorms in preformed cloudiness. Additionally, the weather charts for these days show significant horizontal temperature gradients indicating a warm or cold front, or a squall line. Non-frontal situations are defined as the typical local heat, orographic or advective thunderstorm, originated by clear weather conditions preceding deep convection. Consequently, cloud masking is not a problem that happened often and single thunderstorms spread widely. Only days showing clearly identifiable synoptic conditions are used in this algorithm. The 9th, 15th, 16th, 20th, and 24th of June are assigned to have *frontal* conditions, and the 6th 8th, and 18th of June 2016 are assigned to have *non-frontal* conditions. The frequency distribution of the lifetime class occurrence during the mentioned days is depicted in Figure 3.6.

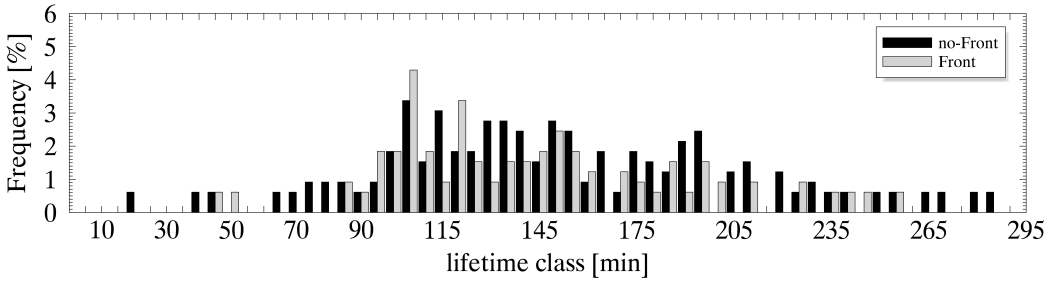

Figure 3.6: Relative frequency distribution of the lifetime classes of thunderstorms in *frontal* (grey) and *non-frontal* (black) situations.

As only five days for *frontal* situations and three days for *non-frontal* situations are considered, the number of thunderstorms for each lifetime class is low (139 thunderstorms in *frontal* situations and 179 thunderstorms in *non-frontal* situations). Although the

number of days considered in the analysis is small, the distribution of the lifetime class occurrence looks very similar for both synoptic categories. Some lifetime classes did not occur during the observed days (for example 5, 10 or 15 min), consequently their life cycle can not be analyzed for these days. Very short-lived (less than 90 min) and long-lived cells (greater than 200 min) are rare for both synoptic situations. Most of the thunderstorms have a lifetime class of 100-195 min. With respect to the small number of thunderstorms, the life cycle of all lifetime classes is averaged for each synoptic situation (see Figure 3.7) for the following analysis.

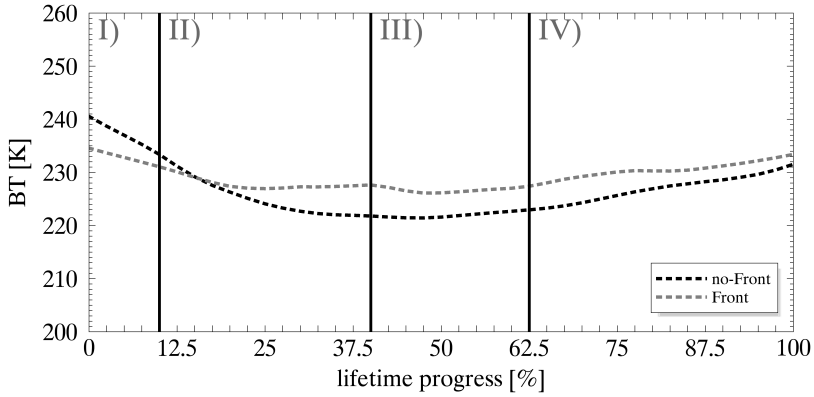

Figure 3.7: Averaged normalized life cycle of thunderstorms that occurred in *frontal* environment (grey dashed line) and in *non-frontal* environment (black dashed line) for the parameter Brightness Temperature (BT).

As seen in Figure 3.7, the parameter BT is presented exemplary for the life cycle of thunderstorms in *frontal* systems (grey dashed line) and *non-frontal* systems (black dashed line), BT is the parameters that shows the strongest differences between those two synoptic situations and was previously identified as parameter with predictive ability. During stage I, BT values are higher for thunderstorms in a *non-frontal* environment than in a *frontal* one, at the beginning the difference is about 5 K, on average. This might be caused by a detection earlier in the life cycle of a thunderstorm in *non-frontal* situation. Early development stages of thunderstorms in *frontal* situations are probably often missed due to cloud masking. At the beginning of stage II, BT of thunderstorms in *frontal* systems do not show further changes, contrary to the further decreasing BT of thunderstorms in a *non-frontal* environment. This decrease of BT nearly ceases at the end of stage II. The temporal changes stay almost constant during stage III. The life cycles of both synoptic situations show an increasing BT at the start of stage IV. At the end of the life cycle, both nearly reach the same BT. The higher BT values for *frontal* than for *non-frontal* thunderstorms during most parts of the life cycle might indicate that *non-frontal* thunderstorms reach higher heights than *frontal* thunderstorms or a lower tropopause exists when *frontal* thunderstorms occur. Further research has to be done with more thunderstorm cases to understand such

differences.

In the previous chapter, *BT* was identified as a parameter with crucial information for the nowcasting of future thunderstorm development. Therefore, the differentiation between the life cycle of *frontal* and *non-frontal* thunderstorms was analyzed. With regard to the result that the characteristics in *BT* of the life cycle phases of *frontal* thunderstorms is less pronounced than those of *non-frontal* thunderstorms, it is possibly more difficult to nowcast the lifetime of *frontal* than of *non-frontal* thunderstorms. Consequently, further research has to be done for the differentiation and nowcasting of thunderstorms in different synoptic situation, this will be discussed in Chapter 5.

3.3.2 Intensity: *Severe* and *non-severe*

One aim of this thesis is, to develop a life cycle model that is able to predict the future intensity of a thunderstorm (*LOC-intensity*). For this purpose, the intensity of a thunderstorm is defined by its reflectivity. The reflectivity is used for intensity categorization, since it is a common indicator for severe weather events related to thunderstorm occurrence such as, hail, heavy rain or lightning. Thunderstorms are separated in the two intensity categories *non-severe* and *severe*. *Non-severe* thunderstorms never reach reflectivities of 46 dBZ during their life cycle, whereas *severe* thunderstorm do so for at least one time step. All thunderstorms in June 2016, May, June, July 2017, and June 2018 are separated this way.

Figure 3.8 shows the frequency distribution of lifetime classes for *non-severe* thunderstorms ($<$ 46 dBZ, grey) and *severe* thunderstorms ($\geq$ 46 dBZ, black). Over the analyzed period almost 600 *severe* thunderstorms and more than 900 *non-severe* thunderstorms occurred. Short- and long-lived thunderstorms are observed for both intensity categories. The strong increase of the number of thunderstorms with a lifetime between 90 min and 175 min is especially pronounced for *non-severe* thunderstorms. This increase exists for both categories due to the definition of the thunderstorms life cycle based on the $A_{\tau>0.1}$ criterion (see Chapter 2.2). *Severe* thunderstorms also show a maximum during this period, however, the maximum is weak compared to the maximum of *non-severe* thunderstorms. It is possible that *non-severe* thunderstorms with a lifetime of 100-145 min occur more frequently than *severe* thunderstorms, because they dissipate more quickly after their early development and consequently, reach a well developed stage less frequently. Long-lived thunderstorms occurred for both severity categories at the same rate, whereas very long-lived thunderstorms ($>$ 240 min) mainly show high intensities.

Regarding intensity prediction, the question that raised is: Are there differences in the life cycle between *severe* and *non-severe* thunderstorms? With the purpose to answer this question, the life cycle is analyzed in the same manner as in the previous analyses.

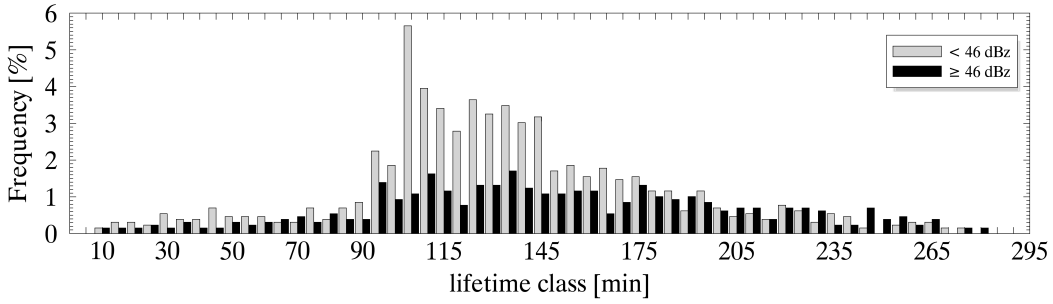

Figure 3.8: Relative frequency distribution of the lifetime classes for thunderstorms that are categorized as *non-severe* (grey) and *severe* (black).

At least one parameter for each data source is shown in Figure 3.9. For reasons of clarity and comprehensibility, only the averaged life cycle and its 25th and 75th percentiles are depicted for every parameter and intensity class. In stage I, the values of BT are very similar for *non-severe* and *severe* thunderstorms. During stage II, BT shows lower values for *severe* thunderstorms than for *non-severe* thunderstorms. This difference remains until the life cycle ends. A reason for this difference might be that thunderstorms with high reflectivities reach higher altitudes due to a more intense updraft. Thunderstorms with high intensities also reach greater areal expanse during their life cycle as depicted in $A_{\tau>0.1}$. The maximum of *severe* thunderstorms during stage III is more than two times higher than of the maximum of *non-severe* thunderstorms. These large $A_{\tau>0.1}$ values exist until the thunderstorm life cycle ends. This great expansion might indicate an intense updraft and a corresponding accumulation of the upcoming air at the tropopause.

Non-severe thunderstorms reach slightly higher values of r_e during their life cycle than *severe* thunderstorms, consequently most parts of the percentile polygons overlap. As the severity is defined by the radar reflectivity, it is not surprising that the reflectivity related parameter VIL of *severe* thunderstorms shows values more than twice as high than that of *non-severe* thunderstorms. These large differences occur especially during stage II and stage III. Additionally, the number of lightning observations differs largely between the two intensity categories. The parameter Li is more than four times greater for *severe* thunderstorms than for *non-severe* thunderstorms. The maximum of Li occurs for thunderstorms with low intensity at the end of stage II, while the maximum of intense thunderstorms is reached at a later time, at the beginning of stage II. High values of Li for *severe* thunderstorms persist throughout stage IV. These high values of Li are consistent with previous studies about reflectivity, lightning, and hail occurrence (Wapler, 2017). The glaciation indicated by high reflectivity values, favors lightning formation. The model parameter $CAPE$ shows a relatively constant difference between *severe* thunderstorms and *non-severe* thunderstorms, during the whole thunderstorm life cycle. The parameter $CAPE$ shows almost twice as high

values for intense thunderstorms as for *non-severe* thunderstorms. This result is not surprising, since $CAPE$ is a well known indicator of thunderstorm intensity as several studies evaluated (see Chapter 1.3).

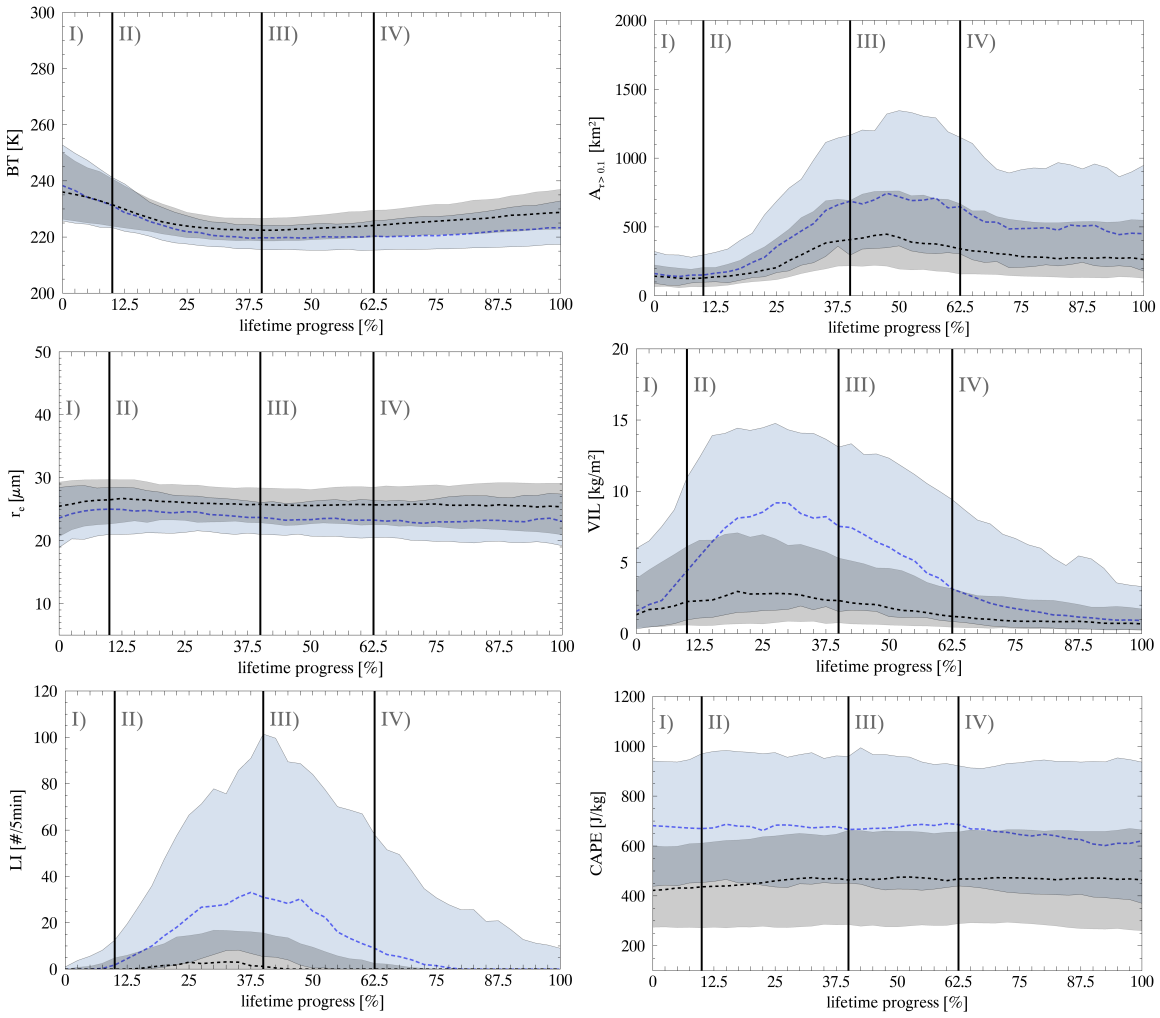

Figure 3.9: The averaged life cycle separated into early growth (I), advanced growth (II), mature (III), and decay (IV) for the observational parameters Brightness Temperature (BT), Area inside A_{cb} where $\tau > 0.1$ ($A_{\tau>0.1}$), effective radius (r_e), Vertically Integrated Liquid water (VIL), and Lightning detection (Li), and the model parameter Convective Available Potential Energy ($CAPE$) of *severe* thunderstorms (blue dashed line) and *non-severe* thunderstorms (black dashed line) and the corresponding 25th and 75th percentiles (blue polygon: *severe*, black polygon: *non-severe*).

Overall, for almost every parameter the life cycle of *severe* thunderstorms shows large overlaps with the life cycle of *non-severe* thunderstorms. This is an indicator that an

intensity prediction based on these parameters could be difficult. Therefore only a first approach of intensity prediction is presented in Chapter 4.3 and discussed further in Chapter 5.

3.4 Summary of the life cycle analyses

The life cycles of thunderstorms that occurred over Germany were analyzed. Thunderstorms are defined as objects detected by the satellite based thunderstorm detection algorithm Cb-TRAM. Since aim of this analyses is a nowcasting of the lifetime and intensity of the thunderstorm and no algorithm is available that is able to differentiate between the thunderstorm organization types reliable, all organization types detected by Cb-TRAM are considered in these analyses. Consequently, incomplete life cycles are possible as a result of detection (late detection due to higher cloud coverage) or organization (for example, coexistence of several life cycle stages in one thunderstorm as it is a multicell). Satellite, ground-based radar, lightning and model data sources were chosen for the life cycle analyses. The life cycle was separated into stages by characteristics in the temporal changes of Brightness Temperature (BT) and Area of the Cb-TRAM cell (A_{cb}). The life cycle consists of the following stages: *Early growth* (stage I), *advanced growth* (stage II), *mature* (stage III), and *decay* (stage IV).

The first focus of the life cycle analyses is the identification of stage characteristics in the different parameters. The following characteristics were found for each life cycle stage. In stage I, a strong decrease in BT and increases in cloud optical thickness (τ), effective radius (r_e), ice fraction at the cloud top (*phase*), precipitation radar signal maximum reflectivity (R_{max}), and Vertically Integrated Liquid water (VIL) can be observed. Stage II is characterized by an ongoing decrease in BT and increases in Area inside A_{cb} where $\tau > 0.1$ ($A_{\tau>0.1}$), τ, and *phase*. There, r_e, R_{max}, and VIL reach their maximums. The parameter Lightning detection (Li) starts to increase. It reaches its maximum at the beginning of stage III. Here, BT then reaches its minimum, and $A_{\tau>0.1}$ its maximum, while r_e, R_{max}, and VIL decrease. Stage IV is characterized by an increasing BT and decreasing R_{max} and VIL. In the second half of stage IV lightning activity comes to an end.

The second focus of the life cycle analyses is the identification of the differences between the typical life cycles of long- and short-lived thunderstorms. Observations on short-lived thunderstorms begin typically with lower BT values and higher τ values than long-lived thunderstorms. This observation can be attributed to the fact that many cells can not be detected as individual developments before they have reached some characteristic intensity, for example, due to cloud obscuration.

Apart from these observational parameters, which can be analyzed for each individual thunderstorm, additional parameters describing the general convective environment are

used to investigate the differences between long- and short-lived thunderstorms. The model parameters Convective Available Potential Energy ($CAPE$), Relative Humidity at 700 hPa (RH), and vertical velocity at 700 hPa (ω) are averaged over a certain surrounding area, and they along with the propagation velocity (c), are treated as environmental parameters. Consequently, these parameters do not show individual trend characteristics over the life cycle stages, but they still have diagnostic potential for total lifetime. Short-lived thunderstorms have higher RH values, higher c values, and lower $CAPE$ values over their entire life cycle. Therefore, these parameters seem to have predictive abilities in terms of the lifetime of thunderstorms.

It was shown by the 25th and 75th percentiles, that all parameters contain large variabilities. These large variabilities are probably a result of the consideration of all organization types detected, that probably rarely show a single thunderstorm cell that is not merging with other thunderstorms or splits into separated thunderstorms.

Additionally, the life cycles of *non-severe* (< 46 dBZ) and *severe* (≥ 46 dBZ) thunderstorms were compared. Severe thunderstorms show larger values over their life cycles for $A_{\tau>0.1}$, R_{max}, VIL, Vertically Integrated Ice (VII), and Li and in the model parameter $CAPE$, than *non-severe* thunderstorms.

These results are used as basis for the implementation of two life cycle models. The fuzzy logic-based models developed predict, on the one hand, the remaining lifetime (*LOC-lifetime*) and, on the other hand, the future intensity (*LOC-intensity*) of thunderstorms. In addition to the nowcasting of the remaining lifetime, the current stage is also calculated by the *LOC-lifetime* model. That are described in Chapter 4.

4 Nowcasting of the thunderstorm life cycle

The previous results of the life cycle analyses are used for parameter selection and the fuzzy logic-based nowcasting of the remaining thunderstorm lifetime, the calculation of its current stage (*LOC-lifetime*) and the prediction of its intensity (*LOC-intensity*). First of all, parameter selection for the nowcasting method *LOC-lifetime* is described, then the selected parameters are presented. Next, the fuzzy logic life cycle method is explained in detail including the various fuzzy logic steps. Thereafter, the nowcasting method is validated and compared with other existing nowcasting methods. Additionally, a sensitivity study is presented for the prediction of the remaining thunderstorm lifetime, taking into account the data sources used and membership functions. Afterwards, a first approach for intensity prediction with the nowcasting model *LOC-intensity* is presented in a similar way.

4.1 Combination of data used to nowcast thunderstorms lifetime

The second part of this thesis evaluates whether or not the life cycle information in the analyzed data can improve the nowcasting of thunderstorms by observing if this combination has lower false alarm ratio (FAR) compared to the existing extrapolation method. The results of the previous life cycle study are used for this purpose. A method will be presented for calculating the current stage and predicting the remaining lifetime of a thunderstorm (*LOC-lifetime*). As seen in the life cycle analyses, not every parameter contains information about the current stage or lifetime; thus, parameters selection must be done and is presented next. Following the parameter selection, the *LOC-lifetime* is described in detail. Afterwards, the verification of the *LOC-lifetime* is presented. The robustness of *LOC-lifetime* is also tested for various set ups. Furthermore, the sensitivity of *LOC-lifetime* with regard to the data sources as well as the definition of the thresholds of the membership functions and the membership function itself is evaluated.

4.1.1 Parameter selection for lifetime nowcasting

The aim of parameter selection is to analyze as many parameters as necessary to extract all information without too much redundancy. Since *LOC-lifetime* calculates both the remaining lifetime and the current stage of a thunderstorm, parameters meeting different criteria will be considered.

In Chapter 3.1.1, the parameters with predictive value were evaluated. Now, correlation analyses are done to identify those strongly correlated parameters providing redundant information. The decision to remove strongly correlated parameters is made to avoid amplifying "false information". For example, if there are several strongly correlated parameters from one data source that indicate a decaying thunderstorm, while other parameters rightly indicate a growing thunderstorm, the false prediction "decay" could predominate. Such an incorrect prediction can be avoided by filtering redundant information. In Table 4.1, the correlations between all analyzed parameters are shown. For each calculation, the *Linear Pearson Correlation Coefficient* r is used. Here,

$$r_{xy} = \frac{\sum_{i=1}^{n}(x_i - \bar{x})(y_i - \bar{y})}{\sqrt{\sum_{i=1}^{n}(x_i - \bar{x})^2}\sqrt{\sum_{i=1}^{n}(y_i - \bar{y})^2}}$$

where n is the size of each normalized life cycle step, x_i and y_i are the values of the parameters for the single life cycle time steps, and $\bar{x}$ and $\bar{y}$ are the mean values of the two parameters being compared over the entire life cycle. This correlation coefficient is calculated for every possible parameter combination. It becomes positively or negatively large if the two compared parameters are strongly correlated, in the case of no correlation, the *Linear Pearson Correlation Coefficient* is zero.

A correlation coefficient greater than 0.9 or smaller than -0.9 is assumed to identify parameters with strongly redundant information. In each case of strong correlated coefficients, one of the two strongly correlated parameters is chosen for *LOC-lifetime* with respect to a multi-sourced data set. The aim of the selection is to select at least one parameter from every data source to obtain a life cycle model that is as independent of the data sources as possible.

First, the parameters of the satellite data are compared. The parameters A_{cb} and $A_{\tau>0.1}$ are correlated, due to their similar calculations. The parameter $A_{\tau>0.1}$ is used for *LOC-lifetime* since it contains the additional information from τ. At the beginning of the life cycle, BT shows a characteristic decrease with no further significant changes. To the contrary, *phase* indicates an ongoing glaciation during the first stages and no further changes afterwards. These complementary temporal changes are present in the *Linear Pearson Correlation Coefficient* (r = -0.9). It is not surprising that a thunderstorm elevating to the tropopause glaciates almost completely at the cloud top. The *phase* calculation involves more arithmetic steps than BT since BT is a simple

measurement. As these additional calculation steps might lead to higher uncertainties, the parameter BT is selected for *LOC-lifetime*.

In addition to the correlations between satellite parameters, there exists redundant information in the radar data as well. The radar parameter VIL represents the water content from the surface up to the cloud top, whereas VII is part of VIL, as it is calculated from the height at which 0 °C is reached to the cloud top. Consequently, they are strongly correlated ($r = 0.98$) due to their related calculation. Thus, since VIL exhibits higher absolute values and stronger temporal changes, VIL will be considered for *LOC-lifetime*. Additionally, R_{max} is a measure of the amount of water inside a certain area; therefore, it is very similar to VIL ($r = 0.95$). The parameter VIL will be used in *LOC-lifetime* since it shows larger temporal changes compared to its absolute values than R_{max} (not shown).

In the previous life cycle analyses, the model parameters showed no significant temporal changes compared to their absolute values. Consequently, the correlation coefficient is large for $CAPE$ and RH (r = -0.92). The parameter $CAPE$ shows a slight increase, whereas RH shows a slight decrease. In this case, making a selection between the two would not be beneficial because both parameters had lifetime-dependent values in the previous life cycle analyses (see Chapter 3.1.2).

In addition to the correlations of parameters from the same data sources, parameters from different data sources also contain strongly redundant information. The radar parameter Area of the 46 dBZ contour (RA_{46}) describes areas of very high reflectivity that indicate severe weather, for example, the occurrence of lightning. Consequently, RA_{46} correlates with the lightning parameter Li. Since it is advantageous to collect parameters from different data sources, Li is considered further. The parameter $CAPE$ correlates strongly with the selected parameter VIL. Although no life cycle is captured by the parameter $CAPE$ this strong correlation is the result of a slight increase at the beginning of the life cycle followed by a slight decrease corresponding to the temporal changes in VIL over the life cycle. These changes were not depicted in the life cycle analysis of $CAPE$ because they are small compared to the absolute values of about 600 J kg^{-1}. Despite the fact that $CAPE$ correlates with VIL, $CAPE$ and VIL will be considered for *LOC-lifetime* with regard to a mutli-sourced data set. The parameters c and RH are also highly correlated. Since parameters should be selected from different data sources, the model parameter RH will be considered in *LOC-lifetime* since there are already three satellite parameters ($A_{\tau>0.1}$, τ, and BT) in *LOC-lifetime*.

Table 4.1: *Linear Pearson Correlation Coefficients (r)* of the averaged life cycles of all thunderstorms normalized to one lifetime progress for all the parameters from satellite, radar, lightning, and model data analyzed in Chapter 3.

	A_{cb}	$A_{\tau>0.1}$	BT	τ	r_e	$phase$	c	R_{max}	RA_{46}	VII	VIL	Li	$CAPE$	RH	ω
A_{cb}	1	0.99	-0.89	0.7	-0.66	0.8	0.65	0.05	0.59	0.1	-0.4	0.8	-0.13	-0.42	0.13
$A_{\tau>0.1}$	0.99	1	-0.88	0.68	-0.69	0.77	0.67	0.03	0.54	0.05	-0.08	0.79	-0.13	-0.43	0.09
BT	-0.89	-0.88	1	-0.85	0.38	-0.9	-0.5	-0.31	-0.7	-0.37	-0.24	-0.86	-0.09	-0.28	-0.17
τ	0.7	0.68	-0.85	1	-0.04	0.69	0.1	0.7	0.87	0.7	0.6	0.89	0.5	-0.15	0.49
r_e	-0.66	-0.69	0.38	-0.04	1	-0.41	-0.81	0.56	0.1	0.59	0.68	-0.17	0.58	-0.68	0.33
$phase$	0.8	0.77	-0.9	0.69	-0.41	1	0.71	0.02	0.4	0.1	0	0.59	-0.25	0.59	-0.22
c	0.65	0.67	-0.5	0.1	-0.81	0.71	1	-0.63	-0.18	-0.59	-0.7	0.1	-0.78	0.94	-0.65
R_{max}	0.05	0.03	-0.31	0.7	.0.56	0.02	-0.63	1	0.76	0.93	0.95	0.58	0.96	-0.79	0.81
RA_{46}	0.59	0.54	-0.7	0.87	0.1	0.4	-0.18	0.76	1	0.83	0.76	0.94	0.63	-0.39	0.78
VII	0.1	0.05	-0.37	0.7	0.59	0.1	-0.59	0.93	0.83	1	0.98	0.66	0.86	-0.69	0.81
VIL	-0.4	-0.08	-0.24	0.6	0.68	0	-0.7	0.95	0.76	0.98	1	0.54	0.91	-0.79	0.81
Li	0.8	0.79	-0.86	0.89	-0.17	0.59	0.1	0.58	0.94	0.66	0.54	1	0.42	-0.13	0.63
$CAPE$	-0.13	-0.13	-0.09	0.5	0.58	-0.25	-0.78	0.96	0.63	0.86	0.91	0.42	1	-0.92	0.86
RH	-0.42	-0.43	-0.28	-0.15	-0.68	0.59	0.94	-0.79	-0.39	-0.69	-0.79	-0.13	-0.92	1	-0.8
ω	0.13	0.09	-0.17	0.49	0.33	-0.22	-0.65	0.81	0.78	0.81	0.81	0.63	0.86	-0.8	1

In addition to the correlation criterion, the parameter must fulfill a second criterion in order to be considered in *LOC-lifetime*. This second criterion is that they have characteristics indicating the current stage also for possible variations inside the 25th and 75th percentile polygon. The median value of r_e presents a characteristic maximum value in the deep convection stage, but this maximum is small compared to the possible variation inside the 25th and 75th percentiles (shown in Chapter 3.1.1, Figure 3.5). In particular, the minimum of the 75th percentile must be less than the maximum of the median line, and the maximum of the 25th percentile must be greater than the minimum of the median line. If this is not the case, it indicates that r_e is very variable (compared to its averaged life cycle characteristics) and consequently not advantageous for *LOC-lifetime*. The model parameter ω does not contain robust information about the lifetime or life cycle stage and is therefore not considered in the life cycle model *LOC-lifetime*.

Hence, the following parameters are used in *LOC-lifetime* to calculate the remaining lifetime and current stage of a thunderstorm: the observational parameters $A_{\tau>0.1}$, BT, τ, VIL, Li, and the model parameters $CAPE$ and RH. Since the selected observational parameters show characteristic temporal changes over the life cycle indicating the current stage in combination with their absolute values, these temporal changes (difference of one time step, 5 min) and absolute values will be included in *LOC-lifetime*. The model parameters do not exhibit any significant characteristics over the life cycle: however, their absolute values indicate the lifetime of the thunderstorm. Thus, only the absolute values of the model parameters will be considered in *LOC-lifetime* in order to calculate the remaining lifetime and current stage.

4.1.2 Lifetime nowcasting and stage determination

The fuzzy logic mathematical method is used to combine the selected parameters and to nowcast the remaining lifetime of thunderstorms. Fuzzy logic is currently used in weather event prediction due to its possibility to categorize more like nature and human thinking, as described in Chapter 2.3.

In addition to the nowcast of the remaining lifetime, the current stage is calculated. The output "current stage" is categorized into the stages *growth*, *mature*, and *decay*. This categorization differs from the life cycle definition used in the previous analyzes: however, when taking into consideration the high variability between single thunderstorm and their life cycles, the separation into three stages makes more sense for *LOC-lifetime*. Additionally, the definition of a thunderstorm's lifetime for *LOC-lifetime* differs from the thunderstorm's lifetime definition used in the previous analyses. The definition of a thunderstorm for *LOC-lifetime* only covers the actual by Cb-TRAM detected cells without their backward- and forward-extrapolations. This shorted thunderstorm life cycle is used here since the actual thunderstorm detected by Cb-TRAM describes

an area of possible severe weather events. This period of possible severe events is of interest for nowcasting and therefore tried to predict.

As mentioned in Chapter 2.3, fuzzy logic consists of three main steps:

(a) fuzzification of the input data to the fuzzified input

(b) combination of the fuzzified input to the fuzzified output

(c) defuzzification of the fuzzified output to the "readable" output

These steps are described for *LOC-lifetime* in the following paragraphs. In addition, the derivation of the remaining lifetime, based on the analysis of the current stage, is explained below.

The remaining lifetime of thunderstorms that currently exist (Cb-TRAM detection only) is calculated via a combination of the previous selected parameters $A_{\tau>0.1}$, BT, τ, VIL, and Li from the observational data sources, and $CAPE$ and RH from the model parameters. Since the absolute values of $A_{\tau>0.1}$, τ, VIL, and Li do not indicate the current stage, their temporal changes will be considered in *LOC-lifetime*. For instance, low $A_{\tau>0.1}$ values indicate that the thunderstorm is either in stage I and growing or in stage IV and already dissipating. However, an increasing $A_{\tau>0.1}$ indicates a growing thunderstorm, and a negative temporal change in $A_{\tau>0.1}$ indicates a decaying thunderstorm. The model parameters hardly change over the life cycle. Therefore, only the absolute values of the model parameters are used. The absolute values and temporal changes of these parameters must be fuzzified for the fuzzy logic-based nowcasting model *LOC-lifetime*.

(a) Fuzzification

The fuzzifier allocates a certain fuzzy score value, also called membership grade, for every parameter in the defined fuzzy set. Figure 4.1 shows the method for the threshold selection for the membership functions for the temporal changes of the parameter BT. Figure 4.2 shows the corresponding membership functions.

In this case, the fuzzy sets are *growth* and *decay*. *Growth* is comparable to the life cycle stage I (early growth) as defined in Chapter 2.5. *Decay* is equal to stage IV. Values of the 25th or 75th percentile are used to calculate the thresholds of the membership functions. The relevant time steps are the end of the early growth (stage I) for the *growth* class and the beginning of the decay (stage IV) for the *decay* class. In Figure 4.1, the 25th and 75th percentiles of the temporal changes of BT during the life cycle are shown. The red cross marks the threshold for the fuzzy set *growth*, in this case at -0.5 K/5min, meaning that temporal changes of -0.5 K/5min or less are allocated with a membership grade > 0 to the fuzzy set *growth*, see also Figure 4.2. For the threshold of the fuzzy set *decay*, the 75th percentile of the temporal changes of BT at the beginning of stage IV (decay) are used (marked by a blue cross in Figure 4.1). The

difference between these two thresholds (-0.8 to -0.5) marks the overlap seen in 4.2. The membership function and the allocation to a fuzzy value is explained next.

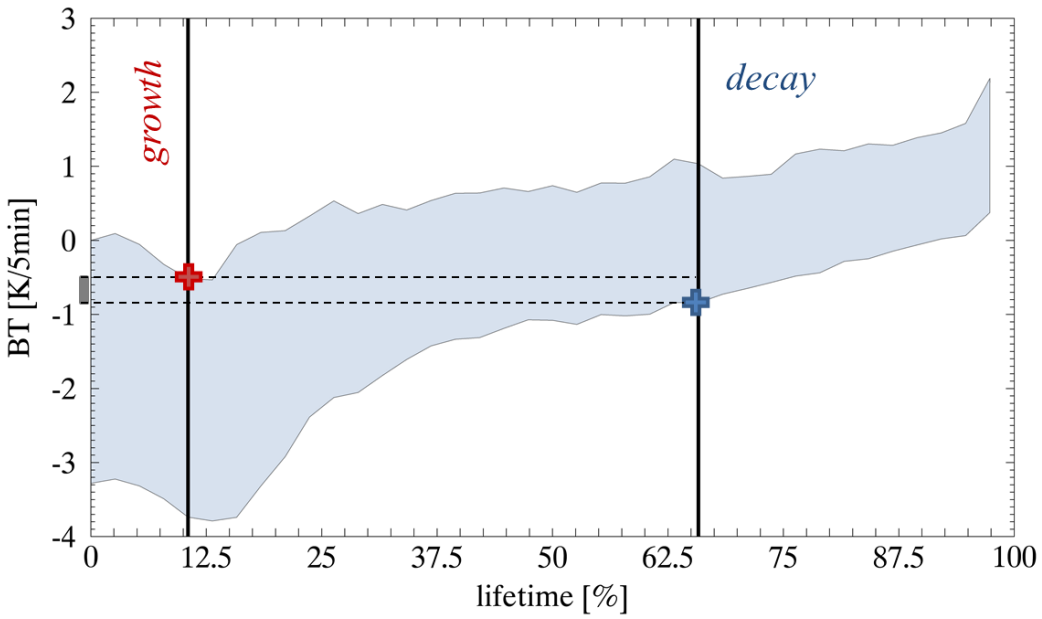

Figure 4.1: The polygone limited by the 25th and 75th percentiles of the temporal changes of Brightness Temperature in [K/5min] over the life cycle is shown. The red cross marks the threshold for the fuzzy set *growth* and the blue cross for the fuzzy set *decay*.

The allocation is done via membership functions. The blue line represents the values allocated to the fuzzy set *decay* and the red line depicts the values allocated to the fuzzy set *growth* for certain values of the trend of the parameter BT. The *mature* stage is presented by the overlap between these two classes and therefore comparable to the life cycle stages II (advanced growth) and stage III (mature) of the definition used for the life cycle analyses (Chapter 3) and described in Chapter 2.5. The aim is to select a wide range for each fuzzy set that contains an overlap to reduce the influence of the high variability of thunderstorms. Indeed, this overlap is one of the advantages of the fuzzy logic method. As presented in Figure 4.2, a thunderstorm is allocated to the set *growth* if it has temporal changes of BT of -0.5 K/5min or less; if it shows BT values of -0.8 K/5min or greater, then it is allocated with a membership grade greater than 0 to the fuzzy set *decay*. The sum of the allocated membership grades of the two classes is always 1 for all parameter values. If the value of the parameter is between the thresholds of the classes, both classes are assigned a value greater than 0, however, the sum of both is still 1 (grey shaded area).

These membership functions are calculated for every parameter individually (see thresholds in Table 4.2). As a result, the input from the parameters is converted to a

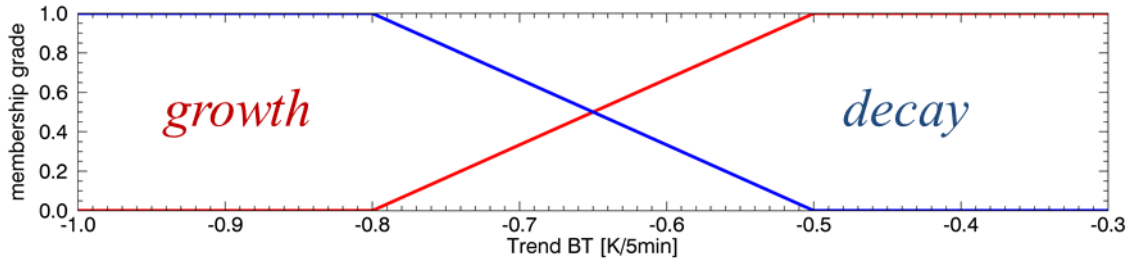

Figure 4.2: Membership functions of the fuzzy sets *growth* (red) and *decay* (blue) for the parameter BT.

fuzzified input (membership grades between 0 and 1 for every fuzzy set and parameter) by these membership functions.

Table 4.2: Threshold of the membership functions for the selected parameters. The trend thresholds present the difference between two time steps of 5 min. The percentual trend is only calculated for the parameter $A_{\tau>0.1}$.

	growth		*decay*	
Parameter	Absolute	Trend	Absolute	Trend
BT [K]	> 224.8	< -0.5	< 226.8	> -0.8
$A_{\tau>0.1}$	-	$> -14.5\%$	-	$< 67.5\%$
τ	-	> -4.3	-	< 6.1
VIL [kg m^{-2}]	-	> -0.4	-	< 0.6
Li [#/5min]	-	> 0.2	-	< 1.7
$CAPE$ [J kg^{-1}]	> 424	-	< 963	-
RH [%]	< 84	-	> 76	-

(b) Combination

For every parameter, one membership grade for each fuzzy set (*growth* and *decay*) is now available. The combination is found by subtracting the average of the membership grade of the *growth* set from the average of the membership grade of the *decay* set. Consequently, one value between -1 and 1 is calculated. This value presents the fuzzified output. In Figure 4.3, the mean fuzzified output value of each lifetime class and detection step is presented. Therefore for every thunderstorm at every detection step the fuzzy output value is calculated and averaged for all thunderstorms with the same total lifetime at the same detected lifetime so far. The values in the table are smoothed with their nearest neighbors, i.e., the mean value of each cell and its four nearest neighbors (if available: above, left, right, and beneath the cell) is calculated.

(c) Defuzzification

The table in Figure 4.3 is used to defuzzify the fuzzified output. The actual stage is allocated directly with the available fuzzy output, and the current stage can be read. The colors indicate whether a thunderstorm is growing (green) or decaying (red), according to the fuzzified output. The yellow color indicates an overlap between a growing and decaying thunderstorm, consequently the *mature* stage. On average, the thunderstorms exhibit typical life cycle (first *growth*, then *mature*, and, at lastly, *decay*). There are exceptions, i.e., very short-lived thunderstorms. At first detection, they are already in *decay*, reflecting the fact that the early development of very short-lived thunderstorms impedes detection. Thus, short-lived thunderstorms are already well developed at first Cb-TRAM detection.

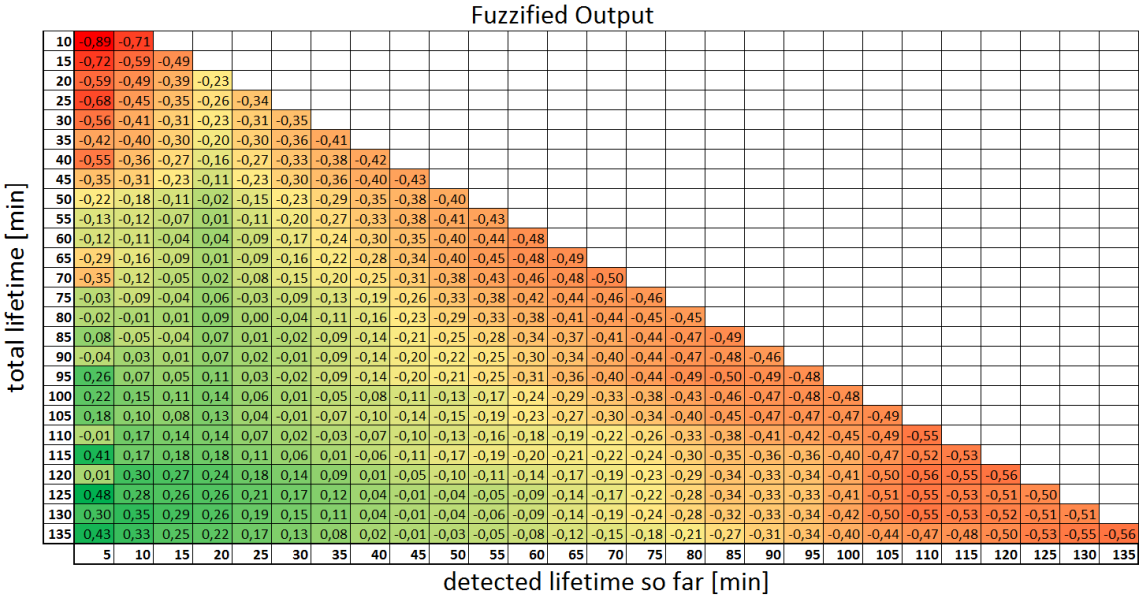

total lifetime [min] \ detected lifetime so far [min]	5	10	15	20	25	30	35	40	45	50	55	60	65	70	75	80	85	90	95	100	105	110	115	120	125	130	135
10	-0,89	-0,71																									
15	-0,72	-0,59	-0,49																								
20	-0,59	-0,49	-0,39	-0,23																							
25	-0,68	-0,45	-0,35	-0,26	-0,34																						
30	-0,56	-0,41	-0,31	-0,23	-0,31	-0,35																					
35	-0,42	-0,40	-0,30	-0,20	-0,30	-0,36	-0,41																				
40	-0,55	-0,36	-0,27	-0,16	-0,27	-0,33	-0,38	-0,42																			
45	-0,35	-0,31	-0,23	-0,11	-0,23	-0,30	-0,36	-0,40	-0,43																		
50	-0,22	-0,18	-0,11	-0,02	-0,15	-0,23	-0,29	-0,35	-0,38	-0,40																	
55	-0,13	-0,12	-0,07	0,01	-0,11	-0,20	-0,27	-0,33	-0,38	-0,41	-0,43																
60	-0,12	-0,11	-0,04	0,04	-0,09	-0,17	-0,24	-0,30	-0,35	-0,40	-0,44	-0,48															
65	-0,29	-0,16	-0,09	0,01	-0,09	-0,16	-0,22	-0,28	-0,34	-0,40	-0,45	-0,48	-0,49														
70	-0,35	-0,12	-0,05	0,02	-0,08	-0,15	-0,20	-0,25	-0,31	-0,38	-0,43	-0,46	-0,48	-0,50													
75	-0,03	-0,09	-0,04	0,06	-0,03	-0,09	-0,13	-0,19	-0,26	-0,33	-0,38	-0,42	-0,44	-0,46	-0,46												
80	-0,02	-0,01	0,01	0,09	0,00	-0,04	-0,11	-0,16	-0,23	-0,29	-0,33	-0,38	-0,41	-0,44	-0,45	-0,45											
85	0,08	-0,05	-0,04	0,07	0,01	-0,02	-0,09	-0,14	-0,21	-0,25	-0,28	-0,34	-0,37	-0,41	-0,44	-0,47	-0,49										
90	-0,04	0,03	0,01	0,07	0,02	-0,01	-0,09	-0,14	-0,20	-0,22	-0,25	-0,30	-0,34	-0,40	-0,44	-0,47	-0,48	-0,46									
95	0,26	0,07	0,05	0,11	0,03	-0,02	-0,09	-0,14	-0,20	-0,21	-0,25	-0,31	-0,36	-0,40	-0,44	-0,49	-0,50	-0,49	-0,48								
100	0,22	0,15	0,11	0,14	0,06	0,01	-0,05	-0,08	-0,11	-0,13	-0,17	-0,24	-0,29	-0,33	-0,38	-0,43	-0,46	-0,47	-0,48	-0,48							
105	0,18	0,10	0,08	0,13	0,04	-0,01	-0,07	-0,10	-0,14	-0,15	-0,19	-0,23	-0,27	-0,30	-0,34	-0,40	-0,45	-0,47	-0,47	-0,47	-0,49						
110	-0,01	0,17	0,14	0,14	0,07	0,02	-0,03	-0,07	-0,10	-0,13	-0,16	-0,18	-0,19	-0,22	-0,26	-0,33	-0,38	-0,41	-0,42	-0,45	-0,49	-0,55					
115	0,41	0,17	0,18	0,18	0,11	0,06	0,01	-0,06	-0,11	-0,17	-0,19	-0,20	-0,21	-0,22	-0,24	-0,30	-0,35	-0,36	-0,36	-0,40	-0,47	-0,52	-0,53				
120	0,01	0,30	0,27	0,24	0,18	0,14	0,09	0,01	-0,05	-0,10	-0,11	-0,14	-0,17	-0,19	-0,23	-0,29	-0,34	-0,33	-0,34	-0,41	-0,50	-0,56	-0,55	-0,56			
125	0,48	0,28	0,26	0,26	0,21	0,17	0,12	0,04	-0,01	-0,04	-0,05	-0,09	-0,14	-0,17	-0,22	-0,28	-0,34	-0,33	-0,33	-0,41	-0,51	-0,55	-0,53	-0,51	-0,50		
130	0,30	0,35	0,29	0,26	0,19	0,15	0,11	0,04	-0,01	-0,04	-0,06	-0,09	-0,14	-0,19	-0,24	-0,28	-0,32	-0,33	-0,34	-0,42	-0,50	-0,55	-0,53	-0,52	-0,51	-0,51	
135	0,43	0,33	0,25	0,22	0,17	0,13	0,08	0,02	-0,01	-0,03	-0,05	-0,08	-0,12	-0,15	-0,18	-0,21	-0,27	-0,31	-0,34	-0,40	-0,44	-0,47	-0,48	-0,50	-0,53	-0,55	-0,56

Figure 4.3: Table of fuzzy output values averaged for each total lifetime and detected lifetime so far. Values range between -1 and 1 where values near -1 are colored reddish (comparable to decay), values near 1 are colored greenish (comparable to growth) and values between -1 and 1 are colored yellowish (indicating mature).

In order to decide whether a thunderstorm is growing or decaying, a membership function is once again calculated. This membership function is used to evaluate the actual stage of the thunderstorm via its fuzzified output, as presented in Figure 4.4. To define the thresholds of the classes, the range that includes 50% of the values in Figure 4.3 around 0 is used. The overlap between the set *growth* and *decay* is categorized as the *mature* stage. An overlap of 50% of the values for allocation to the *mature* seems large compared to the time period that is covered by stage III in the analyzed life cycle (see Chapter 3.1.1). The fact that stage I and large parts of stage IV are

not detected by Cb-TRAM must be taken into consideration; thus the life cycle of a Cb-TRAM-detected cell is reduced by time steps at the beginning and end of its life cycle.

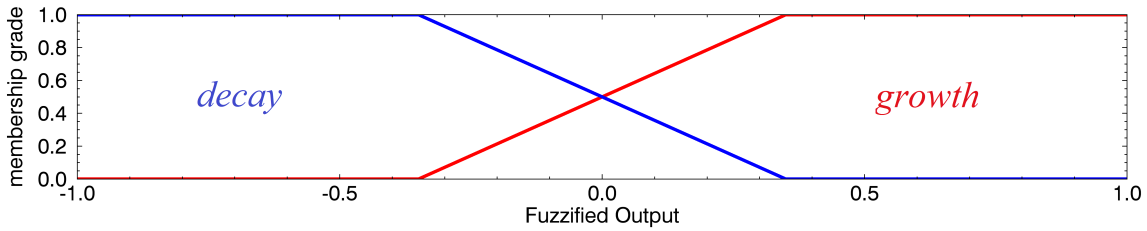

Figure 4.4: Membership function to classify fuzzified output into *growth* (red line), *mature* (overlap between blue and red line), or *decay* (blue line).

The colors depicted in Table 4.3 indicate an average life cycle comprising the *growth*, *mature*, and *decay* stages for long-lived thunderstorms. For almost every lifetime class, *LOC-lifetime* calculates a fuzzy logic value of 0.3 or greater (indicating a *growth* stage) at the beginning; afterwards, the *mature* stage takes over (-0.3 $\geq$ fuzzy logic value $\leq$ 0.3), then, at the end, the *decay* stage comes into play (fuzzy logic value $<$ -0.3). This cycle works for, on average, thunderstorms with lifetimes (detections by Cb-TRAM only) greater than 45 min. The thunderstorms with lifetimes between 10 and 45 min show strong decay at the beginning, with decreasing afterwards. As a result, on average, short-lived thunderstorm do not exhibit a textbook life cycle, but the rest of the thunderstorm lifetime classes indicate that short-lived thunderstorms are often the product of a missed detection due to cloud masking. Hence, most short-lived thunderstorms are already well developed at the first Cb-TRAM detection.

When consideration is narrowed to textbook-like behavior in thunderstorm life cycle, as defined by a *growth* stage, followed by a *mature* stage, and then a *decay* stage, the following statistical values are calculated. Only 19% of all thunderstorms that occurred in June of 2016; May, June, and July of 2017; and June of 2018 exhibited this textbook-like behavior. The other 81% of the thunderstorms indicated a change from *decay* to *growth* during their life cycles. This result points out again the high variability present in the thunderstorms life cycle, as already shown in Chapter 3.2. On average, the life cycle exhibits textbook-like behavior, but individual thunderstorms often cannot be described by this behavior. On average a text-book-like picture is given, since the change from *decay* back to *growth* may occur only for one time step and the time of reversed life cycle differs for the individual thunderstorms. One possible explanation for this high number of thunderstorms with non-textbook-like life cycles is that thunderstorms are dynamical and variable systems consisting of several cells each in an other stage as described in Chapter 1.2.

In Figure 4.5 the percentages of thunderstorms with textbook-like life cycles and those

without such life cycles are depicted for every lifetime class. Very short-lived thunderstorms almost always exhibit non-textbook-like life cycle behavior. Approximately 30% of long-lived thunderstorms have textbook-like life cycles. Short-lived thunderstorms being less likely than long-lived thunderstorms to have textbook life cycles is again a hint that short-lived thunderstorms often develop from existing thunderstorms and are therefore already well developed and often in the *decay* stage. Although, long-lived thunderstorms contain more time steps during their life cycles, which leads to statistically higher chances of non-textbook-like life cycles, one-third of the time, they exhibit a *decay* stage after a *growth* stage.

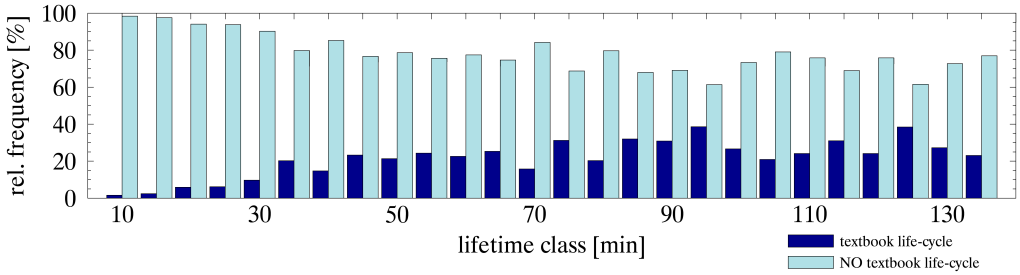

Figure 4.5: Dark blue bars show the percentages of thunderstorms with textbook-like life cycles and light blue bars show the percentages of those with non-textbook-like life cycles.

In addition to the calculation of its current stage, *LOC-lifetime* predicts a thunderstorms remaining lifetime. For this purpose, the fuzzified output of a current thunderstorm is compared to the values in Table 4.3. The lifetime is known for an observed thunderstorm; therefore, the values of the matching column (detected lifetime so far) in Figure 4.3 can be compared to the fuzzified output derived from the parameters that are actually observed. For instance, if a thunderstorm has been detected for 20 min and the actual calculated fuzzified output is about 0.1, then all values in the column 20 "detected lifetime so far [min]" are compared to the actual calculated fuzzified output. The difference from 0.1 in column "20 min" is lowest for a thunderstorm with a total lifetime of 95 min. Thus, the lifetime of the current thunderstorm is allocated to this lifetime class, and its remaining lifetime is calculated as 75 min (95-20 min).

As depicted in Figure 4.3, the averaged fuzzy logic values do not differ that much from each other. Additionally, a lifetime prediction with an accuracy of 5 min is very difficult due to the well-known high variability presented in Chapter 3.1.1. In order to quantify this high uncertainty, the *standard deviations* of the fuzzy logic values are calculated for every detection step and every lifetime. Therefore, the fuzzy logic values calculated for every detection step of every thunderstorm in the analyzed period (June 2016; May, June, July 2017; June 2018) are used. Each fuzzy logic value is assigned to the total lifetime the thunderstorm lived and its detected lifetime so far, when the fuzzy logic value is calculated. The fuzzy logic values of thunderstorms with the same lifetime at

the same detection step are used to calculate the *standard deviation* (as introduced in Chapter 2.4) of this total lifetime and detection step. The *standard deviations* are depicted in Figure 4.6. They are used to calculate an interval around each calculated fuzzy logic value, for which the lifetime prediction interval consists of the median plus or minus the *standard deviation*. In the previous example, (remaining lifetime of 75 min) employing the *standard deviation* leads to a lifetime prediction of 30-115 min. The colors in Figure 4.6 indicate the values of the *standard deviations*. Dark blue cells indicate larger *standard deviations* than the light blue cells have. In some cases, the *standard deviations* are greater than 0.4. The smallest value is about 0.24. Compared to a possible fuzzy logic value range of -1 to 1, these values are large, indicating the highly variable thunderstorm life cycle and possible challenges for nowcasting.

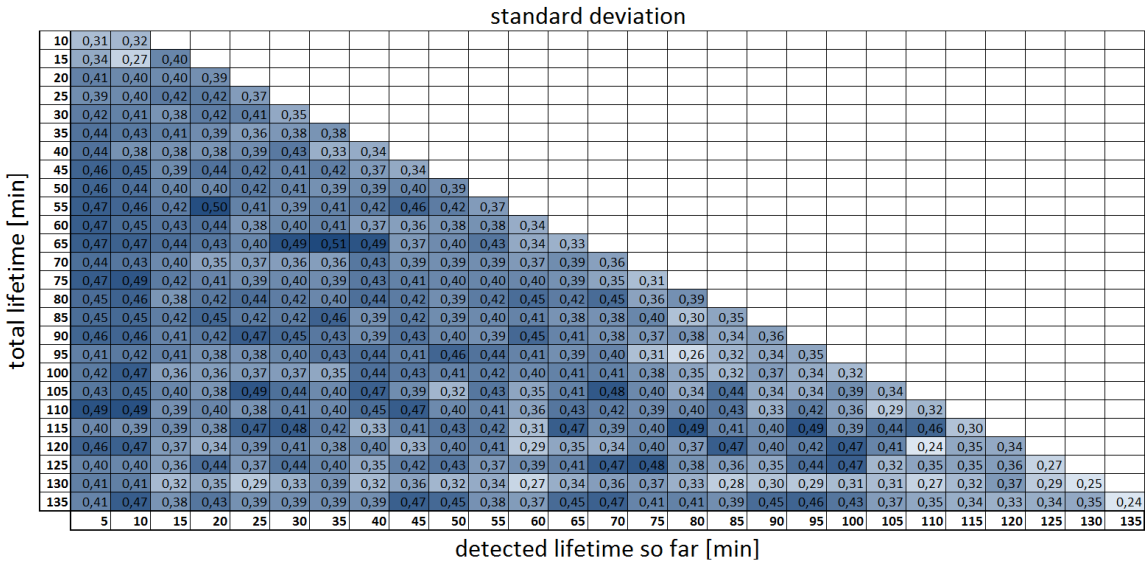

total lifetime [min] \ detected lifetime so far [min]	5	10	15	20	25	30	35	40	45	50	55	60	65	70	75	80	85	90	95	100	105	110	115	120	125	130	135
10	0,31	0,32																									
15	0,34	0,27	0,40																								
20	0,41	0,40	0,40	0,39																							
25	0,39	0,40	0,42	0,42	0,37																						
30	0,42	0,41	0,38	0,42	0,41	0,35																					
35	0,44	0,43	0,41	0,39	0,36	0,38	0,38																				
40	0,44	0,38	0,38	0,38	0,39	0,43	0,33	0,34																			
45	0,46	0,45	0,39	0,44	0,42	0,41	0,42	0,37	0,34																		
50	0,46	0,44	0,40	0,40	0,42	0,41	0,39	0,39	0,40	0,39																	
55	0,47	0,46	0,42	0,50	0,41	0,39	0,41	0,42	0,46	0,42	0,37																
60	0,47	0,45	0,43	0,44	0,38	0,40	0,41	0,37	0,36	0,38	0,38	0,34															
65	0,47	0,47	0,44	0,43	0,40	0,49	0,51	0,49	0,37	0,40	0,43	0,34	0,33														
70	0,44	0,43	0,40	0,35	0,37	0,36	0,36	0,43	0,39	0,39	0,39	0,37	0,39	0,36													
75	0,47	0,49	0,42	0,41	0,39	0,40	0,39	0,43	0,41	0,40	0,40	0,40	0,39	0,35	0,31												
80	0,45	0,46	0,38	0,42	0,44	0,42	0,40	0,44	0,42	0,39	0,42	0,45	0,42	0,45	0,36	0,39											
85	0,45	0,45	0,42	0,45	0,42	0,42	0,46	0,39	0,42	0,39	0,40	0,41	0,38	0,38	0,40	0,30	0,35										
90	0,46	0,46	0,41	0,42	0,47	0,45	0,43	0,39	0,43	0,40	0,39	0,45	0,41	0,38	0,37	0,38	0,34	0,36									
95	0,41	0,42	0,41	0,38	0,38	0,40	0,43	0,44	0,41	0,46	0,44	0,41	0,39	0,40	0,31	0,26	0,32	0,34	0,35								
100	0,42	0,47	0,36	0,36	0,37	0,37	0,35	0,44	0,43	0,41	0,42	0,40	0,41	0,41	0,38	0,35	0,32	0,37	0,34	0,32							
105	0,43	0,45	0,40	0,38	0,49	0,44	0,40	0,47	0,39	0,32	0,43	0,35	0,41	0,48	0,40	0,34	0,44	0,34	0,34	0,39	0,34						
110	0,49	0,49	0,39	0,40	0,38	0,41	0,40	0,45	0,47	0,40	0,41	0,36	0,43	0,42	0,39	0,40	0,43	0,33	0,42	0,36	0,29	0,32					
115	0,40	0,39	0,39	0,38	0,47	0,48	0,42	0,33	0,41	0,43	0,42	0,31	0,47	0,39	0,40	0,49	0,41	0,40	0,49	0,39	0,44	0,46	0,30				
120	0,46	0,47	0,37	0,34	0,39	0,41	0,38	0,40	0,33	0,40	0,41	0,29	0,35	0,34	0,40	0,37	0,47	0,40	0,42	0,47	0,41	0,24	0,35	0,34			
125	0,40	0,40	0,36	0,44	0,37	0,44	0,40	0,35	0,42	0,43	0,37	0,39	0,41	0,47	0,48	0,38	0,36	0,35	0,44	0,47	0,32	0,35	0,35	0,36	0,27		
130	0,41	0,41	0,32	0,35	0,29	0,33	0,39	0,32	0,36	0,32	0,34	0,27	0,34	0,36	0,37	0,33	0,28	0,30	0,29	0,31	0,31	0,27	0,32	0,37	0,29	0,25	
135	0,41	0,47	0,38	0,43	0,39	0,39	0,39	0,39	0,47	0,45	0,38	0,37	0,45	0,47	0,41	0,41	0,39	0,45	0,46	0,43	0,37	0,35	0,34	0,33	0,34	0,35	0,24

Figure 4.6: Table of *standard deviations* to define a tolerance interval around the predicted lifetime (calculation see text).

4.2 Verification of lifetime prediction

The verification of *LOC-lifetime* is performed using the Probability Of Detection (POD), False Alarm Ratio (FAR), as well as the Critical Success Index (CSI) and the Heidke Skill Score (HSS) defined in Chapter 2.4. Additionally, the Root-Mean-Squared Error (RMSE) is presented and a tolerance interval is used to evaluate the accuracy in min.

The following verification scores are calculated by the fuzzy logic-based model with an input consisting of four months out of the whole data set (June of 2016; May, June, and July of 2017; and June of 2018), whereby the fifth month is used as independent

data for nowcasting. This method is called *cross validation*. With respect to *LOC-lifetime* validation, the statistical values of all validation months are summed up and averaged.

Figure 4.7 shows the true frequency of the thunderstorms within certain lifetime classes that occurred in the analyzed period for each month. As depicted, the month of June 2016 contained 720 thunderstorms in total spread out over almost every lifetime class. In contrast, to the thunderstorm-weak month June of 2017 has only 213 detected thunderstorms.

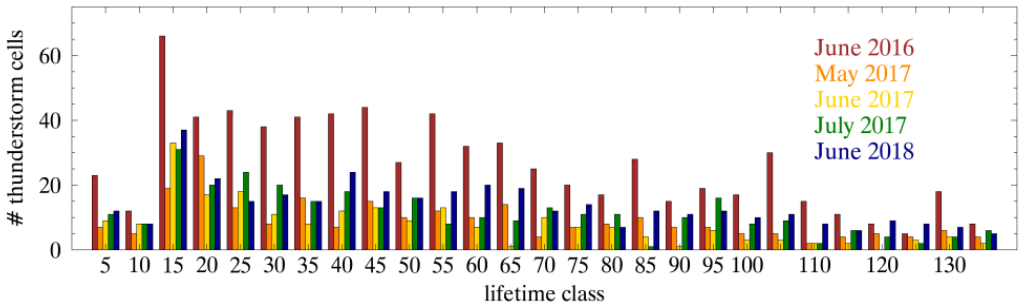

Figure 4.7: Frequency for every lifetime class in the analyzed month of June 2016 (total of 720 thunderstorms), May 2017 (243), June 2017 (213), July 2017 (306), and June 2018 (373).

Next, the remaining lifetime is calculated for every Cb-TRAM detection stop. Each thunderstorm's remaining lifetime is calculated with the newest available information at every 5 min time step. The upper figure in Figure 4.8 shows the POD and FAR for each lifetime class. To calculate the POD and FAR, *hits*, *misses*, and *false alarms* must be defined. A *hit* is defined as a remaining lifetime being equal to the observed lifetime, a *miss* occurs when an observed lifetime is not predicted, and a *false alarm* means that a remaining lifetime is falsely predicted. Hence, if the lifetime class is predicted correctly the POD is high. If a lifetime class is predicted that is not observed, the FAR of the predicted lifetime is larger. Now, nowcasted lifetimes are categorized as "correct" if they are equal to the observed lifetime, so no tolerance interval is added. As depicted in the figure, most of the cases are incorrectly predicted (yellow bars). Most lifetime classes that are correctly predicted, are in the range of 35 min up to 70 min. Remaining lifetimes greater than 100 min are very seldom predicted and never correctly. The high FAR of about 0.95 is due to the fact that only the correctly predicted remaining lifetimes are classified as "true" plus a temporal resolution of 5 min is very small for prediction. Therefore, it appears to make sense to create a tolerance interval around the predicted value, whereby the prediction of the remaining lifetime is classified as being correct if it is inside this tolerance interval. The tolerance interval is calculated for *LOC-lifetime* via the *standard deviations* presented in Figure 4.6.

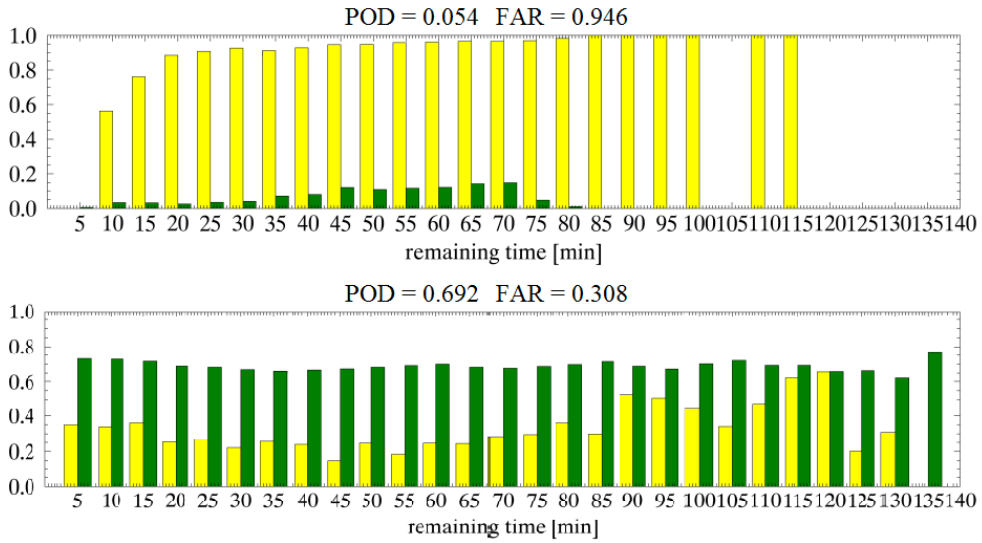

Figure 4.8: POD (green) and FAR (yellow) of *LOC-lifetime* output for the remaining lifetime for every lifetime class. The upper figure shows the output of an interval range of 0 min, and the lower figure shows the output for an interval range determined by he *standard deviation*.

The lower part of Figure 4.8 represents an example of the POD and FAR values of the prediction of a remaining lifetime with a tolerance interval calculated using the *standard deviation* (see Table 4.6). Hence, every fuzzy logic value is correct for a remaining lifetime within one *standard deviation* ($\pm$ value in Figure 4.6) around the predicted remaining lifetime at the detected lifetime so far, resulting in lower FAR values of about 0.31. Although the data set is independent of the defuzzification table, 69 % of the predictions are correct, indicating, that the variability within the single analyzed month can not be that high. In conclusion, the *LOC-lifetime* model appears to be robust for the analyzed period (in the case of the summer months May, June, and July).

In Figure 4.9, the tolerance interval in minutes is depicted for every remaining lifetime prediction category. It is assumed that the tolerance interval is similar to that produced by the *standard deviation*. In particular, the values of the *standard deviation* presented in Table 4.6 are translated here into a tolerance interval measured in minutes for the real remaining lifetime. Therefore, the importance of the *standard deviation* for the accuracy of the lifetime prediction is preserved. As expected the prediction of short remaining lifetimes is more accurate than of long remaining lifetimes (see Figure 4.9), as seen in an increased tolerance interval with an increased predicted lifetime. Therefore, to predict almost 68% of the lifetimes of 10 min correctly, a tolerance interval

of ±25 min is necessary. Whereas, since the prediction of a remaining lifetime of 105 min is less accurate, so a tolerance interval of almost ±40 min is necessary to obtain a POD of 68% for the prediction "105 min". This result is not surprising due to the fact that the quality of a prediction decreases with increasing prediction time.

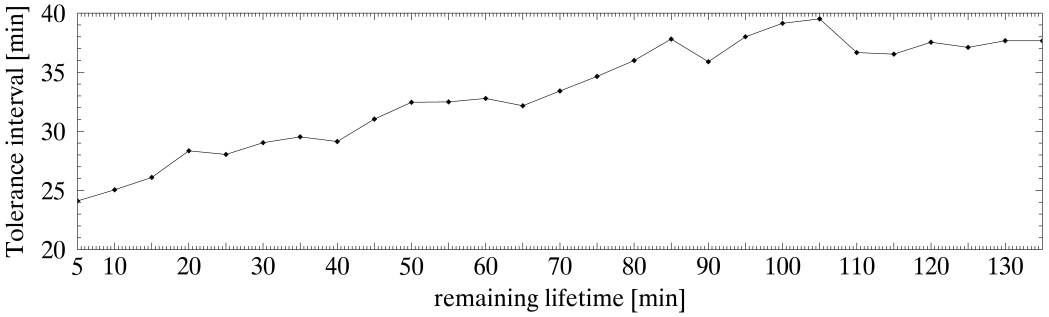

Figure 4.9: Averaged tolerance interval (in min) for lifetime predictions incorporating *standard deviation*.

The question that is now raised is: how many *standard deviations* are necessary to obtain usable predictions and how dependent is the quality of the nowcasting model on the tolerance interval?

In Figure 4.10, the POD, FAR, CSI, HSS, RMSE, and the corresponding tolerance interval are given for certain *standard deviations*. The tolerance interval indicates the time interval range for a certain multiple of the *standard deviation*. The RMSE is the corresponding time scale indicating the range that the predicted remaining lifetime is away from the real remaining lifetime. Due to the fact that all lifetime predictions are summed up here, the FAR is equal to the POD-1. This is the case because every *miss* is a *false alarm* elsewhere. Therefore, when considering all thunderstorm lifetime predictions, FAR and POD have complementary values. Additionally, the CSI is calculated while considering the *false alarms*, *hits*, and *misses* together. The HSS is calculated in order to obtain an accurate gain in the forecast relative to the forecast produced by random chance.

As mentioned in the previous section, an interval around the median of plus or minus one *standard deviation* contains about 68 % of all values. Similar percentages are examined over multiples of the *standard deviation* ranging from 0 to 4. The POD with no tolerance interval is very low, almost 0.05, and an HSS of about 0.025 indicates little prediction skill. The skill increases with an increasing tolerance interval. With a tolerance interval of width two *standard deviations* (multiple of 1), the POD is relatively high, indicating that large tolerance intervals are necessary. On average, using the *standard deviation* results in a tolerance interval of almost ≥ 25 min min. This high tolerance interval is not surprising, due to the large *standard deviations* compared to

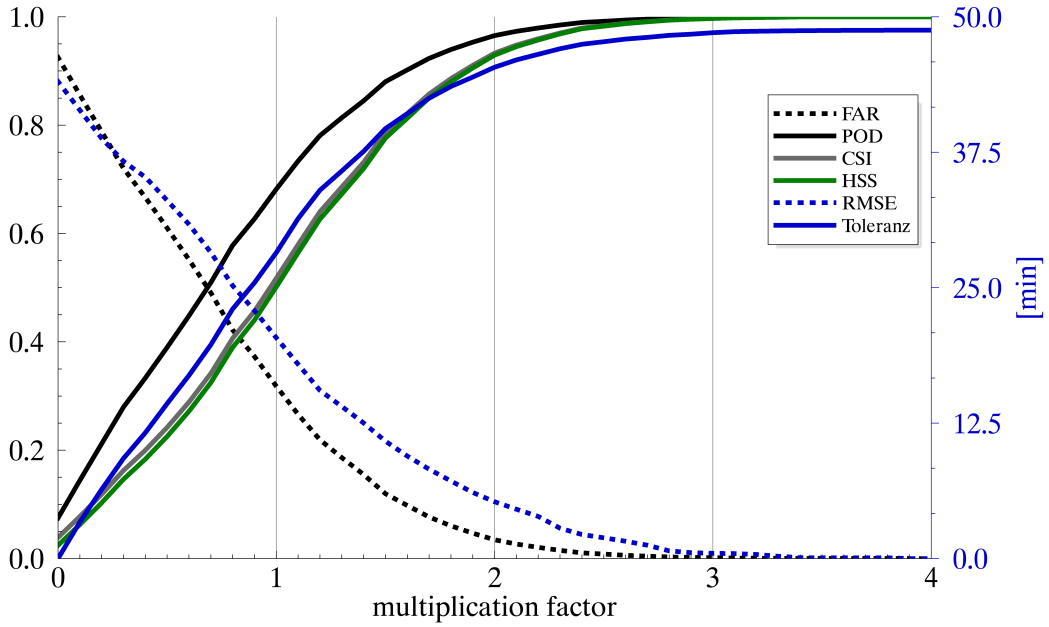

Figure 4.10: POD (solid black line), FAR (dashed black line), CSI (solid grey line), HSS (solid green line), RMSE (dashed glue line), and tolerance interval (solid blue line) of *LOC-lifetime* output for the "remaining lifetime", depending on the tolerance interval calculated with a certain multiple of the *standard deviation*.

the possible range, depicted in Table 4.6. The variability in thunderstorms life cycle is too high to obtain a more accurate prediction.

Consequently, a second remaining lifetime prediction is done by differentiating the thunderstorms into just the categories short-lived (< 60 min) and long-lived thunderstorms (≥ 60 min) and with no tolerance interval. This calculation only requires the values of the parameters at the fist detection time step. The results are depicted in the contingency table, Table 4.3. The prediction of the short-lived thunderstorms has a slightly lower POD (0.62) than the prediction of the long-lived thunderstorms (0.63). As the lifetime prediction for short-lived thunderstorms has a lower FAR value (0.29) than the lifetime prediction of long-lived thunderstorms (0.47), the prediction of short-lived thunderstorm might be more reliable. This suggestion is validated by the Gilbert Gill Score (GSS), which is an indicator of how well the forecast of the event corresponds to the real observed events in comparison with a statistical hit chance. The GSS for short-lived thunderstorms is about 0.3 and higher than that of the prediction of long-lived thunderstorms (0.13).

Correspondingly that the prediction of long-lived thunderstorms is over forecast (BIAS=1.2) and the prediction of short-lived thunderstorms is slightly under forecast (BIAS=0.9). Thus, the HSS is a measure of the accuracy of the forecasting

compared to the random chance of a correct prediction, which is calculated as well. The HSSs for the prediction of lifetimes, separated into the two categories short- and long-lived thunderstorms on the basis of the parameters at the first detection by Cb-TRAM, are about 0.25 (for both categories). Therefore, an improvement has been made over a random forecast. The prediction of short- and long-lived thunderstorms will be used to compare the results of the intensity prediction as presented in Chapter 4.3. Both predictions are based on information of the first detection step, therefore, the quality of lifetime prediction in comparison with the intensity prediction only based on the information of the first detection step can be evaluated.

Table 4.3: *Hits*, *misses*, *false alarms*, and *correct* negatives for the prediction of short-lived (< 60 min, left), and long-lived thunderstorms (≥ 60 min, right).

		Observed	
		YES	NO
forecast	YES	625	255
	NO	350	407

		Observed	
		YES	NO
forecast	YES	470	350
	NO	255	625

In conclusion, the prediction of the remaining lifetime has a very large range around the real lifetime, as indicated by the high RMSE for a tolerance interval range of 0. The quality of *LOC-lifetime* (remaining lifetime in 5 min interval) compared to the quality of other nowcasting models is presented in the following.

4.2.1 Comparison of the skill score values of simpler methods

Comparisons with the lifetime prediction abilities of previously existing nowcasting models must be made in order to identify the gain made by the newly developed nowcasting model *LOC-lifetime* for the nowcasting of thunderstorms. The newly developed nowcasting model provides two outputs: 1. current stage, and 2. remaining lifetime. The first output is more a definition of the actual stage and behavior of the thunderstorm than a prediction. There are no models yet, that characterize the current stage automatically. Therefore, a comparison of the ability of the nowcasting model to identify the current stage with other nowcasting models can not be done. Consequently, only the output "remaining lifetime" is compared to those of other nowcasting algorithms.

The core purpose of the related extrapolation algorithms is to predict the future displacement of a thunderstorm. There are a number of position extrapolating methods, but the remaining lifetime often is not included. Commonly, a fix time range is used to calculate the future location for this period. For instance, Cb-TRAM is able to

predict the future location for the next 60 min in 5 min intervals. Therefore, every thunderstorm is predicted to live another 60 min at every detection step.

The developed nowcasting model is able to calculate the remaining lifetime for every detected time step. Taking into account that the thunderstorm is predicted to have a remaining lifetime of 60 min at every detected time step, the POD is 0.038 (see Figure 4.11, purple line at 0). In this case, no tolerance interval is added.

The quality of the output "remaining lifetime" is compared to a random prediction that considers climatology information, i.e. it represents the probability of a lifetime occurrence based on a real frequency distribution. Considering the predictions during the whole life cycle, a POD of 0.037 is calculated. The HSS, depicted in Figure 4.10, has a value of 0.024 for a prediction without a tolerance interval.

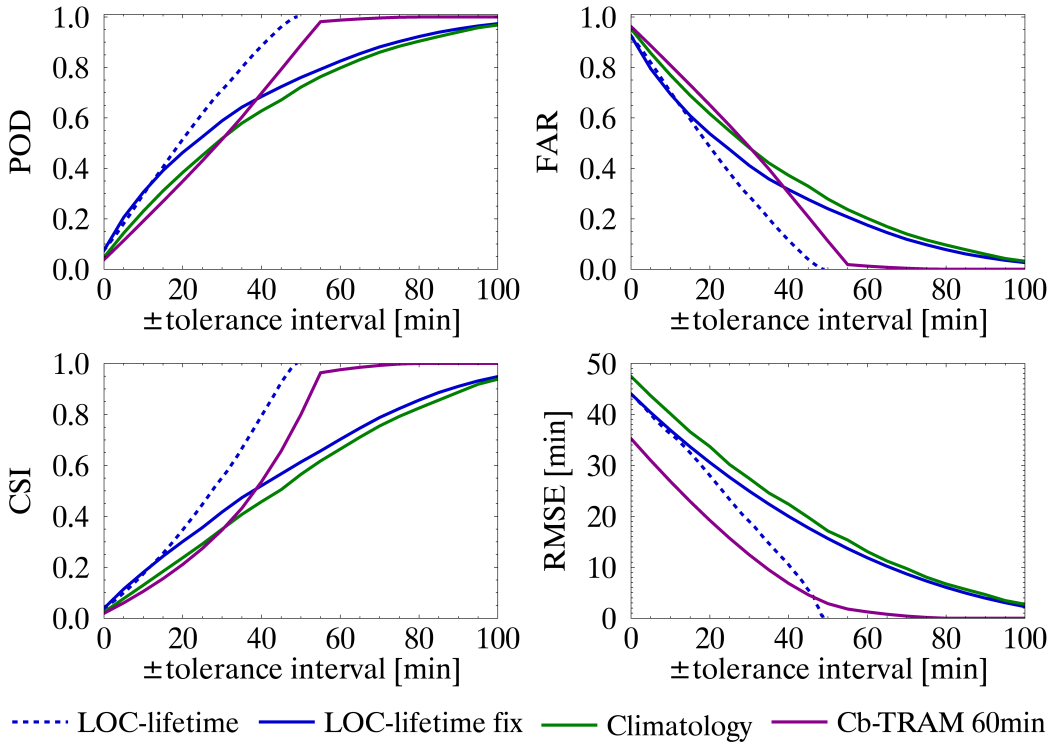

Figure 4.11: POD, FAR, CSI, and RMSE for the newly developed nowcasting model using the *standard deviation* (blue, dashed) and a fix tolerance interval (blue, solid), a random prediction using climatology information (green), and the Cb-TRAM nowcast that always expects the remaining lifetime to be 60 min (purple), depicted over the tolerance interval.

In Figure 4.11, the POD, FAR, CSI and RMSE are depicted for the newly developed nowcasting model for both; a fixed tolerance interval and a tolerance interval utilizing the *standard deviation*, in the cases of a random prediction of the remaining lifetime

utilizing climatology information and the Cb-TRAM assumption that every Cb-TRAM cell has a remaining lifetime of 60 min. The tolerance interval is calculated with the standard deviation for *LOC-lifetime*. The tolerance intervals used in the other methods are certain time ranges that are added to the predicted lifetime. Hence, a prediction with a tolerance interval indicating 50 min of remaining lifetime, is categorized as correct if the detected remaining lifetime lies in an interval of ±50 min around the predicted remaining lifetime.

The previously described POD values for a tolerance interval of 0 can be read off of Figure 4.11. The newly developed nowcasting model shows the best results for every tolerance interval, when its tolerance interval is calculating using the *standard deviation*. The prediction for *LOC-lifetime* with a fixed tolerance interval is, for small tolerance intervals, as good as the prediction obtained with a tolerance interval calculated using the *standard deviation*. For larger tolerance intervals (greater than 15 min), the improvement in the model when using the *standard deviation* to calculate the tolerance interval increases with an increasing tolerance interval. Therefore, *LOC-lifetime*, with its variable tolerance interval reaches, a POD of 1 for the lowest tolerance interval. The nowcasting of Cb-TRAM reaches a POD of 1 for the second-lowest tolerance interval. This result is not surprising because the remaining lifetime of 60 min is almost in the middle of the analyzed lifetime classes. Hence, the entire time range is covered by a tolerance interval of 60 min. The random prediction has the worst results for almost every tolerance interval. Results similar to those obtained for two other methods are found when the tolerance interval is very small. A related result shows the comparison of the RMSE values, which also depends on the tolerance interval. Additionally, the RMSE, FAR, and CSI values are shown. The improvement in the forecasting skill on the part of *LOC-lifetime* is visible in almost every statistical parameter. The RMSE is better for an assumption that the lifetime is always 60 min than *LOC-lifetime*. Such a result is not surprising because the largest difference between the predicted lifetime and the observed lifetime is about 75 min (if the remaining lifetime is 135 min). Due to the fact that these large differences do not occur very often, the RMSE is limited naturally to a prediction of 60 min.

In conclusion, the *LOC-lifetime* model predicts the remaining lifetime better than all the less sophisticated methods. Also, a reduced FAR is depicted. However, for high POD and CSI values and low RMSE and FAR values, very large tolerance intervals are needed. In the case of a tolerance interval calculated using the *standard deviation*, the interval is already about 25 min wide.

In Table 4.4, the statistical values are presented for every single verification month with the assumption that a tolerance interval using the *standard deviation* has been added. The verification months show very similar values. Therefore, it can be assumed that the quality of the life cycle model *LOC-lifetime* concerning the remaining lifetime prediction is relatively independent of the month used for verification. Consequently,

a data base of four months seems to be large enough to obtain a relatively robust result.

Table 4.4: Statistical values POD, FAR, and CSI describing the output quantitatively, with the RMSE used as a quality measure of the output for each month used as a verification month while the other months are used to determine the membership function thresholds and the *standard deviation*.

	POD	FAR	CSI	averaged tolerance interval	RMSE
June 2016	0.66	0.34	0.5	27 min	16 min
May 2017	0.68	0.32	0.51	28 min	17 min
June 2017	0.71	0.29	0.55	31 min	19 min
July 2017	0.74	0.26	0.59	33 min	23 min
June 2018	0.72	0.28	0.56	30 min	19 min

4.2.2 Sensitivity of nowcast to data sources

In the following section, the sensitivities concerning the data sources that are used as input, as well as the fuzzy set functions and thresholds are presented. The POD, FAR, CSI, RMSE and HSS for data sets based on different data sources or fuzzy logic set ups are depicted in Table 4.5. The relative skill differences in terms of percentages of the standard *LOC-lifetime* model with a tolerance interval of 0 are calculated for every statistical parameter. The standard *LOC-lifetime* is based on parameters from satellite, ground-based radar, lightning, and model data, which were selected in Chapter 4.1.1. The membership functions are linear, and the thresholds are calculated using the 25th, and 75th percentiles, as described previously. Now the results of *LOC-lifetime* based on a step function and thresholds defined by the 5th and 95th percentiles are compared with the output of the original *LOC-lifetime* model.

Data sources

LOC-lifetime inputs consisting of satellite, radar, lightning, and model data. The sensitivity of *LOC-lifetime* is tested for different data sources. Several runs are made, where, for each run, one data source is removed from the input data. First, the remaining lifetime is calculated with different data sources. Due to the fact that a thunderstorm is defined by a Cb-TRAM cell, satellite data is always crucial for the nowcasting. But the other satellite parameters can be left out of the input of the lifetime prediction. The POD, CSI, HSS, RMSE, and FAR are calculated for a tolerance

interval range of 0. The standard *LOC-lifetime* is based on the satellite parameters $A_{\tau>0.1}$, BT, and τ, the radar data parameter VIL, the parameter Li from the lightning observations, and the model parameters $CAPE$ and RH.

In Table 4.5, the POD, FAR, CSI, HSS, and RMSE for several runs are depicted, where, for each run, one data source is not considered in the calculations. Additionally, the output is validated for a data set consisting of all parameters, that were analyzed in Chapter 3.1.1. The radar data has the most positive effect on the *LOC-lifetime* output. Thus, the removal of radar data parameter VIL shows large adverse effects. The POD is reduced by 13.4 % compared to in the *LOC-lifetime* model. Additionally, the satellite parameters show the largest positive effects on the RMSE value. Therefore, leaving out the satellite parameters increases the RMSE by about 2.5 min. The model data parameters have almost no effect on the output. Leaving out of the model parameters only reduces the POD by about -0.4 %. In the case in which every parameter is considered in the *LOC-lifetime* model, the deterioration of the quality of the output is comparable to an omission of the lightning data. The result that all parameters contribute to lower POD, CSI, and HSS and to higher FAR and RMSE can be explained by the variability during the life cycle as shown in 3.1.1, which is higher for the parameters determined in Chapter 4.1.1.

Table 4.5: Percent difference in POD, FAR, CSI, RMSE, and HSS for the *LOC-lifetime* model for different set ups.

%	POD	FAR	CSI	HSS	RMSE
"LOC-lifetime"	0	0	0	0	0
No satellite	-1.9	0.2	-2.0	-7.3	2.5
No model	-0.4	0.0	-0.4	-0.9	0.3
No radar	-13.4	1.1	-13.8	-21.3	1.7
No lightning	-8.7	0.7	-9.1	-13.3	1.7
All analyzed parameters	-7.1	0.9	-8.5	-14.2	0.8
step fct	-4.4	0.4	-4.6	-11.1	1.8
0595 pctl	4.8	-0.4	5.0	7.1	-6.8
min/max	-38.9	2.9	-38.0	-78.1	2.8

Membership function

In Table 4.5, two more set ups are presented for a possible *LOC-lifetime* variation. One is the calculation of a membership function that has the shape of a step function, and the other is using the 5th and 95th percentiles to define the membership thresholds.

Since the basic model is based on a linear membership function, the opposite function type, a step function, was chosen here. Furthermore, it was chosen in such a manner

that it could detect the impact of the shape of the membership function on the *LOC-lifetime* output. With a step function, it is not possible that both categories can contain values above 0, i.e., there must be one category with a fuzzy logic value of 1 and another with a fuzzy logic value of 0. As seen in Table 4.5 the output of the model-based on the step function is worse than output obtained via the linear function-based model. This result is not surprising, since, when using a linear function, more detailed information is available.

Additionally, a larger range of overlap was chosen by using the 5th and 95th percentiles. This strategy shows improvement, over using the 25th and 75th percentiles to define the membership thresholds, indicating that the larger the range, the better the *LOC-lifetime* quality might be. The standard *LOC-lifetime* is based on the 25th and 75th percentiles because it was assumed that a wide range would be affected by outliers and might affect the model quality adversely. As depicted by the last row in Table 4.5, where the threholds for the membership functions are the minimum and maximum values of the parameters, the quality of the nowcasting decreases extremely if the range is set too large. Consequently the thresholds have to set carefully. As this sensitivity study hinted at an improved *LOC-lifetime* here, possible methods for finding suitable thresholds are discussed in Chapter 5.

All in all, the selection of data sources as well as the shape and calculation of the membership function, influence the quality and quantity of the *LOC-lifetime* model. In addition to the previous sensitivity categorizations, further thunderstorm features are expected to influence the nowcasting models output; these features will be described in Chapter 7.

4.3 First approach for intensity prediction

Until this point, the fuzzy logic nowcasting model was presented that can be used to predict the remaining lifetime of a thunderstorm. The question that raises now is: Is it sensible and possible to predict the future intensity of a thunderstorm via this method? The life cycle analyses in Chapter 3.3.2 showed that there is a difference in the averaged life cycles of *severe* thunderstorms ($\geq$ 46 dBZ) and *non-severe* thunderstorms ($<$ 46 dBZ), but they also showed large scatter. As shown in Chapter 4.2, it is possible to estimate whether a thunderstorm will last for a long time ($\geq$ 60 min) or for a short time ($<$ 60 min) with regard to the first Cb-TRAM detection step. Is it possible to predict the future intensity based only on information from the first detection step as well? For this purpose, the parameter information from the first detection from Cb-TRAM will be used in the prediction of the future intensity. This new approach is titled *LOC-intensity*. The output of the model *LOC-intensity* is separated into the classes *non-severe* and *severe*, as defined in Chapter 3.1.1. Thus, *LOC-intensity*

predicts, that a thunderstorm will develop high intensity ($\geq$ 46 dBZ) or low intensity ($<$ 46 dBZ). In the following, the parameters that are useful for *LOC-intensity* are selected and, afterwards, the fuzzy logic set up for *LOC-intensity* is described. Finally, the results of *LOC-intensity* are presented and validated.

Parameter selection for intensity prediction

Parameter selection for the intensity prediction is necessary because the parameters show on average, different characteristics in the life cycles of thunderstorm with high and low intensities. Thus, one aim is to calculate the intensity via information available at the first Cb-TRAM detection, the overlaps in the values of the parameters for *non-severe* and *severe* thunderstorms are calculated for the first detection step. In Figure 4.12, this overlap is depicted in percentages. The black symbols represent the percentage of the values for *severe* thunderstorms that are in the range of the 25th and 75th percentiles of *non-severe* thunderstorms. The grey symbols represent the percentage of *non-severe* thunderstorm overlapping the 25th and 75th percentile range of the *severe* thunderstorms. As seen in Figure 4.12, the overlap is large for all parameters, for example, BT has more than 80% overlap. This result is not surprising since the polygon of the percentiles in Figure 3.9 showed a large overlap already. Only the lightning values of *non-severe* thunderstorms and the lightning values of *severe* thunderstorms show an overlap of less than 50 %. The large number of overlapping values indicates that it is difficult to differentiate between *non-severe* and *severe* thunderstorms by using only the first detection step. As the aim of this study is to try to predict the future intensity at the first detection step, the parameters with the lowest overlaps are used for *LOC-intensity*. The criterion that must be fulfilled in order to be considered for intensity prediction is that both categories showing an overlap of less than 50%. This criterion is chosen because fuzzy logic is based on allocations to different categories via the values of the parameters. If no different values for some parameter exist, then it is not possible to differentiate between these categories.

As depicted in Figure 4.12, there are only two parameters that show an overlap of less than 50% between the two categories. Therefore, the parameters $CAPE$, and Li are chosen to predict the future intensity. The intensity life cycle study in Chapter 3.3.2 showed that there are lower values of $CAPE$ and Li for *non-severe* thunderstorms (on average) than for *severe* thunderstorms. The other parameters are eliminated due to the large overlaps for these parameters between *non-severe* and *severe* thunderstorms at the first detection step. No parameter from the satellite data shows an overlap of less than 50%, indicating that satellite parameter values from the first Cb-TRAM detection step are not suited for future intensity predictions. Consequently, no satellite and radar parameters are considered for *LOC-intensity*. Thus, only the information available at the first Cb-TRAM detection is considered in LOC-intensity, and no temporal change information is used for intensity prediction.

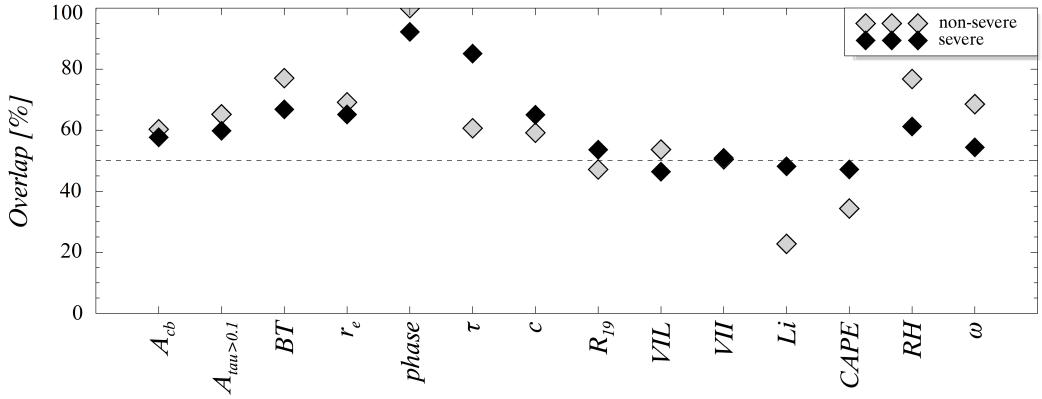

Figure 4.12: Overlap in percentage of *severe* thunderstorms with the 25th and 75th percentiles for the *non-severe* thunderstorms (black), and overlap in percentages of the *non-severe* thunderstorms with the 25th and 75th percentiles for the *severe* thunderstorms (grey).

Prediction of future intensity

Fuzzification The fuzzification of the input data for the calculation of the future intensity is more or less equivalent to the fuzzification of the input data for calculating the remaining lifetime and current stage of a thunderstorm. The input data are different due to the predictive skills of the parameters concerning the thunderstorm's intensity. As described above, the input parameters $CAPE$ and Li are used to calculate the intensity. Next, the thresholds of the membership functions are calculated by using the 25th percentiles of the parameters (seen in Figure 3.9) at the first Cb-TRAM detection step, to define the lowest threshold allocated to *severe* and the 75th percentiles to define the highest value for which a thunderstorm is allocated to the *non-severe* category.

Combination The fuzzified inputs are then numbers between 0 and 1 for the fuzzy sets *non-severe* and *severe* for each of the parameters Li and $CAPE$. To combine the input data, the values of the fuzzy set *non-severe* are summed up, as are the values of the set *severe*. Therefore, the tendency of each intensity class is calculated at the first detection step. Finally, there is one value between 0 and 2 for the set *severe*, and one value between 0 and 2 for the fuzzy set *non-severe* (since the fuzzified inputs of the two parameters $CAPE$ and Li are summed up).

Defuzzification The defuzzification for the calculation of the intensity differs from the defuzzification of the remaining lifetime calculation. Here, the defuzzification is done via the maximum-method, i.e, the maximum value of each category is found, and the category with the highest maximum over all categories is chosen for prediction. So,

if the category *non-severe* has a fuzzy value of 1.5, and the class *severe* has a fuzzy value of 0.5, then the predicted future intensity is *non-severe*. If both classes have the same fuzzy output, then *severe* will be predicted. In the following section, how often the nowcasting model predicts the intensity classes *non-severe* and *severe* is shown.

Verification of intensity prediction

The intensity prediction is categorized into the two classes *non-severe* (low intensity, < 46 dBZ) and *severe* (high intensity, ≥ 46 dBZ). The selected parameters $CAPE$ and Li are used to calculate this output using only the first detection time step of Cb-TRAM. The calculation is based only on this time step because the highest intensity is reached very early, as seen in the previous life cycle analyses. Thus, later time steps only show the actual high or low intensities and therefore have no predictive skill.

The following results are based on the thunderstorms in the analyzed period. In Figure 4.13, the number of *severe* and *non-severe* thunderstorms is presented for every month in the analyzed period. As depicted in this figure, the most thunderstorms occurred in the month of June 2016. This information was also presented in previous figures. In every analyzed month, *non-severe* thunderstorms occurred more frequently than *severe* thunderstorms. The ratio of the *non-severe* thunderstorms to the *severe* thunderstorms is almost 5 : 2. This ratio is more or less the same for all analyzed months.

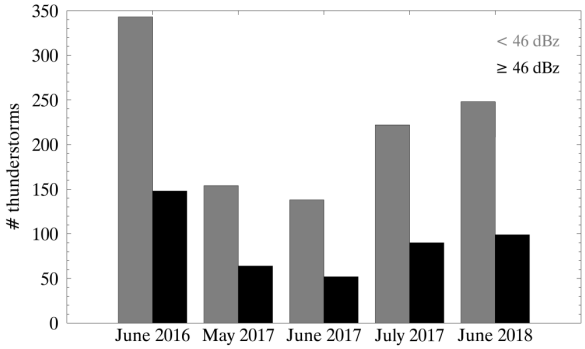

Figure 4.13: Number of thunderstorms with *non-severe* and *severe* intensities for each month in the analyzed period.

Due to the cross validation above, it is possible to use a data set consisting of five independent validation months and therefore five different model runs. The results of these runs are presented in the contingency tables 4.6 for the prediction of *non-severe* thunderstorms and 4.7 for the prediction of *severe* thunderstorms. In each, the results of the five independent model runs are summed up.

Next, it is possible to calculate the POD, CSI, BIAS, HSS, GSS, and FAR for the prediction of *non-severe* thunderstorms by using the values in the contingency table. The

Table 4.6: *Hits, misses, false alarms,* and *correct negatives* for the prediction of *non-severe* thunderstorms.

		observed	
		YES	NO
forecast	YES	543	182
	NO	642	280

intensity of every thunderstorm that occurred during the analyzed period encompassing June of 2016, May; June, and July of 2017; and June of 2018 is predicted, resulting in a POD of 0.46, CSI of 0.39, BIAS of 0.62, HSS of 0.05, GSS of 0.62 and FAR of 0.25 for the prediction of *non-severe* thunderstorms on the basis of the first detection with Cb-TRAM and the values of the parameters Li and $CAPE$ at this time. Although the POD is not very high, the prediction of the *non-severe* intensity has a relatively low FAR. Only every fourth prediction is false. The value of BIAS indicates that *non-severe* thunderstorms are under forecast. Additionally, the GSS - representing a random forecast containing the probability of a hit - is low, thus indicating that the prediction does not have much predictive skill, as confirmed by a HSS near 0.

The same analysis is done for the prediction of *severe* thunderstorms. They are not as frequent as *non-severe* thunderstorms. By using the values in Table 4.7, POD, CSI, BIAS, HSS, GSS, and FAR can be calculated. The prediction *severe* has POD of 0.6, CSI of 0.25, BIAS of 1.95, HSS of 0.05, GSS of 0.03 and FAR of 0.69. The high FAR indicates that *severe* thunderstorms might be over predicted. This over-prediction is also indicated by a BIAS of 1.95. The weak predictive skill is confirmed by the low values of GSS and HSS. Compared to the prediction of *non-severe* thunderstorms, the prediction of *severe* thunderstorms is worse.

These statistical values point out, that the differences in Li and $CAPE$ between *non-severe* and *severe* thunderstorms at the first detection time step is not that high for each individual thunderstorm, as it was suggested previously. It is noticeable that the life cycles of the thunderstorms with different intensities differ greatly within the single analyzed month. Consequently, the nowcasting for all five analyzed months, showed better results than the nowcasting via cross validation (nowcasting the month not included in the basic data set). These results are discussed further in Chapter 5.

4.4 Summary of the nowcasting

Basis for the nowcasting of the lifetime (*LOC-lifetime*) and intensity (*LOC-intensity*) are the results of the life cycle analyses in Chapter 3. In order to be considered for the *LOC-lifetime* model, the parameters have to fulfill two criteria. First, the individual life

Table 4.7: *Hits, misses, false alarms,* and *correct negatives* for the prediction of *severe* thunderstorms.

		observed	
		YES	NO
forecast	YES	280	642
	NO	182	543

cycle stage characteristics have to be present in the 25th, and 75th percentiles as well. Second, the parameters must have correlation coefficients of less than 0.9 with other parameters. During parameter selection, it was decided to use the satellite parameters BT, τ, and $A_{\tau>0.1}$; the ground-based radar parameter VIL; the lightning parameter Li; and the model parameters RH and $CAPE$ in the fuzzy logic-based *LOC-lifetime* model. The results for the lifetime prediction indicate that *LOC-lifetime* shows better results than the extrapolation-based Cb-TRAM algorithm. Cb-TRAM assumes that every thunderstorm has 60 min more to live at every detection step. If no tolerance interval is considered, the FAR is reduced by 0.2 % when using *LOC-lifetime* instead of Cb-TRAM. When a tolerance interval using the *standard deviation* is included, gain is produced for *LOC-lifetime* that increases as the tolerance interval grows. For example, when a tolerance interval of 20 min is considered, the FAR is reduced by 27 % when using *LOC-lifetime* instead of Cb-TRAM. Additionally, improvements in CSI and POD were shown. Thus, high tolerances are needed to reach applicable FAR and POD values, a separation into the categories short-lived (< 60 min) and long-lived (≥ 60 min) thunderstorms, takes place. Next, only the first detection step was used for nowcasting. The results indicate that the first detection step contains enough information to obtain a nowcasting of the lifetime that is better than a random nowcasting using the frequencies of the remaining lifetimes. This improvement is shown by the HSS which is about 0.25 (no tolerance interval added). The large tolerance intervals for the reliable lifetime prediction are necessary, due to the high variability in thunderstorms. This variability may occur due to the consideration of several thunderstorm organization types as well as technically limits (cloud masking).

The sensitivity of *LOC-lifetime* was evaluated as well. In doing so, one data source was left out for every run, and the linear membership function was replaced by a step function. In another run, the membership thresholds were based on the 5th and 95th percentiles instead of the previously used 25th and 75th percentiles. The results of this sensitivity study show that the model parameters are not necessary for the prediction of the remaining lifetime. Radar and satellite data have the most positive impact on the model quality, and better results are obtained when using the 5th and 95th percentile values for the thresholds. This might be the case because using a larger range of thresholds means that more detailed information is obtained; accordingly, the usage of a step function for the membership function shows worse results than using

the linear function.

In addition to nowcasting the remaining lifetime, a fuzzy logic-based model was developed to predict future thunderstorm intensity using only the first detection step (for lead time for warnings). *LOC-intensity* uses the intensity classes *non-severe* (< 46 dBZ) and *severe* (≥ 46 dBZ). Thus, the prediction is based on parameter values from the first detection step only. The criterion for the parameters that are used in the model is that there should be overlaps in parameter values that are as small as possible for *non-severe* and *severe* thunderstorm at the first detection step. The analysis showed that there exists a large overlap ($> 50\%$) for almost every parameter. This result indicates that it will be difficult to predict the intensity on just the basis of the first detection step. The parameters with the smallest overlaps between these two intensity classes were the observational parameter Li and the model parameter $CAPE$. Hence, these two parameters are used to predict the future intensity. In the end, *LOC-intensity* did not prove to be better than a random forecast (HSS=0.05). Possible reasons for such a low skill are discussed in Chapter 5.

In a nutshell, for high tolerance intervals *LOC-lifetime* shows reliable results. The model parameters $CAPE$ and RH show the smallest positive impacts on the quality of *LOC-lifetime*. It is possible to predict the remaining lifetimes but not the future intensities with the information obtained in the first detection step only.

5 Discussion

Several results shown in this thesis are influenced by the peculiarities of observational data sets and of the combination method. Some of these influences are inevitable others could perhaps be improved by additional efforts. In the following, these points as well as consistencies and inconsistencies with the literature are discussed.

The shorter the observed lifetime, the stronger the statistical results are influenced by thunderstorms which do not develop in a clear non-precipitating environment, but within or at least indistinguishably close to systems already existing. For instance at the beginning of the observed life cycles Brightness Temperature (BT) is high for long-lived cells and low for short-lived cells. Together with the other satellite observations of cloud optical thickness (τ), effective radius (r_e), Area of the Cb-TRAM cell (A_{cb}) and ice fraction at the cloud top ($phase$), it becomes obvious that the reason for this difference in BT is high cloud cover masking the formation of new convective cells until they can be identified as individual updrafts. While satellite observed parameters suggest that optically thick clouds are already present at high altitudes at this point of first detection of the "short-lived thunderstorm" category, the missing lightning activity still points to relatively young convective developments. To some extent this is all influenced by the core definition of a "thunderstorm object" based on satellite data. While this seems to be the correct interpretation, as it facilitates the seamless integration of early stages and late stages of a convective life cycle with no or weak unspecific precipitation and no lightning observations, limitations of the satellite based detection process become apparent. Nevertheless, the life cycle analyses were done with respect to a thunderstorm nowcasting and since the thunderstorms (Cb-TRAM objects) that were nowcasted contain the same technical and observational limits, they have to be considered in the life cycle analyses. Thus, the influence to the nowcasting models *LOC-lifetime* is classified as low as the life cycle analyses act as input data for nowcasting of such object oriented cells. Consequently, excluding such incomplete life cycles, for example, by adding a threshold of BT might reduce the variability of the life cycle but might also reduce the quality of the nowcasting models *LOC-lifetime* and *LOC-intensity*, since the input data of the nowcasting models do not contain the variability of the life cycles of thunderstorms detected with a satellite based method.

The parameter maximum reflectivity (R_{max}) shows very high reflectivities already at the beginning of the thunderstorm life cycle. Unfortunately, this hampers the possibility to distinguish between the convective environment with scattered precipitating cells and

the new developments. To remove these incorrect assignments, it would be necessary to isolate reflectivities that only exist in the Cb-TRAM cell. This would be possible, if the radar output of the DWD, in which every measurement point of the radar is available, was used. However, this inaccurate allocation of reflectivities to thunderstorms only has impact on the life cycle, but not on the nowcasting because R_{max} is not used there. In the nowcasting, the only radar parameter considered in *LOC-lifetime* is the Vertically Integrated Liquid water (VIL). The values of VIL are very low compared to reports in the literature, for example, in Amburn and Wolf (1997). The low VIL values can be explained by the mathematical method that was used to assign VIL to the corresponding thunderstorm. The average of the highest 10% of values inside the Cb-TRAM cell was calculated. If the Cb-TRAM cell is extended over a large area (this is the case in mature stage) 10% correspond to many pixels. If extreme high values of VIL exist only for a few pixel, the average of 10% blurs the high values. Amburn and Wolf (1997) used the maximum VIL value and therefore get higher VIL than with the method used in this thesis. The impact of the method used here on the nowcasting of *LOC-lifetime* is low, since the nowcasting model is based on the averaged life cycle calculated with the same method.

The correlation of a thunderstorms size with its lifetime as described in the life cycle analyses was also shown in Mathon and Laurent (2001) and Feng et al. (2012). A correlation between lightning occurrence and thunderstorm area, that was described in Mattos and Machado (2010), was also found in this study. Thunderstorms with larger areas had a higher frequency of lightning occurrence.

The model parameters do not show specific development characteristics during the single life cycle stages. The reason for that might be the way model parameters were allocated to the thunderstorms. The model data pixels inside the Cb-TRAM cell and, additionally, inside a radius of 50 km around the Cb-TRAM cell were considered for the analyses. This enlarged area is used, due to a possible shift in time and space that may exist in the model data, as the model data is not accurate enough to resolve these small scale processes at the exact right location and time. Therefore, it is not surprising that specific local life cycles are represented not very exactly in the model. Therefore, an enhanced updraft indicated by an increasing R_{max} that correlates with growing r_e, as it was observed by Setvák and Doswell (1991) can not be seen in this data. This is the case because in the Setvák and Doswell (1991) study, the updraft was physically measured and in this life cycle analysis the updraft - represented by vertical velocity at 700 hPa (ω) - is a model parameter.

As one aim of this thesis is to predict the future lifetime, it is crucial to identify differences in the life cycle of long- and short-lived thunderstorms. For this purpose, all lifetime classes were normalized to one lifetime progress. Hence, the life cycle stages are selected independently of the lifetime class. Therefore, every stage of short-lived thunderstorms has the same percentage portion of the life cycle as long-

lived thunderstorms. On average, the common characteristics can be assigned to the life cycle in the analyzed data. However, this separation does not work for every single thunderstorm contour since the duration of a stage can differ depending on the environmental conditions. It is necessary to consider that the life cycle stages of short-lived thunderstorms are presented by less data points than that of long-lived thunderstorms. For instance, thunderstorms lasting for 10 min contain only 2 data points that represent a life cycle consisting of four stages after the normalization. Consequently, the life cycle of especially very short-lived thunderstorms is difficult to depict completely. Nevertheless, the impact of the life cycle of the short-lived thunderstorms is considered to be low for the prediction since *LOC-lifetime* and *LOC-intensity* are based on the 25th and 75th percentiles averaged over all lifetimes and the number of short-lived thunderstorms considered in the analyses is very low.

Since the life cycle analyses are often affected by a missing detection of the earlier life cycle stages due to cloud masking, and since frontal environments often show large cloud cover, the thunderstorm life cycle was analyzed separately for frontal and non-frontal environments. As suspected, the life cycles differ from each other. The life cycle of frontal thunderstorms does not show as strong characteristics as of non-frontal thunderstorms. This might be the case due to the previously mentioned cloud masking. However, only thunderstorms in June of 2016 were analyzed due to the time-consuming identification of the synoptic situation. The low number of thunderstorms considered in this analysis might affect the results. It would be beneficial to analyze additional month and consequently more thunderstorms in the same way.

Additionally, the thunderstorm life cycle was analyzed for non-severe (< 46 dBZ) and severe (≥ 46 dBZ) thunderstorms. Severe thunderstorms show much higher values of Area inside A_{cb} where $\tau > 0.1$ ($A_{\tau>0.1}$), R_{max}, VIL, Vertically Integrated Ice (VII), and Lightning detection (Li), Convective Available Potential Energy ($CAPE$), and Relative Humidity at 700 hPa (RH) over the life cycle than non-severe thunderstorms. Kitzmiller et al. (1995) already showed that the areal expansion as well as the VIL can be used to distinguish between severe and non-severe thunderstorms.

The validation of the nowcasting model *LOC-lifetime* showed that it is difficult to predict the remaining lifetime accurately if a prediction to the minute is expected. The nowcasting model *LOC-lifetime* showed higher Probability Of Detection (POD) and lower False Alarm Ratio (FAR) values than existing extrapolation techniques, although, large tolerance intervals were needed to reach high POD and low FAR values. These large tolerance intervals indicate the high variability of the thunderstorm life cycle. An averaged tolerance interval of 30 min is needed to predict 68% of the remaining lifetimes correctly. Already the variability analysis in Chapter 3.2 indicates the highly variable life cycle that happens on the one hand due to the consideration of several thunderstorm organization types and on the other hand due to a miss of parts of

the life cycle, for example, because of cloud masking. Advantageous for *LOC-lifetime* prediction is that the basic data set is also affected by these technical peculiarities.

These high variabilities due to missing development stages affect the results of *LOC-intensity* as well, leading to an unreliable prediction of the future intensity based on information available at the first detection step. Already the selection of the parameters that show differences between *non-severe* and *severe* thunderstorms was difficult due to the large degree of overlap between *non-severe* and *severe* thunderstorm contours. As mentioned before, *LOC-intensity* is a first approach for intensity prediction via fuzzy logic. Only the values of the first Cb-TRAM detection step were used for nowcasting, resulting in low POD, critical success index (CSI), and high FAR values. Further, the Heidke Skill Score (HSS) indicated almost no skill (HSS=0.05). This is the case, because more than one third of the thunderstorms that reach 46 dBZ (or more) during their life cycle already show 46 dBZ (or more) before their first detection by Cb-TRAM. The time of the first occurrence of 46 dBZ (or greater) during the Cb-TRAM detection is depicted in Figure 5.1. About 10% of the 46 dBZ (or more) reaching cells show already 46 dBZ or more -30 min or earlier before Cb-TRAM detects a thunderstorm for the first time. The bar at -30 min represents thunderstorms showing reflectivities higher or equal to 46 dBZ at -30 min. The -30 min time point shows an especially high percentage due to severe thunderstorm occurrence in frontal systems. In such frontal systems, high reflectivity values are present over a long period leading to an incorrect allocation of reflectivity to the backward-extrapolated thunderstorm. In addition, frontal systems cover developing thunderstorms, and as a consequence the thunderstorm is already well developed at its first detection. This indicates that the satellite based detection of Cb-TRAM might be not an appropriate thunderstorm definition for intensity prediction. Mecikalski et al. (2016) presented a study about thunderstorm intensity prediction. They mainly used the geostationary satellite parameters cloud top temperature and effective radius to predict severe storms. They used the "European Severe Weather Database reports" to detect severe weather and tracked the clouds manually to avoid cloud-tracking errors. The aim was, to calculate whether or not a thunderstorm will be intense during the next 2-3 hours after its convective initiation. The HSS values of the prediction of Mecikalski et al. (2016) shows better results (HSS=0.14) than *LOC-intensity* (HSS=0.05). This might be the case due to the fact that in Mecikalski et al. (2016) the beginning of a thunderstorm is defined by a certain reflectivity threshold and furthermore an already well developed thunderstorm is excluded. This "not object-oriented" thunderstorm definition might be necessary for an intensity prediction early in the life cycle.

As a result, the late detection of severe thunderstorms by Cb-TRAM is one reason for the low skill of *LOC-intensity*. Consequently, a thunderstorm definition based on Cb-TRAM detection might not be a suited definition of such weather events with respect to the intensity prediction. An earlier detection of convective regions would probability improve a future intensity prediction.

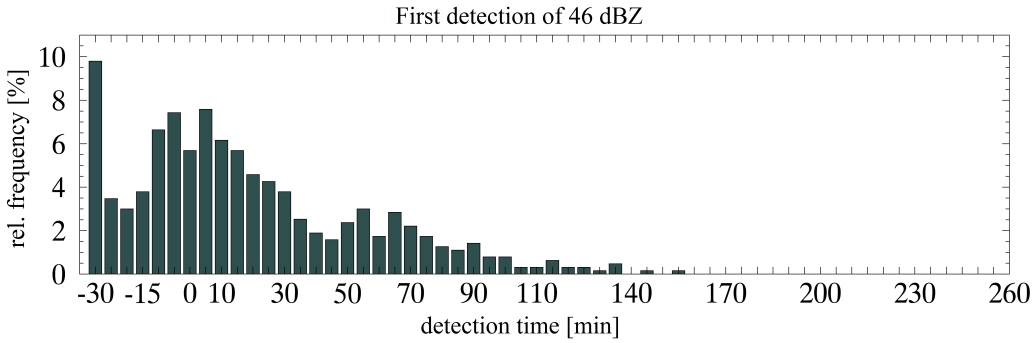

Figure 5.1: The relative frequency of the first detected 46 dBZ contour during Cb-TRAM detection is depicted. Detection time 0 indicates the first detection by Cb-TRAM and -30 min refers to 30 min before Cb-TRAM detection. Only severe storms ($\geq$ 46 dBZ) were selected.

For lead time for warnings the predictive skill of Cb-TRAM was evaluated for the quality of the nowcasting models *LOC-intensity* and *LOC-lifetime* based on the information of the first detection step. To sum up, no statement can be made by *LOC-intensity* about the future intensity at the first Cb-TRAM detection step (HSS=0.05) since many of the *severe* thunderstorms already reached high reflectivities. Nevertheless, the model *LOC-lifetime* showed that it is possible to make a prediction of the remaining lifetime at the first detection step by separating into the categories short- and long-lived. An HSS of 0.25 indicates that there is a gain for the lifetime prediction by using the fuzzy logic based model compared to a random prediction. Consequently, a Cb-TRAM based thunderstorm definition is suited for the prediction of remaining lifetime rather than for the intensity prediction.

6 Conclusion

In this thesis the life cycle of thunderstorms - where thunderstorms are defined as Cb-TRAM detection and consequently contain several thunderstorm organization types - was analyzed in observational and model data. This was done to validate the first hypothesis of this thesis "the life cycle or lifetime characteristics of thunderstorms are present in observational and model data". Additionally to the characteristics of the single life cycle stages, the differences between short- and long-lived thunderstorms in satellite, ground-based radar, lightning, and model data was analyzed with the purpose to use the results in a thunderstorm nowcasting. This was done to test the second hypothesis "the usage of a life cycle description improves the lifetime prediction of thunderstorms compared to existing extrapolation methods as present in a reduced False Alarm Ratio (FAR)". For validation of the second hypothesis a fuzzy logic-based nowcasting model was developed predicting the remaining lifetime.

Following the first hypothesis, parameters from observational and model data should show characteristics for single life cycle stages (early development, advanced development, mature, and decay) or lifetime. Main findings of the life cycle analyses are that parameters from observational data show characteristics in the different life cycle stages, while the life cycle stages can not be identified by using only model data. Although not every observational parameter could be used to differentiate between all four defined life cycle stages, at least one stage could always be identified. A qualitative overview is depicted in Figure 6.1. The behavior of every analyzed parameter is shown for the single life cycle stages. Additionally, an overview of life cycle stage information content and potential use for single life cycle stage identification is given. The last column shows information whether or not the parameter can be used for lifetime prediction.

The thunderstorm life cycle stages can be differentiated via observational data. Stage I (early development) is characterized by a decreasing BT and an increasing τ, r_e, $phase$, VIL and Li, for example. The subsequent stage, stage II (advanced development), shows a strongly decreasing BT, a horizontal ($A_{\tau>0.1}$) growth and ongoing glaciation ($phase$). The parameter Li increases and r_e as well as VIL show a maximum during this stage. Most of the observational parameters show a maximum during stage III (mature). The following stage IV (decay) is characterized by a decrease in almost every parameter and an increase in BT. The analyzed observational parameters originate from satellite, ground-based radar, and lightning measurements. On average, every satellite parameter

Data source	Param.	Stage I	Stage II	Stage III	Stage IV	Life cycle	Lifetime
Satellite	BT	↘	↘	→	↗	✓	✓
	$A_{\tau>0.1}$	→	↗	↗ ↘	↘	✓	✓
	τ	↗	↗	→	↘	✓	✓
	r_e	↗	↗ ↘	↘	↘	(✓)	
	PHA	↗	↗	→	→	(✓)	
Radar	VII/VII	↗	↗ ↘	↘	↘	(✓)	✓
	R_{max}	↗	↗	↗ →	↘	✓	✓
	$ARef_{46}$		↗	↗ ↘	↘	✓	✓
LINET	LI		↗	↗ ↘	↘	✓	✓
COSMO-DE	$CAPE$	↘	↘	↘	↘		✓
	RH	↗	↗	↗	↗		✓
	ω	↘	↘	↘	↘		

Figure 6.1: Analyzed data sources with corresponding parameters and averaged behavior during the four life cycle stages (early development, advanced development, mature, and decay). Life cycle and lifetime column: Checks indicate parameters containing information for life cycle stage, identification or lifetime prediction. Bracketed checks indicate parameters that can not be used to identify every life cycle stage (but at least one). The stages containing maximum or minimum are shaded in grey.

shows life cycle stage dependent characteristics enabling an identification of at least one stage.

In the following, the thunderstorm life cycle illustrated by model parameters is compared to the hypothesis. Therefore, the parameters $CAPE$, RH at 700 hPa and ω at 700 hPa were analyzed over the life cycle, in the same manner as the observational data. As described in Figure 6.1, no temporal changes occurred between the life cycle stages in the model parameters. Over the whole life cycle analyzed an almost constant decrease of $CAPE$ and ω was observed. The parameter RH increases slightly over the thunderstorm life cycle.

In addition to the characteristics of the single life cycle stages in the multi-sourced data set, the life cycle differences between short- and long-lived thunderstorms were analyzed. As mentioned previously, parameters containing certain lifetime information show a check in the column "lifetime" in Figure 6.1. Only the observational parameters BT, $A_{\tau>0.1}$, and τ from the satellite data, the radar parameters VII, VIL, R_{max}, and Area of the 46 dBZ contour (RA_{46}), and the lightning parameter Li show lifetime related

information. Furthermore the model parameters $CAPE$ and RH showed lifetime dependent information. Short-lived thunderstorms showed lower $CAPE$ and higher RH values than long-lived thunderstorms. As explained earlier, no characteristic temporal changes during the life cycle were identified. Since this lifetime information is available already at the first detection step, it might be useful for lifetime prediction. The model parameter ω did not show any lifetime related characteristics that are comparable robust and, therefore, was not used for lifetime prediction.

To summarize, hypothesis I "Model and observational data are able to represent the thunderstorm life cycle or to indicate the lifetime" is valid for observational and model data sources. While observational parameters are able to represent the thunderstorm life cycle and tho indicate the lifetime, model parameters are not accurate enough in space and time to visualize single life cycle stages. Nevertheless, observational as well as model parameters contain lifetime related information.

The second hypothesis implies an improved thunderstorm nowcasting by the fuzzy logic-based, life cycle information containing model compared to extrapolation methods. For verifying this hypothesis several statistical values were calculated and compared to simpler nowcasting methods. The extrapolation method, as it is mentioned in hypothesis II, is the lifetime nowcasting of the algorithm Cb-TRAM. In Cb-TRAM a thunderstorm's location is always nowcasted for 60 min. As no lifetime information is available the thunderstorm will last for a fixed period (60 min). Consequently, the lifetime model is compared to the results of a nowcasting that always predicts a remaining lifetime of 60 min. If no tolerance interval is considered, the FAR of *LOC-lifetime* is about 0.95, and the FAR of Cb-TRAM is about 0.97. Concluding, the fuzzy logic-based model *LOC-lifetime* shows a reduced FAR compared to the lifetime prediction of the extrapolation method based Cb-TRAM algorithm.

This reduction of FAR equals almost 2 %. The improvement of *LOC-lifetime* compared to the lifetime prediction of Cb-TRAM increases with a growing tolerance interval calculated by adding the standard deviation with a certain multiplication factor. Adding a tolerance interval of 20 min around the predicted lifetime, the improvement of *LOC-lifetime* is about 27 % compared to Cb-TRAM (since FAR of *LOC-lifetime* is about 0.49 and FAR of Cb-TRAM is about 0.69).

The model quality depends on the choice of membership threshold definition, as indicated by a sensitivity study. Using a larger threshold difference results in a higher model quality, as the 5th and 95th percentiles showed, for example, lower FAR for *LOC-lifetime* than the model output based on the 25th and 75th percentiles. However, the thresholds can be choosen too large as the sensitivity study with the maximum and minimum values indicated. Additionally, the set of parameters affect the model quality. Especially the radar parameter VIL improves the lifetime prediction for the fuzzy logic-based model. Therefore, the results of *LOC-lifetime* are dependent on the set of parameters that were selected via different criteria regarding life cycle characteristics

and correlation. Consequently, other parameter sets or parameter criteria would influence the quality of the model output, similarly to the definition of the fuzzy logic membership functions.

To conclude, the nowcasting of thunderstorm lifetime by using the life cycle information containing fuzzy logic-based model *LOC-lifetime* showed better statistical values than a lifetime prediction without life cycle information, for example, by the extrapolation based algorithm Cb-TRAM. However, large tolerance intervals are needed to reach low FAR values. These large tolerances are necessary, due to the high variability of thunderstorms during their life cycle. Along with this, the textbook life cycle of growth, mature, and decay is present only in 19 % of all analyzed thunderstorms. This result indicates, that the quality of *LOC-lifetime* is restricted by the high variability of the thunderstorm life cycle. Nevertheless, the multi-sourced data set showed an improvement compared to the usage of a data set consisting of less data sources.

While the previously mentioned possibility of a miss of the early development of the thunderstorm life cycle and the consideration of several organization types might be problematic for the life cycle analyses and *LOC-lifetime*, it is necessary to consider the thunderstorms as they were actually detected by Cb-TRAM - since this is the actual thunderstorms definition. Excluding non-textbook life cycles, for example, by adding a threshold indicating an early development stage would be contradicting to the goal to use the actually available data for prediction.

The new developed model for lifetime prediction of thunderstorms is able to improve the thunderstorm nowcasting, as shown. Since thunderstorms are highly variable and complex systems the contribution to a better quality of thunderstorm nowcasting is small but might lead to a more accurate prediction. As the sensitivity study has shown, some data sources are more relevant for such an - in time and space high resolved - prediction than others. This information might be beneficial for further research.

7 Outlook

The presented analyses about the life cycle of thunderstorms in *frontal* and *non-frontal* situations indicated, on average, life cycle related differences between those two categories. The nowcasting model *LOC-lifetime* does not differentiate between these synoptic situations yet. If information about the current synoptic situation is available, incorporation into *LOC-lifetime* via an adapted data input is likely to improve the quality of *LOC-lifetime*. In case the synoptic situation can be identified, the input data for *LOC-lifetime* can be adapted. Consequently, if *frontal* environment dominates, then the life cycle of thunderstorms in *frontal* environment can be used as input data and vice versa for a *non-frontal* environment. As seen in Chapter 3.3, the life cycle characteristics of BT are not as strong for thunderstorms in a *frontal* environment than in *non-frontal* environment. Thus, a new algorithm has to be developed to be able to determine the actual synoptic situation. This algorithm could separate the historical thunderstorms into the two categories and consequently the life cycle characteristics for both synoptic situations could be evaluated. The algorithm could further be used in *LOC-lifetime* to identify which averaged life cycle characteristic is more likely for the current synoptic situation.

One result of *LOC-intensity* is that it is not possible to predict the future intensity by using only the information of the first Cb-TRAM detection step. The reason for this is a delayed detection of thunderstorms by Cb-TRAM leading to a first detection although the thunderstorm is already classified as *intense* (in about 30% of the cases). Consequently, another thunderstorm definition has to be used for intensity prediction. One possibility might be to define different areas of convective regions that are likely for thunderstorm development resulting in a possibly earlier detection of thunderstorms in their life cycle. The future intensity of these regions could then be predicted. Such a "no object-oriented" definition should be more applicable for intensity prediction.

As shown in the sensitivity study, the definition of the membership thresholds for the fuzzy logic-based nowcasting of the lifetime affects the model quality. The usage of the 25th and 75th percentiles as well as the usage of the maximum and minimum values showed worse results than the usage of the 5th and 95th percentiles. This leaves the question, which thresholds would show the best results for *LOC-lifetime*. An answer could be found by implementing an artificial neural network that calculates the best thresholds for the model, although, it is possible that percentiles are not the best way to define the thresholds. The combination of fuzzy logic and the threshold definition

via the methods of artificial neural networks is called “Neuro-Fuzzy” and is already used in weather forecasting (Deg-Hyo et al., 2007).

The life cycle analyses as well as the developed nowcasting models *LOC-lifetime* and *LOC-intensity* are based on the assumption that a thunderstorm is equal to a Cb-TRAM cell. For the life cycle analyses an extended period of -30 min before and 60 min after detection by Cb-TRAM was considered to try to detect the whole life cycle. Consequently, the results of the life cycle analyses and the fuzzy logic-based nowcasting models are dependent on the Cb-TRAM algorithm and, therefore, also convey its uncertainties as well. As seen in the life cycle analyses the thunderstorms are in some cases not detected at the beginning but later in the life cycle. This delayed detection of convection may happen due to an overlaying cloud mask that impedes the detection of the early development. This miss of the early life cycle phases of a developing thunderstorm due to cloud obscuration is a fundamental limit of the satellite detection. Therefore, it would be interesting, if the definition by another thunderstorm tracking algorithm not based on satellite data, for example, the radar data based algorithms Rad-TRAM or KONRAD, would show similar results for the life cycle analyses and the nowcasting. Concluding, it would be vital to test other tracking algorithms in order to evaluate the reliability of the results of this thesis and to transfer found characteristics of the life cycle to other nowcasting methods.

Acronyms and Symbols

A_{cb}	Area of the Cb-TRAM cell
$A_{\tau>0.1}$	Area inside A_{cb} where $\tau > 0.1$
ANC	Auto-Nowcast Sytem
APICS	Algorithm for the Physical Investigation of Clouds with SEVIRI
B	Buoyancy
BT	Brightness Temperature
$CAPE$	Convective Available Potential Energy
Cb − TRAM	Cumulonimbus Tracking And Monitoring
CG	Cloud-to-Ground
CI	Convective Initiation
CIN	Convective Inhibition Energy
COALITION	COntext And scaLe orIented Thunderstorm satellIte predictOrs developmeNt
COSMO − D2	COnsortium for Small scale MOdeling with a grid spacing of 2.2 km has been operated since May 2018
COSMO − DE	COnsortium for Small scale MOdeling with a grid spacing of 2.8 km operated until May 2018
CSI	Critical Success Index
DC	Deep Convection
DLR	Deutsches Zentrum fr Luft- und Raumfahrt e.V.
DMC	Deep Moist Convection
DWD	Deutscher Wetterdienst
EL	Level of Equilibrium
FAR	False Alarm Ratio

FCL	Free Convective Layer
g	gravitational force
GSS	Gilbert Skill Score
HRV	High Resolution Visible channel
HSS	Heidke Skill Score
IC	Intra Cloud
IR	Infra-Red channel
LF	Low Frequency
Li	Lightning detection
LI	Lifted Index
LINET	European ground-based Lightning Network
$LOC - intensity$	Model for intensity prediction
$LOC - lifetime$	Model for remaining lifetime prediction and actual stage calculation
NIR	Near Infra-Red
NWP	Numerical Weather Prediction
ω	vertical velocity at 700 hPa
PC	Pre-Convection
POD	Probability Of Detection
PPI	Plan Position Indicator scan
$phase$	ice fraction at the cloud top
r_e	effective radius
R_{max}	maximum reflectivity
RA_{46}	Area of the 46 dBZ contour
Rad − TRAM	Radar Tracking and Monitoring
RH	Relative Humidity at 700 hPa
RMSE	Root Mean Squared Error
s	*standard deviation*

SEVIRI	Spinning Enhanced Visible and Infra-Red Imager
SI	Showalter Index
τ	cloud optical thickness
TITAN	Thunderstorm Identification and Tracking, Analysis and Nowcasting
T	temperature of a parcel
T'	temperature of the surrounding environment
UTC	Universal Time Coordinated
c	propagation velocity
VII	Vertically Integrated Ice
VIL	Vertically Integrated Liquid water
VIS	Visible channel
VLF	Very Low Frequency
WV	Water Vapor channel
z	height
z_{EL}	height of the equilibrium level
z_{LFC}	height of the level of free convection

List of Figures

List of Tables

Bibliography

Adler, R. F. and Fenn, D. D. (1979). Thunderstorm Intensity as Determined from Satellite Data. *Journal of Applied Meteorology*, 18:502–517. https://doi.org/10.1175/1520-0450(1979)018%3C0502:TIADFS%3E2.0.CO;2.

Amburn, S. A. and Wolf, P. L. (1997). VIL Density as a Hail Indicator. *Weather and Forecasting*, 12(3):473–478. https://doi.org/10.1175/1520-0434(1997)012%3C0473:VDAAHI%3E2.0.CO;2.

Baldauf, M., Stephan, K., Klink, S., Schraff, C., Seifert, A., Förstner, J., Reinhardt, T., and Lenz, C.-J. (2006). The new very short range forecast model LMK for the convection-resolving scale. *Second THORPEX International Science Symposium*, Volume of extended abstracts Part B:148–149.

Bergeron, T. (1935). On the physics of clouds and precipitation. *Proces Verbaux de l'Association de Mètèorologie*, pages 156–178.

Betz, H.-D., Schmidt, K., Laroche, P., Blanchet, P., Oettinger, W. P., Defer, E., Dziewit, Z., and Konarski, J. (2009). LINET - An international lightning detection network in Europe. *Atmospheric Research*, 91(2-4):564–573. doi: 10.1016/j.atmosres.2008.06.012.

Brooks, H. and Dotzek, N. (2008). The spatial distribution of severe convective storms and an analysis of their secular changes. *Climate Extremes and Society*, pages 35–53. doi: 10.1017/CBO9780511535840.006.

Bugliaro, L., Zinner, T., Keil, C., Mayer, B., Hollmann, R., Reuter, M., and Thomas, W. (2011). Validation of cloud property retrievals with simulated satellite radiances: a case study for SEVIRI. *Atmospheric Chemistry Physics*, 11(12):5606–5624. doi: 10.5194/acp-11-5603-2011.

Byers, H. R. and Braham Jr., R. R. (1948). Thunderstorm structure and circulation. *Journal of Meteorology*, 5(3):71–86. doi: https://doi.org/10.1175/1520-0469(1948)005%3C0071:TSAC%3E2.0.CO;2.

Cintineo, R. M. and Stensrud, D. J. (2013). On the Predictability of Supercell Thunderstorm Evolution. *Journal of Atmospheric Science*, 70:1993–2011. doi: https://doi.org/10.1175/JAS-D-12-0166.1.

Darden, C. B., Nadler, D. J., Carcione, B. C., Blakeslee, R. J., Stano, G. T., and Buechler, D. E. (2010). Utilizing total lightning information to diagnose convective trends. *Bulletin of American Meteorological Society*, 91(2):167–175. doi: https://doi.org/10.1175/2009BAMS2808.1.

Davini, P., Bechini, R., Cremonini, R., and Cassardo, C. (2012). Radar-Based Analysis of Convective Storms over Northwestern Italy. *Atmosphere*, 3(1):33–58. doi: 10.3390/atmos3010033.

Deg-Hyo, B., Jeong, D. M., and Kim, G. (2007). Monthly dam inflow forecasts using weather forecasting information and neuro-fuzzy technique. *Hydrological Science Journal*, 52(1):99–113. doi: 10.1623/hysj.52.1.99.

Dixon, M. and Wiener, G. (1993). TITAN: Thunderstorm identification, tracking, analysis, and nowcasting - A radar based methodology. *Journal of Atmospheric Oceanic Technology*, 10(6):785–797. https://doi.org/10.1175/1520-0426(1993)010%3C0785:TTITAA%3E2.0.CO;2.

Doswell III, C. A. (1985). The operational meteorology of convective weather, Volume II: Storm scale analysis. *national oceanic and atmospheric administration*, page 240 p.

Doswell III, C. A. (2001). Severe Convective Storms - An Overview. *Meteorologicas Monographs*, (50):1–26. https://doi.org/10.1175/0065-9401-28.50.1.

Dvorak, V. R. (1975). Tropical Cyclone Intensity Analysis and Forecasting from Satellite Imagery. *Monthly Weather Review*, 130:420–430. https://doi.org/10.1175/1520-0493(1975)103%3C0420:TCIAAF%3E2.0.CO;2.

Emanuel, K. A. (1994). *Atmospheric Convection*. Oxford Press. ISBN 0-19-506630-8.

Farnell, C., Rigo, T., and Pineda, N. (2017). Lightning jump as a nowcast predictor: Application to severe weather events in Catalonia. *Atmospheric Research*, 183:130–141. http://dx.doi.org/10.1016/j.atmosres.2016.08.021.

Feng, Z., dong, X., Xi, B., McFarlane, S. A., Kennedy, A., Ling, B., and Minnis, P. (2012). Life cycle of midlatitude deep convective systems in a Lagrangian framework. *Journal of geophysical Research*, 117(D23201). doi: 10.1029/2012JD018362.

Feynman, R. P., Leighton, R. B., and Sands, M. (1964). Electricity in the atmosphere. The Feynman Lectures on Physics. Vol. II: Mainly Electromagnetism and Matter. *Addison-Wesley, Reading, MA*, page 11 pp.

Findeisen, W. (1938). Die kolloidmeteorologischen Vorgänge bei der Niederschlagsbildung. *Meteorologische Zeitschrift*, 55:131–133.

Foote, G. B. (1985). Aspects of cumulonimbus classification relevant to the hail problem. *Journal de recherches atmosphériques.*, 19:61–74.

Forster, C., Ritter, A., Gemsa, S., Tafferner, A., and Stich, D. (2016). Satellite-Based Real-Time Thunderstorm Nowcasting for Strategic Flight Planning En Route. *Journal of Air Transportation*, 24(4):113–124. DOI:10.2514/1.D0055.

Freud, E., d. Rosenfeld, Andreae, M. O., Costa, A. A., and Artaxo, P. (2008). Robust relations between CCN and the vertical evolution of cloud drop size distribution in deep convective clouds. *Atmospheric Chemistry and Physics*, 8:1661–1675. https://doi.org/10.1175/1520-0434(1998)013%3C1148:ABCOSD%3E2.0.CO;2.

Galway, J. G. (1956). The lifted index as a predictor of latent instability. *Bulletin of American Meteorological Society*, 37:528–529. https://doi.org/10.1175/1520-0477-37.10.528.

Goodman, S. J., Buechler, D. E., and Meyer, P. J. (1988). Convective Tendency Images Derived from a Combination of Lightning and Satellite Data. *Weather and Forecasting*, 3:173–188. https://doi.org/10.1175/1520-0434(1988)003%3C0173:CTIDFA%3E2.0.CO;2.

Goodman, S. J. and MacGorman, D. R. (1986). Cloud-to-Ground Lightning Activity in Mesoscale Complexes. *Monthly Weather Review*, 114:2320–2328. https://doi.org/10.1175/1520-0493(1986)114%3C2320:CTGLAI%3E2.0.CO;2.

Greene, D. R. and Clark, R. A. (1972). Vertically integrated liquid Water - A New Analysis Tool. *Monthly Weather Review*, 100(7):548–552. https://doi.org/10.1175/1520-0493(1972)100%3C0548:VILWNA%3E2.3.CO;2.

Han, L., Sund, J., Zhang, W., Xiu, Y., Feng, H., and Lin, Y. (2017). A machine learning nowcasting method based on real-time reanalysis data. *Journal of Geophysical Research: Atmosphere*, 122:4038–4051. doi: 10.1002/2016JD025783.

Hansen, B. K. (1997). SIGMAR: a fuzzy expert system for critiquing marin forecasts. *AI Applications*, 11(1):59–68.

Hansen, B. K. (2007). A Fuzzy Logic-Based Analog Forecasting System for Ceiling and Visibility. *Weather and Forecasting*, (22):1319–1330. https://doi.org/10.1175/2007WAF2006017.1.

Hartung, D. C., Sieglaff, J. M., Cronce, L. M., and Feltz, W. F. (2013). An intercomparison of UW Cloud-Top Cooling Rates with WSR-88D Radar Data. *Weather and Forecasting*, 28:463–480. https://doi.org/10.1175/WAF-D-12-00021.1.

Helmert, K., Tracksdorf, P., Steinert, J., Werner, M., Frech, M., Rathmann, N., Hengstebeck, T., Mott, M., Schumann, S., and Mammen, T. (2014). DWDs new radar network and post-processing algorithm chain. *Proc. Eighth European Conf. on Radar in Meteorology and Hydrology (ERAD 2014)*. http://www.pa.op.dlr.de/erad2014/programme/ExtendedAbstracts/237_Helmert.pdf.

Hertl, S. and Schaffar, G. (1998). An autonomous approach to road temperature prediction. *Meteorological Applications*, 5(3):227–238. https://doi.org/10.1017/S1350482798000838.

Hoffmann, J. M. (2008). Entwicklung und Anwendung von statistischen Vorhersage-Interpretationsverfahren für Gewitternowcasting und Unwetterwarnungen unter Einbeziehung von Fernerkundungsdaten. *Dissertation, FU-Berlin*, page 205pp.

Höller, H. (1994). Mesoscale Organization and Hailfall Characteristics of Deep Convection in Southern Germany. *Beiträge zu Physik der Atmosphäre - Contributions to Atmospheric Physics*, 67(3):219–234. http://elib.dlr.de/31866/1/94-hoeller.pdf.

Huntrieser, H., Schiesser, H., Schmid, W., and Waldvogel, A. (1997). Comparison of Traditional and Newly Developed Thunderstorm Indices for Switzerland. *Weather and Forecasting*, 12:108–125. https://doi.org/10.1175/1520-0434(1997)012%3C0108:COTAND%3E2.0.CO;2.

Jurković, P. M., Mahović, N. S., and Počakal, D. (2015). Lightning, overshooting top and hail characteristics for strong convective storms in Central Europe. *Atmospheric Research*, 161-162:153–168. http://www.sciencedirect.com/science/article/pii/S0169809515001155.

Kitzmiller, D. H., McGovern, W. E., and Saffle, R. F. (1995). The WSR-88D Sevre Weather Potential Algorithm. *Weather and Forecasting*, 10:141–159. https://doi.org/10.1175/1520-0434(1995)010%3C0141:TWSWPA%3E2.0.CO;2.

Kober, K. and Tafferner, A. (2009). Tracking and Nowcasting of convective cells using remote sensing data from radar and satellite. *Meteorologische Zeitschrift*, 18(1):75–84. https://dx.doi.org/10.1127/0941-2948/2009/359.

Lang, P. (2001). Cell tracking and warning indicators derived from operational radar products. *30th Conf. Radar Met., Munich, Germany, AMS Boston*, pages 245–247.

Leekwijck, W. V. and Kerre, E. E. (1999). Defuzzification: criteria and classification. *Fuzzy Sets and Systems*, 108(2):159–178. https://doi.org/10.1016/S0165-0114(97)00337-0.

Liu, W. and Li, X. (2016). Life cycle characteristics of warm-season severe thunderstorms in central united states from 2010 to 2014. *Climate*, 4(45). doi: 10.3390/cli4030045.

Machado, L. A. T., Rossow, W. B., Guedes, R. L., and Walker, A. W. (1997). Life Cycle Variations of Mesoscale Convective Systems over the Americas. *Monthly Weather Review*, 126(6):1630–1654. https://doi.org/10.1175/1520-0493(1998)126%3C1630:LCVOMC%3E2.0.CO;2.

MacKeen, P. L., Brooks, H. E., and Elmore, K. L. (1998). Radar Reflectivity-Derived Thunderstorm Parameters Applied to Storm Longevity Forecasting. *Weather and Forecasting*, 14:289–295. https://doi.org/10.1175/1520-0434(1999)014%3C0289:RRDTPA%3E2.0.CO;2.

Markowski, P. and Richardson, Y. (2010). *Mesoscale meteorology in midlatitudes*. John Wiley & Sons.

Mathon, V. and Laurent, H. (2001). Life cycle of Sahelian mesoscale convective cloud systems. *Quarterly Journal of the Royal Meteorological Society*, 127(572):377–406. https://doi.org/10.1002/qj.49712757208.

Mattos, E. V. and Machado, L. A. T. (2010). Cloud-to-ground lightning and Mesoscale Convective Systems. *Atmospheric Research*, 99:377–390. doi:10.1016/j.atmosres.2010.11.007.

Mecikalski, J., Bedka, K., and König, M. (2012). Best Practice Document. *EUMETSAT Convection Working Group*, Version 2.0.

Mecikalski, J., Rosenfeld, D., and Manzato, A. (2016). Evaluation of geostationary satellite observations and the development of a 1-2h prediction model for future storm intensity. *Journal of Geophysical Research: Atmosphere*, 121:6374–6392. doi:10.1002/2016JD024768.

Mecikalski, J., Watts, P. D., and König, M. (2011). Use of Meteosat Second Generation optimal cloud analysis field for understanding physical attributes of growing cumulus clouds. *Atmospheric Research*, 102(1-2):175–190. https://doi.org/10.1016/j.atmosres.2011.06.023.

Mecikalski, J., Williams, J. K., Jewett, C. P., Ahijevych, D., LeRoy, A., and Walker, J. (2015). Probabilistic 0-1-h Convective Initiation Nowcasts that Combine Geostationary Satellite Observations and Numerical Weather Prediction Model Data. *Journal of applied meteorology and climatology*, 54:1039–1059. doi:10.1175/JAMC-D-14-0129.1.

Mikus, P. and Mahovic, N. S. (2013). Satellite-based overshooting top detection methods and analysis of correlated weather conditions. *Atmospheric Research*, 123:268–280. https://doi.org/10.1016/j.atmosres.2012.09.001.

Mueller, C., Saxen, T., Roberts, R., Wilson, J., Betancourt, T., Dettling, S., Oien, N., and Yee, J. (2003). NCAR Auto-Nowcast System. *Weather and Forecasting*, 18:545–561. https://doi.org/10.1175/1520-0434(2003)018%3C0545:NAS%3E2.0.CO;2.

Murphy, A. H. (1998). The Early History of Probability Forecasts: Some Extensions and Clarifications. *Weather and Forecasting*, 13:5–15. https://doi.org/10.1175/1520-0434(1998)013%3C0005:TEHOPF%3E2.0.CO;2.

Nisi, L., Ambrosetti, P., and Clementi, L. (2014). Nowcasting severe convection in the Alpine region: the COALITION approach. *Quarterly Journal of the Royal Meteorological Society*, 140:1684–1699. DOI:10/1002/qj.2249.

Pope, M., Jakob, C., and Reeder, M. J. (2008). Convective Systems of the North Australian Monsoon. *Journal of Climate*, 21:5091–5512. https://doi.org/10.1175/2008JCLI2304.1.

Rädler, A. T., Groenemeijer, P. H., Faust, E., Sausen, R., and Pùčik, T. (2019). Frequency of severe thunderstorms across Europe expected to increase in the 21st century due to rising instability. *Climate and Atmospheric Science*, 2(30). https://doi.org/10.1038/s41612-019-0083-7.

Rasmussen, E. N. and Blanchard, D. O. (1998). A Baseline Climatology of Sounding-Derived Supercell and Tornado Forecast Parameters. *Weather and Forecasting*, 13:1148–1164. https://doi.org/10.1175/1520-0434(1998)013%3C1148:ABCOSD%3E2.0.CO;2.

Reynolds, S. E., Brook, M., and Gourley, M. F. (1957). Thunderstorm Charge Separation. *Journal of Meteorology*, 14:426–436. https://doi.org/10.1175/1520-0469(1957)014%3C0426:TCS%3E2.0.CO;2.

Roberts, R. D. and Rutledge, S. (2003). Nowcasting Storm Initiation and Growth Using GOES-8 and WSR-88D Data. *Weather and Forecasting*, 18(4):562–584. https://doi.org/10.1175/1520-0434(2003)018%3C0562:NSIAGU%3E2.0.CO;2.

Rosenfeld, D., Woodley, W. L., Lerner, A., and Kelman, G. (2008). Satellite detection of severe convective storms by their retrieved vertical profiles of cloud particle effective radius and thermodynamic phase. *Journal of geophysical research*, 113:D04208. DOI:10.1029/2007JD008600.

Sander, J. (2011). Extremwetterereignisse im Klimawandel: Bewertung der derzeitigen und zukünftigen Gefährdung. *Faculty of Physics, Disseration, LMU München*, page page 125pp.

Saunders, C. P. (1993). A Review of Thunderstorm Electrification Processes. *Journal of Applied Meteorologic Climatology*, 32:642–655. https://doi.org/10.1175/1520-0450(1993)032%3C0642:AROTEP%3E2.0.CO;2.

Schumann, U. (2012). Atmospheric Physics. *Research Topics in Aerospace*. DOI:10.1007/978-3-30183-4.

Senf, F. and Deneke, H. (2017). Satellite-Based Characterization of Convective Growth and Glaciation and its Relationship to Precipitation Formation over Central Europe. *Journal of Applied Meteorologic Climatology*, 56:1827–1845. https://doi.org/10.1175/JAMC-D-16-0293.1.

Senf, F., Dietzsch, F., Huenerbein, A., and Deneke, H. (2015). Characterization of Initiation and Growth of Selected Severe Convective Storms over Central Europe with MSG-SEVIRI. *Journal of Applied Meteorologic Climatology*, 54:207–224. https://doi.org/10.1175/JAMC-D-14-0144.1.

Setvák, M. and Doswell, C. A. (1991). the AVHRR Channel 3 Cloud Top Reflectivity of Convective Storms. *Monthly Weather Review*, 119:841–847. https://doi.org/10.1175/1520-0493(1991)119%3C0841:TACCTR%3E2.0.CO;2.

Showalter, A. K. (1953). A stability index for thunderstorm forecasting. *Bulletin of American Meteorological Society*, 34(6):250–252. https://doi.org/10.1175/1520-0477-34.6.250.

Stich, D. (2013). Convection initiation. *Faculty of Physics, Disseration, LMU München*. https://nbn-resolving.org/urn:nbn:de:bvb:19-157194.

Sun, J., Xue, M., Wilson, J. W., Zawadzki, I., Ballard, S. P., Onvlee-Hooimeyer, J., Joe, P., Barker, D. M., Li, P., Golding, B., Xu, M., and Pinto, J. (2014). Use of NWP for nowcasting convective precipitation: Recent progress and challenges. *Bulletin of American Meteorology*, 95:209–426. https://journals.ametsoc.org/doi/abs/10.1175/BAMS-D-11-00263.1.

Tafferner, A., Forster, C., Hagen, M., Keil, C., Zinner, T., and Volkert, H. (2008). Development and propagation of severe thunderstorms in the Upper aube catchment area: Towards an integrated nowcasting and forecasting system using real-time data and high-resolution simulations. *Meteorology and Atmospheric Physics*, 101(3-4):211–227. doi: 10.1007/s00703-008-0322-7.

Tessendorf, S. A., Millder, L. J., Wiens, K. C., and Rutledge, S. A. (2005). The 29 June 2000 Supercell Observed during STEPS. Part I: Kinematics and Microphysics. *Journal of Atmosphäreic Science*, 62:4127–4150. https://doi.org/10.1175/JAS3585.1.

Wallace, J. M. and Hobbs, P. V. (2006). Atmospheric Science - An introductory Survey. *Elsevier*. ISBN 978-0-12-732951-2.

Wapler, K. (2017). The life-cycle of hailstorms: Lightning, radar reflectivity and rotation characteristics. *Atmospheric Research*, 193:60–72. https://doi.org/10.1016/j.atmosres.2017.04.009.

Watson, A. I., Holle, R. L., and Lopez, R. E. (1995). Lightning from Two National Detection Networks Related to Vertically Integrated Liquid and Echo-Top Information from WSR-88D Radar. *Weather and Forecasting*, 10:592–605. https://doi.org/10.1175/1520-0434(1995)010%3C0592:LFTNDN%3E2.0.CO;2.

Wegener, A. (1911). Thermodynamik der Atmoshpäre. *Leipzig*, page 331 p.

Westcott, N. E. (1994). Merging of Convective Clouds: Cloud Initiation, Bridging, and Subsequent Growth. *Monthly Weather Review*, 122:780–790. https://doi.org/10.1175/1520-0493(1994)122%3C0780:MOCCCI%3E2.0.CO;2.

Williams, E., Boldi, B., Matlin, A., Weber, M., Hodanish, S., Sharp, D., Goodman, S., Raghavan, R., and Buechler, D. (1999). The behavior of total lightning activity in severe Florida thunderstorms. *Atmospheric Research*, 51(3):245–265. https://doi.org/10.1175/2009BAMS2808.1.

Wilson, J. W., Crook, N. A., Mueller, C. K., Sun, J., and Dixon, M. (1998). Nowcasting thunderstorms: A status report. *Bulletin of American Meteorological Society*, 79:2079–2099. https://doi.org/10.1175/1520-0477(1998)079%3C2079:NTASR%3E2.0.CO;2.

Wilson, J. W., Feng, Y., and Chen, M. (2010). Nowcasting challenges during the Beijing Olympics: Success, failures, and implications for future nowcasting systems. *Weather and Forecasting*, 25:1691–1714. https://doi.org/10.1175/2010WAF2222417.1.

Zadeh, L. A. (1965). Fuzzy sets. *Information and Control*, 8(3):338–353. https://doi.org/10.1016/S0019-9958(65)90241-X.

Zinner, T., Forster, C., de Coning, E., and Betz, H.-D. (2013). Validation of Meteosat storm detection and nowcasting system Cb-TRAM with lightning network data - Europe and South Africa. *Atmospheric Measurement Techniques*, 6(6):1567–1585. doi: 10.5194/amt-6-1567-2013.

Zinner, T., Mannstein, H., and Tafferner, A. (2008). Cb-TRAM: Tracking and monitoring severe convection from onset over rapid development to mature phase using multi-channel Meteosat-8 SEVIRI data. *Meteorology and Atmospheric Physics*, 101(3-4):191–210. doi: 10.1007/s00703-008-0290y.

Data Acknowledgment

I would like to thank the German Weather Service (Deutscher Wetterdienst, DWD) who funded this work within the framework of the extramural research of the DWD for the funding period “Transitional research for an integrated forecasting system with a seamless transition from nowcasting for very-short-range”. Additionally, I am grateful to the following organizations for providing the data sources without which this work would not have been possible:

- the satellite data was provided by the European Organisation for the Exploitation of Meteorological Satellites (EUMETSAT) in form of the MSG SEVIRI rapid scan
- the radar data was provided by the DWD as well as the model data of the COSMO-DE model
- the lightning data was provided by the *nowcast GmbH*

Danksagung

Die Erstellung dieser Dissertation war nur möglich durch die Unterstützung von zahlreichen Menschen, bei denen ich mich herzlichst bedanken möchte.

Als erstes möchte ich mich bei meinen Betreuern bedanken: Arnold Tafferner, Caroline Forster und Tobias Zinner, die die Arbeit mit vielen wissenschaftlichen Diskussionen bereichert haben. Arnold, ich möchte dir dafür danken, dass du vor allem in der Anfangsphase stets ein offenes Ohr hattest, egal ob für technische oder wissenschaftliche Fragen. Du hast mir insbesondere den Einstieg in IDL erleichtert. Caro, danke, dass du nach Arnolds Renteneintritt die Betreuung der Arbeit übernommen hast! Angefangen bei dem Datensupport bis hin zu wissenschaftlichen Fragen hast du die Arbeit immer tatkräftig unterstützt. Vor allem auf der Ziel“geraden” hattest du immer ein offenes Ohr. Zusammen mit Tobias hatten wir viele konstruktive Diskussionen wodurch die Arbeit Stück für Stück an Qualität gewann, ich möchte euch herzlich dafür danken. Caro und Tobias, ich möchte euch auch für das Lesen der Arbeit und die konstruktive Kritik danken. Ebenso möchte ich mich bei Kathrin Wapler für die konstruktiven Beiträge und den Datensupport bedanken. Ebenso mchte ich mich fr die Bereitstellung von Daten bei Luca Bugliaro bedanken. Einen herzlichen Dank auch an meinen Erstgutachter, George Craig, für das Feedback und die konzeptionellen Ideen für die Arbeit. Vielen Dank auch an Markus Rapp für die Übernahme des Zweitgutachters und Unterstützung der Arbeit. Ebenso möchte ich mich bei, Thomas Gerz bedanken, dass ich die Möglichkeit bekommen habe meine Arbeit in seiner Abeilung zu erstellen. Ohne die Zusammenarbeit des DWD und des DLR wäre diese Arbeit nicht möglich gewesen, vielen Dank für die konstruktive Kooperation.

Zu guter Letzt möchte ich meinen Kollegen, Freunden sowie meiner Familie für ihre stetige Unterstützung und ihr Interesse an meiner Arbeit danken. Andy, tausend Dank dir dafür, dass du mich unermütlich motiviert und meine Arbeit Korrektur gelesen hast und mir stets eine Stütze warst und bist!